5. Equatorial waves

Because the atmosphere has in general a better homogeneity in the longitudinal (zonal or rotating) direction, it is quite reasonable to expand any meteorological quantity or forcing term (such as insolation) into a Fourier series as waves with various zonal wavenumbers and frequencies (or their ratios or zonal phase velocities). The zonal mean of such a wave component itself becomes zero, just as defined as a disturbance or an eddy in (4.1). A nonlinear quadratic term does not vanish even if the zonal mean is taken, but it is negligible in the first-order approximation (so almost linear) if the amplitude of the wave component is sufficiently small. Such a linear problem can be solved relatively easily by the Fourier expansion. For a global approach on the spherical Earth it is requested to use a spherical polynomial or Legendre expansion, but for a study near the equator a cylindrical (Bessel. Hermite, etc.) function expansion or even the simplest Fourier expansion becomes sufficiently useful approximation. Those techniques of mathematics to solve wave equations and of data calculations to analyze wave components have been prepared sufficiently for applications in many scientific fields, which is practically convenient background for applying the wave concepts to the tropical meteorology and climatology.

More importantly than practical, in the general fluid dynamics any waves must have concrete restoring forces (such as buoyancy, vorticity conservation, and compressibility) and amplifying mechanisms (forcing sources, instabilities, and free normal modes) determined by characteristics and conditions of the considered fluid system. Therefore, if a phenomenon is proved to be associated with a wave, we may clarify its cause in past and may predict its reoccurrence in future, although nonlinearity (multiple wave interactivity) and irreversibility (transience, dissipation, etc.) make difficulty. Furthermore fluid waves transport energy and momentum without direct circulations (mass transport), just like electromagnetic waves (cf. Chapter 1) in vacuum space, by which tropical regionally excited waves may cause global extratropical abnormal weather/climate, and waves excited in the troposphere may (interact the mean flow and) induce non-diurnal non-annual oscillations of the middle and upper atmospheres.

In spite of such importance the history of wave dynamics in the tropics is very young, almost only during the recent half century. It is clearly because the equatorial region has special situations such as vanishing Coriolis force, strong insolation, high moisture, interaction with the ocean broader than the northern mid latitudes, and so on, which generates special kinds of ‘equatorial waves’ to be described in this chapter. In addition many regions in the tropics have not been observed well until few decade ago, because of unstable politics, slow economic development, and/or insufficient measuring technology. However, in particular economic/political situations the south and southeast Asian countries, as well as fully global satellite remote sounding technologies, have been developed very rapidly. High resolution atmosphere-ocean coupled models also have been constructed. Now we are starting to study the global atmosphere including the tropics almost seamlessly.

5.1. Classification of waves in geophysical fluids

Subtracting the zonal mean equations (4.2)−(4.6) from the basic equations (3.13)−(3.17), we obtain

$$\frac{\overline{D}u'}{Dt} + \left(\frac{\partial \overline{u}}{\partial y} - f\right)v' + \frac{\partial \overline{u}}{\partial z}w' + \frac{\partial \phi'}{\partial x} = G_x{}', \tag{5.1}$$

$$\frac{\overline{D}v'}{Dt} + fu' + \frac{\partial \phi'}{\partial y} = G_y{}', \tag{5.2}$$

$$\frac{\partial \phi'}{\partial z} = \frac{RT'}{H}, \tag{5.3}$$

$$\frac{\overline{D}T'}{Dt} + \frac{\partial \overline{T}}{\partial y}v' + \left(\frac{\partial \overline{T}}{\partial z} + \Gamma\right)w' = Q', \tag{5.4}$$

$$\frac{\partial u'}{\partial x} + \frac{\partial v'}{\partial y} + \frac{1}{\rho_0}\frac{\partial \rho_0 w'}{\partial z} = 0, \tag{5.5}$$

where we have assumed the mean flow only in the zonal direction for simplicity:

$$\frac{\overline{D}}{Dt} \equiv \frac{\partial}{\partial t} + \overline{u}\frac{\partial}{\partial x}, \tag{5.6}$$

and have summarized all the nonlinear terms and non-axisymmetric forcing terms into $G_x{}'$, $G_y{}'$ and Q'.

As the simplest case, we assume also that the meridional and vertical shears of the mean flow are sufficiently weak ($\partial\overline{u}/\partial y \approx \partial\overline{u}/\partial z \approx 0$; then automatically $\partial\overline{T}/\partial y \approx 0$ by the thermal-wind equilibrium (4.11)), apply the equatorial β-plane approximation (4.7) and the Vaisala-Brunt frequency expression for vertical temperature gradient (4.19), and almost free conditions (sufficiently far away from any boundaries and weak internal forcing/dissipation; then $G_x{}' \approx G_y{}' \approx Q' \approx 0$). In this case (5.3)–(5.5) may be summarized into one (so-called shallow-water) equation:

$$-\frac{1}{N^2\rho_0}\frac{\overline{D}}{Dt}\frac{\partial}{\partial z}\rho_0\frac{\partial \phi'}{\partial z} + \frac{\partial u'}{\partial x} + \frac{\partial v'}{\partial y} = 0. \tag{5.7}$$

Thus our problem is to solve three equations (5.1), (5.2) and (5.7) for three dependent variables u', v' and ϕ'.

Assuming the factors of those three equations are strongly dependent only on y, we may put sinusoidal forms (as in the Fourier expansion) concerning x, z and t dependencies:

$$\begin{pmatrix} u' \\ v' \\ \phi' \end{pmatrix} \equiv e^{z/2H} \cdot \Re\left[\begin{pmatrix} \tilde{u}(y) \\ \tilde{v}(y) \\ \tilde{\phi}(y) \end{pmatrix} \exp\{i(kx + mz - \omega t)\}\right], \tag{5.8}$$

where $\Re[\ ]$ denotes to take the real part, k and m are zonal and vertical wavenumbers, and ω is frequency (relative to the ground). A factor dependent on $e^{z/2H}$ implies that the wave is automatically amplified upward to compensate the decrease of atmospheric density ρ_0 to conserve the wave energy $\propto \rho_0 \cdot |\text{amplitude}|^2$. Substituting (5.8) into (5.1), (5.2) and (5.7) and using the 'intrinsic' frequency relative to the wave media moving with the mean flow $\overline{u}$:

$$\hat{\omega} \equiv \omega - k\overline{u}, \tag{5.9}$$

we obtain a set of ordinary differential equation only for y:

$$\begin{pmatrix} -i\hat{\omega} & -\beta y & ik \\ \beta y & -i\hat{\omega} & d/dy \\ ik & d/dy & -i(\hat{\omega}/N^2)(m^2 + 1/4H^2) \end{pmatrix} \cdot \begin{pmatrix} \tilde{u}(y) \\ \tilde{v}(y) \\ \tilde{\phi}(y) \end{pmatrix} = 0,$$

which may be reduced to the following single equation only for one dependent variable $\tilde{v}$:

$$\frac{d^2\tilde{v}}{dy^2} + \left[\left\{\left(m^2 + \frac{1}{4H^2}\right)\frac{\hat{\omega}^2}{N^2} - k^2 - \frac{k\beta}{\hat{\omega}}\right\} - \frac{\beta^2}{N^2}\left(m^2 + \frac{1}{4H^2}\right)y^2\right]\tilde{v} = 0. \tag{5.10}$$

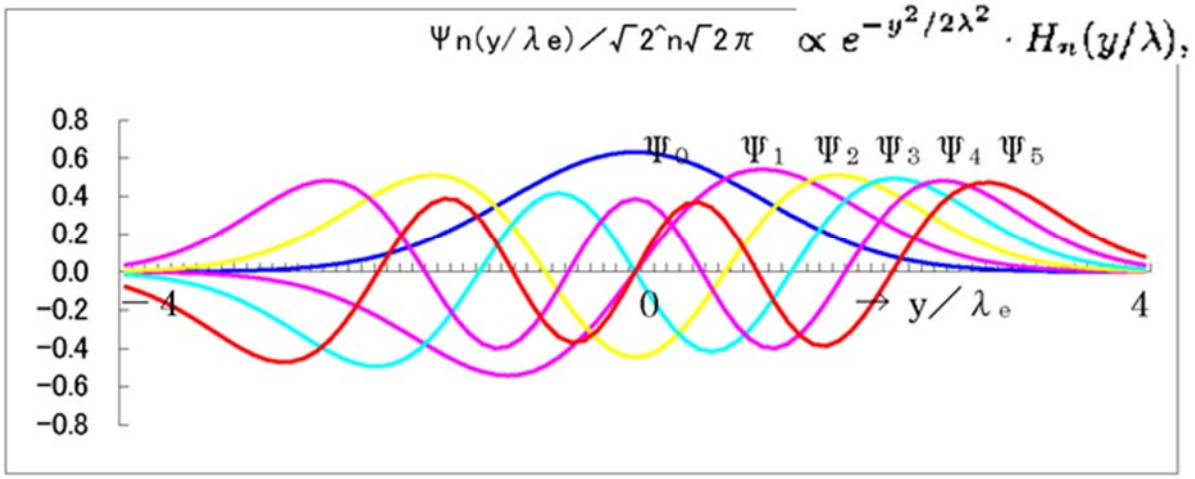

Fig. 5.1 The Hermite polynomials as the meridional structure function of the equatorial shallow water wave equations.

Then the other two variables are obtained from $\tilde{v}$ and its derivative as follows:

$$\tilde{u} = i\frac{kd\tilde{v}/dy - [(m^2 + 1/4H^2)\hat{\omega}\beta y/N^2]\tilde{v}}{k^2 - (m^2 + 1/4H^2)\hat{\omega}^2/N^2}, \quad \tilde{\phi} = i\frac{\hat{\omega}d\tilde{v}/dy - k\beta y\tilde{v}}{k^2 - (m^2 + 1/4H^2)\hat{\omega}^2/N^2}, \tag{5.11}$$

which are called the *polarization relations*. Although earlier studies to solve essentially similar problems (such as tides) used another single equation for $\tilde{\phi}$ with a more complex form, Matsuno (1966) derived (5.9) which was a breakthrough to obtain many important features describe in this section. Almost simultaneously but completely independently Kato (1966) and also Lindzen (1966) noticed that the depth h of truly shallow water (ocean) in the classical tidal theories[37] could be related to the vertical wavenumber as

$$gh = N^2\left(m^2 + \frac{1}{4H^2}\right)^{-1}, \tag{5.12}$$

which could take a negative value for the atmosphere, in case of *external* (upward decaying) modes with imaginary wavenumbers $m = im_i$. The *internal* modes (vertically propagating waves) are labeled by real numbers of m and positive numbers of h. Later we see that for example gravity waves with the diurnal period (related to global tides and local diurnal cycles) are internal and external in the latitudes lower and higher than 30º. An estimation[38] for waves considered here is h~100 m, corresponding to a vertical wavelength $2\pi/m$ ~10 km.

Matsuno (1966) solved (5.10) for a boundary condition:

$$|\tilde{v}| \to 0 \quad \text{for} \quad y \to \pm\infty,$$

corresponding to solutions decaying poleward[39], i.e., trapped near the equator, requested also from the mathematical validity of equatorial β-plane approximation. If a homogeneous equation such as (5.10) has a nontrivial solution (other than $\tilde{v} \equiv 0$) satisfying arbitrary boundary conditions, the factor of the equation must have a special form, namely the bracket { } must take certain values which are called eigenvalues. Fortunately (5.10) is mathematically equivalent to the Hermite equation appeared in quantum mechanics, and the so-called eigensolutions

[37]In the classical tidal theories for the atmosphere, the vertical structure was obtained from (5.7) by separating variables, in which h was used as the separation constant and called '*equivalent depth*'.
[38]The earliest estimation h~10 km was carried out in 1930s based on records of pressure disturbances caused by Krakatau (Krakatoa) eruption in 1883 (cf. Fig. 1.8), but this was due to a special case of acoustic-gravity waves (Lamb wave) filtered out in our basic equations.
[39]The both poles are located at $y = \pm\infty$ in the equatorial β-plane approximation (4.7).

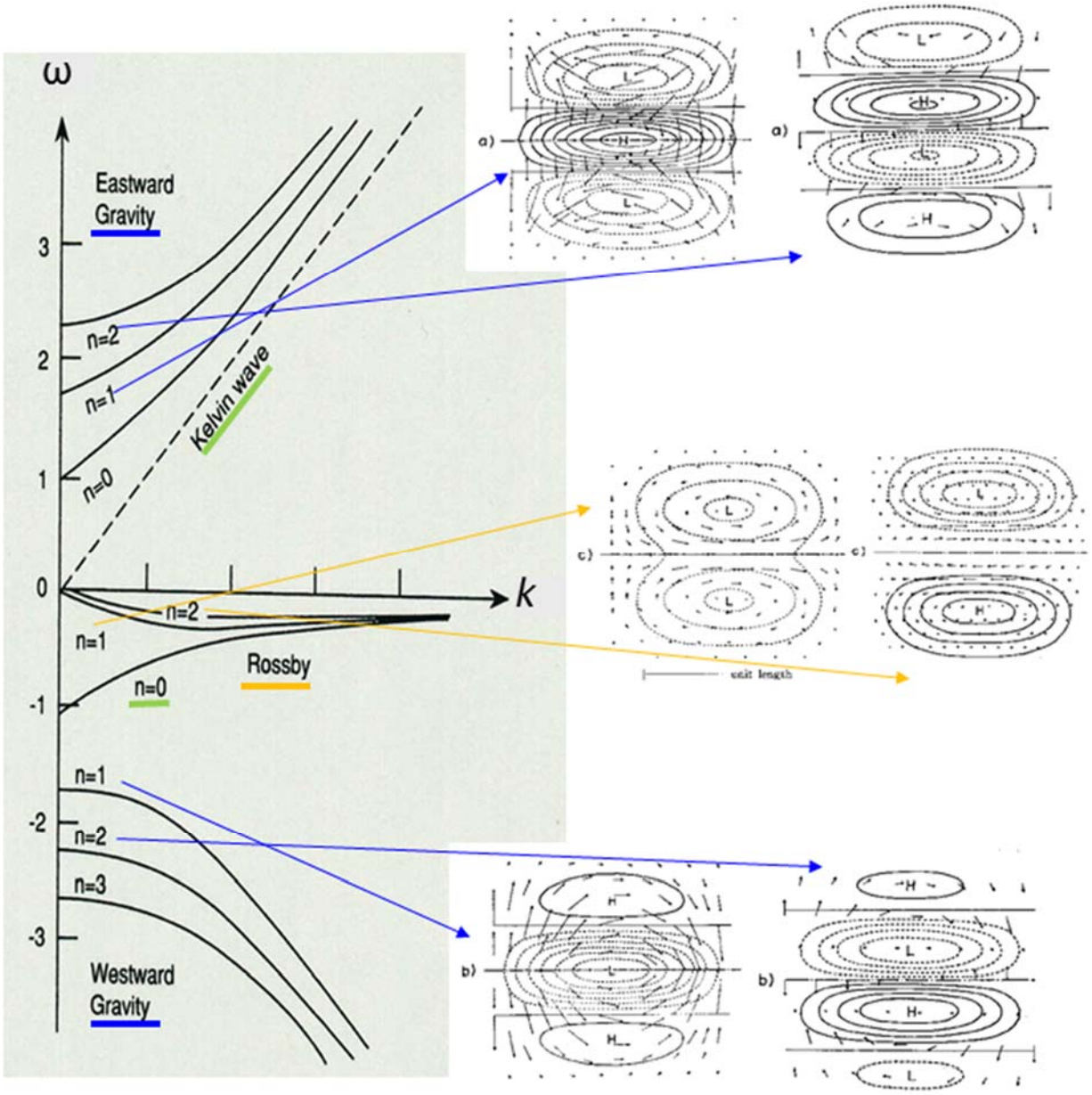

Fig. 5.2 The dispersion (frequency–zonal wavenumber) diagram of shallow-water-approximated equatorially trapped waves solved by Matsuno (1966) with horizontal structures of inertio-gravity and Rossby modes.

satisfying that boundary condition had been known already:

$$\tilde{v}(y) \propto e^{-y^2/2\lambda^2} \cdot H_n(y/\lambda), \qquad \lambda = \left[\frac{N^2}{\beta^2}\Big/\left(m^2 + \frac{1}{4H^2}\right)\right]^{1/4}, \tag{5.13}$$

where λ is the equatorial deformation radius (4.21) for h given by the equivalent depth (5.12), and $H_n(y/\lambda)$ is the nth-degree Hermite polynomials for argument y/λ (see Fig. 5.1). For h~100 m, the equivalent shallow-water gravity-wave phase speed $\sqrt{gh}$~30 m/s~2,600 km/day, and the deformation radius $\lambda = (gh/\beta^2)^{1/4}$~1,000 km ~ 10º latitude. The eigenvalues providing appropriate solutions are

$$\lambda^2\left(\frac{\widehat{\omega}^2}{\lambda^4\beta^2} - k^2 - \frac{k\beta}{\widehat{\omega}}\right) = 2n + 1 \qquad (n = 0, 1, 2, \cdots), \tag{5.14}$$

which may be plotted in the $\hat{\omega}$-k plane as shown in Fig. 5.2. A formula such as (5.14) concerning the wave parameters (k, m and ω in this case) is called the *dispersion relation*, and is mathematically given also by a simple replacement rule such as $(\partial/\partial x,\ \partial/\partial z,\ \partial/\partial t) \to i(k, m, -\omega)$ in the factor of governing equation (5.10) or those of the original ones (5.1)–(5.5), as well as a formal expression of *local wavenumber* considering an approximate wavelike solution $\tilde{v}(y) \propto e^{ily}$ for the meridional direction:

$$l(y)^2 = \frac{2n+1}{\lambda^2} - \frac{y^2}{\lambda^4}. \tag{5.15}$$

Therefore the dispersion relation includes the field (wave media) parameters (β, N, H, $\overline{u}$ in this case) given in factors of the governing equations, and determine the basic structures of waves as the solutions.

The factor $e^{-y^2/2\lambda^2}$ multiplied on the whole solutions (5.13) shows a rapid decay of wave amplitude away from the equator, by which we confirm very easily that the solutions satisfy the boundary condition. (5.15) implies that the eigenvalue number n represents the meridional wave structure (more exactly speaking, the number of nodes of the meridional velocity $\tilde{v}$ profile in the meridional direction), and such a wavelike variation (with a real value of l) is restricted within $|y| < \sqrt{(2n+1)}\lambda$, which may be confirmed by plotting the Hermite function[40] $H_n(y/\lambda)$:

$$H_0\left(\frac{y}{\lambda}\right) = 1, \qquad H_1\left(\frac{y}{\lambda}\right) = 2\frac{y}{\lambda}, \qquad H_2\left(\frac{y}{\lambda}\right) = 4\left(\frac{y}{\lambda}\right)^2 - 2, \quad H_3\left(\frac{y}{\lambda}\right) = 8\left(\frac{y}{\lambda}\right)^3 - 12\frac{y}{\lambda}, \quad \cdots.$$

From these considerations we understand that the equatorial deformation radius λ is essential to define the horizontal scale of tropical wave dynamics.

The dispersion relation (5.14) is a cubic equation (with at maximum three roots) for $\hat{\omega}$, when all the other wave and field parameters are completely given. This number of roots is originated by the number of time derivatives appeared in the basic equations (5.1)–(5.5)[41], and the three roots are those corresponding to eastward and westward moving (inertio-) gravity waves, and westward moving Rossby (planetary) waves. Namely, if we take a limit $\beta \to 0$, (5.10) and (5.13)–(5.15) are reduced to those for the shallow-water gravity waves without Earth's rotation (Fig. 5.3):

$$\frac{d^2\tilde{v}}{dy^2} + \left[\left(m^2 + \frac{1}{4H^2}\right)\frac{\hat{\omega}^2}{N^2} - k^2\right]\tilde{v} = 0, \quad \lambda \to \infty, \quad \left(m^2 + \frac{1}{4H^2}\right)\frac{\hat{\omega}^2}{N^2} - k^2 = l^2.$$

Alternatively, if $h \to \infty$, namely $m^2 + 1/4H^2 \to 0$, we have a Rossby wave with no horizontal divergence:

$$\frac{d^2\tilde{v}}{dy^2} - \left(k^2 + \frac{k\beta}{\hat{\omega}}\right)\tilde{v} = 0, \qquad \lambda \to \infty, \qquad -\frac{k\beta}{\hat{\omega}} - k^2 = l^2.$$

These are too extreme, no restriction for the tropics ($\lambda \to \infty$), and almost continuous spectral band (n disappeared).

More realistic approach is to classify cases by temporal scales, i.e., the magnitude of $|\hat{\omega}|$. On one hand, if the temporal scale is so short as to neglect the last term in the bracket of (5.14), i.e., $|\hat{\omega}| \gg \beta/k$,

$$\hat{\omega}^2 - \beta^2 y^2 \approx \frac{k^2 + l(y)^2}{m^2 + 1/4H^2} N^2, \tag{5.16}$$

which is known as the dispersion relation for *inertio-gravity waves* (Fig. 5.4), applied for the equatorial β-plane. The frequency of internal (vertically propagating) modes with real vertical wave numbers ($m^2 > 0$) must satisfy

---

[40]The definition of the Hermite polynomials has a variety. Here we use $H_n(x) \equiv (-1)^n \cdot e^{x^2} \cdot d^n e^{-x^2}/dx^n$.

[41]The original forms of the basic equations (three components (2.3), and (2.4)–(2.5)) have time derivatives, and there may be five roots for $\hat{\omega}$ corresponding to five modes: Rossby, two gravity and two acoustic waves. The last two roots are omitted in meteorology, by neglecting the time derivatives in the vertical momentum (hydrostatic) and continuity equations (Boussinesq) as in (5.1)–(5.5).

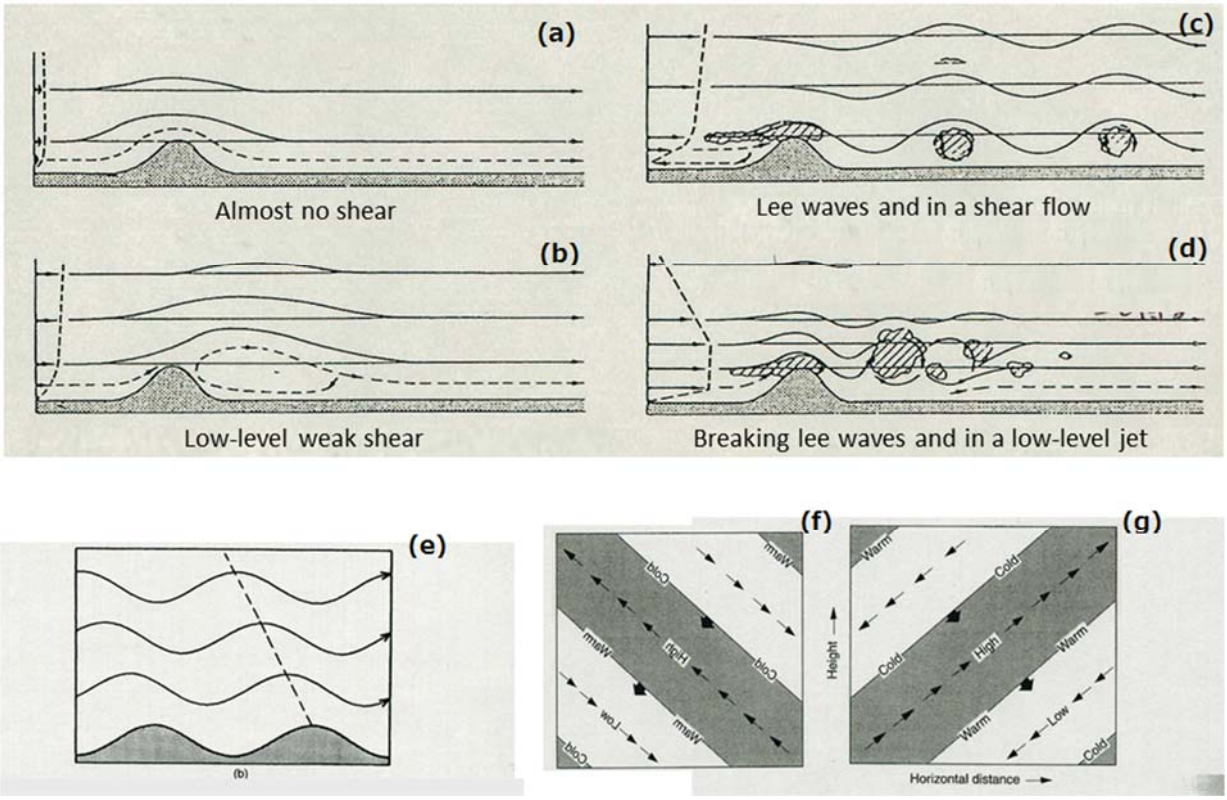

Fig. 5.3 Internal gravity waves (without the inertial (Earth's rotation) effect): (a)−(d) mountain (lee-side) waves for various flows (Corby, 1954); (e) internal waves in a shear flow (Durran, 1990); and (f) −(g) phae structures in the vertical plane including the propagation direction for k and m with the same sign and opposite signs (Holton, 1992).

$$|f|(=|\beta y|) < |\widehat{\omega}| < N.$$

These waves may propagate in any horizontal directions dependent on signs/values of k, l $[=\sqrt{(2n+1)}/\lambda$ at the equator $y = 0]$ and ω, and their 'horizontal' phase speeds relative to the media moving with the mean zonal velocity $\overline{u}$ are commonly given at the equator as

$$\left|\frac{\widehat{\omega}}{\text{horizontal wavenumber}}\right| = \sqrt{\frac{\widehat{\omega}^2}{k^2 + l(y)^2}} \approx \sqrt{\frac{N^2}{m^2 + 1/4H^2}} = \sqrt{gh},$$

which is just the same as gravity waves in a shallow water with mean depth h. Positive/negative roots $\pm|\widehat{\omega}|$ for a given set of the other parameter values correspond to waves propagating symmetrically eastward/westward relative to the media. The frequency ω and zonal phase velocity ω/k relative to the ground are not symmetric. In other words, in the basic flow, waves propagating eastward/westward with the same speed have different values of $|\widehat{\omega}|$, and hence different structures and characteristics, which are essentially important in the wave-mean flow interactions (Section 5.4). Although detailed description of waves common also in the extratropics is out of the scope, it may be shown from (5.11), (5.16) and (5.8) that the perturbed horizontal velocity $\boldsymbol{u}'_{\mathrm{H}} \equiv (u', v')$ makes an elliptic oscillation of which the long axis directs the horizontal propagation direction (parallel to the horizontal wavenumber: $\boldsymbol{k}_{\mathrm{H}} \equiv (k, l)$ $(k,\ l)$)[42]; the short/long axis ratio is $|f/\widehat{\omega}|$ $(=|\beta y/\widehat{\omega}|)$, and the rotation direction is the same as f $(=$

[42]The easiest confirmation is done for a zonal propagation mode ($l = 0$, $d/dy = 0$): from (5.16) $k^2 - (m^2 + 1/4H^2)\widehat{\omega}^2/N^2 \approx -(m^2 + 1/4H^2)f^2/N^2$, and (5.10) becomes , $\tilde{u} = i(\widehat{\omega}/f)\tilde{v}$, $\tilde{\phi} = i[k/\{(m^2 + 1/4H^2)f/N^2\}]\tilde{v} = [kN^2/\{\widehat{\omega}(m^2 + 1/4H^2)\}]\tilde{u}$.

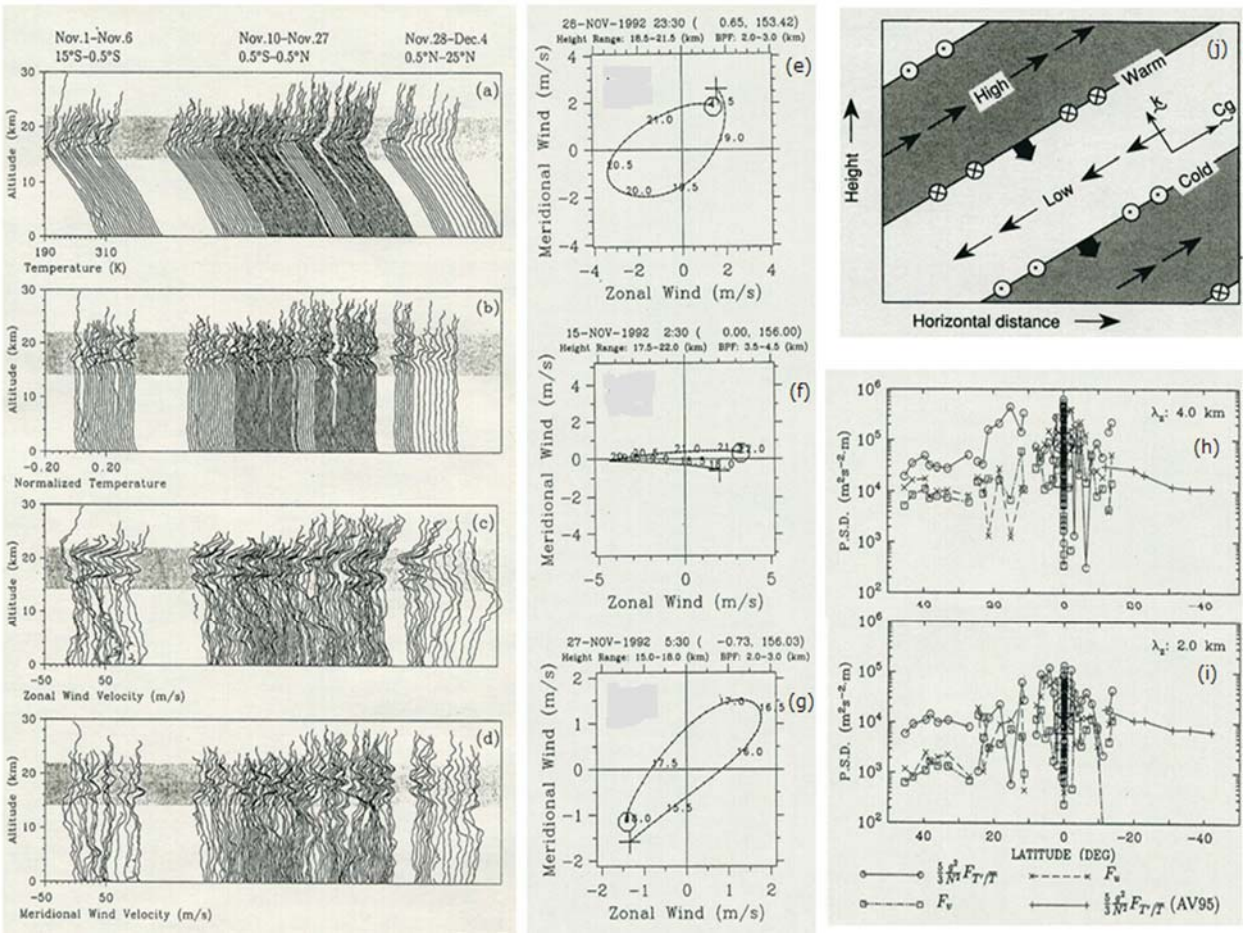

Fig. 5.4 Inertio-gravity waves: intensive radiosonde observations in around the tropics (Ogino et al., 1995) for (a)−(d) temperature and its normalized anomaly, and zonal and meridional winds; (e)−(g) horizontal wind vector hodographs in the northern hemisphere, at the equator and in the southern hemisphere; and (h)−(i) meridional distributions of amplitudes of 4 and 2 km vertical wavelength modes. In addition (j) is theoretical phase structure (Holton. 1992).

βy). It becomes a linear oscillation at the equator ($f = 0$), and becomes an inertial circular motion if the frequency t akes the lowest limit ($|\hat{\omega}| \to |f|$). It is also shown that ϕ' and the long-axis component of wind are in or anti phase, and $\phi' \approx \hat{\boldsymbol{c}}_{\mathrm{H}} \cdot \boldsymbol{u}'_{\mathrm{H}}$ for $f \approx 0$, where $\hat{\boldsymbol{c}}_{\mathrm{H}} \equiv (\hat{\omega}/|\boldsymbol{k}_{\mathrm{H}}|^2)\boldsymbol{k}_{\mathrm{H}}$ is the horizontal phase velocity relative to the media.

On the other hand, if the temporal scale is so long as to neglect the first term in the bracket of (5.14), i.e.,$|\hat{\omega}| \ll N$, we have a dispersion relation for *shallow-water Rossby waves* (Fig. 5.5) over the equatorial β-plane:

$$\hat{\omega} \approx \frac{-k\beta}{k^2 + l(y)^2 + (\beta^2 y^2/N^2)(m^2 + 1/4H^2)}. \tag{5.17}$$

This wave does not exist if $\beta = 0$ (homogeneous or no rotation), and $\hat{\omega} \to -0$ in the limit of $k \to 0$. The zonal phase propagation direction is always westward. Because of small $|\hat{\omega}|$ (corresponding to $|\overline{D}/Dt|$), (5.11) becomes approximately geostrophic: $\tilde{v} \approx i(k/\beta y)\tilde{\phi}$ and $\tilde{u} \approx -(l/k)\tilde{v} \approx -i(l/\beta y)\tilde{\phi}$. There are many good textbooks in which these two classical types of waves are explained in more details (e.g., Holton, 1992; Gill, 1982; Andrews, 2000).

It is for $n \geq 1$ that the general dispersion relation (5.14) with (5.15) has three roots for $\hat{\omega}$, corresponding to those inertio-gravity and Rossby waves common to the extratropics. For $n = 0$ (in this case $\tilde{v}(y) = e^{-y^2/2\lambda^2}$ has

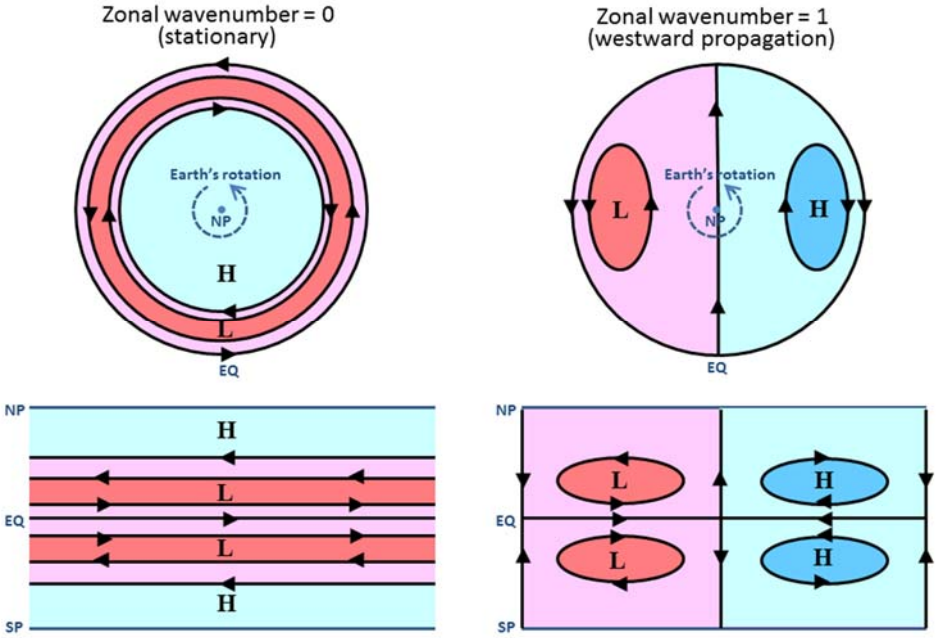

Fig. 5.5 Polar and equatorial views of pressure and wind patterns for Rossby (planetary) waves of $n = 1$ and zonal wavenumber $k \cdot 2\pi a =$ 0 (see Shigehisa, 1983, for derivation) and 1 (same as in Fig. 5.1).

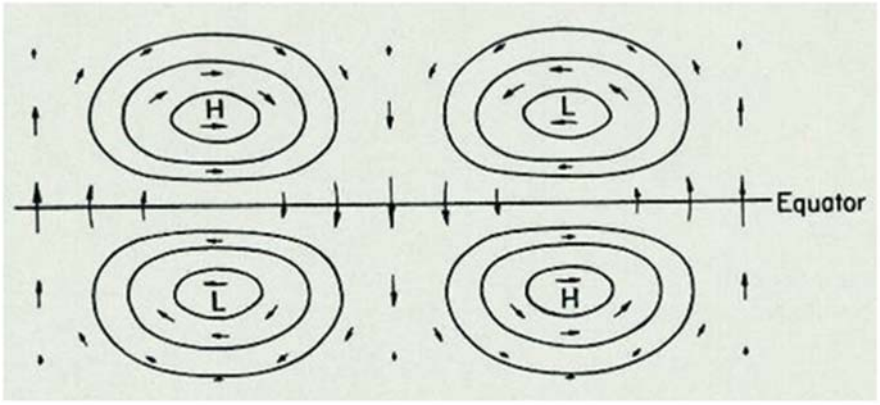

Fig. 5.6 Theoretical horizontal pressure and wind distributions of mixed Rossby-gravity wave (Matsuno, 1966).

a Gaussian-like meridional profile centered at the equator) appropriate roots are only two[43]:

$$\hat{\omega} = \frac{k\beta\lambda^2}{2}\left(1 - \sqrt{1 + \frac{4}{k^2\lambda^2}}\right) = \frac{kN}{(m^2 + 1/4H^2)^{1/2}}\left(\frac{1}{2} - \sqrt{\frac{1}{4} + \frac{\beta(m^2 + 1/4H^2)^{1/2}}{k^2 N}}\right) (< 0), \quad (5.18)$$

and the other one (a positive $\hat{\omega}$) similar to (5.18) with a positive sign replacing the negative sign in the bracket (in front of the root) which is an eastward propagating inertio-gravity wave. The westward propagating wave given by (5.18) becomes similar to Rossby wave in the short zonal wavelength limit ($k \to \infty$), and also to inertio-gravity wave in the long wave limit ($k \to 0$). Therefore this wave with $n = 0$ and negative $\hat{\omega}$ is called by Matsuno (1966) as the *mixed Rossby-gravity wave* (Fig. 5.6), or named after the observational discover(s) (Yanai and Maruyama, 1966) as *Yanai (-Maruyama) wave* (see Section 5.4).

All the waves mentioned above are derived from the reduced equation (5.10) only for $\tilde{v}$, and any other waves

[43]The other solution $\hat{\omega} = -k\beta\lambda^2 = -kN(m^2 + 1/4H^2)^{-1/2}$ is invalid for the polarization relations (5.10).

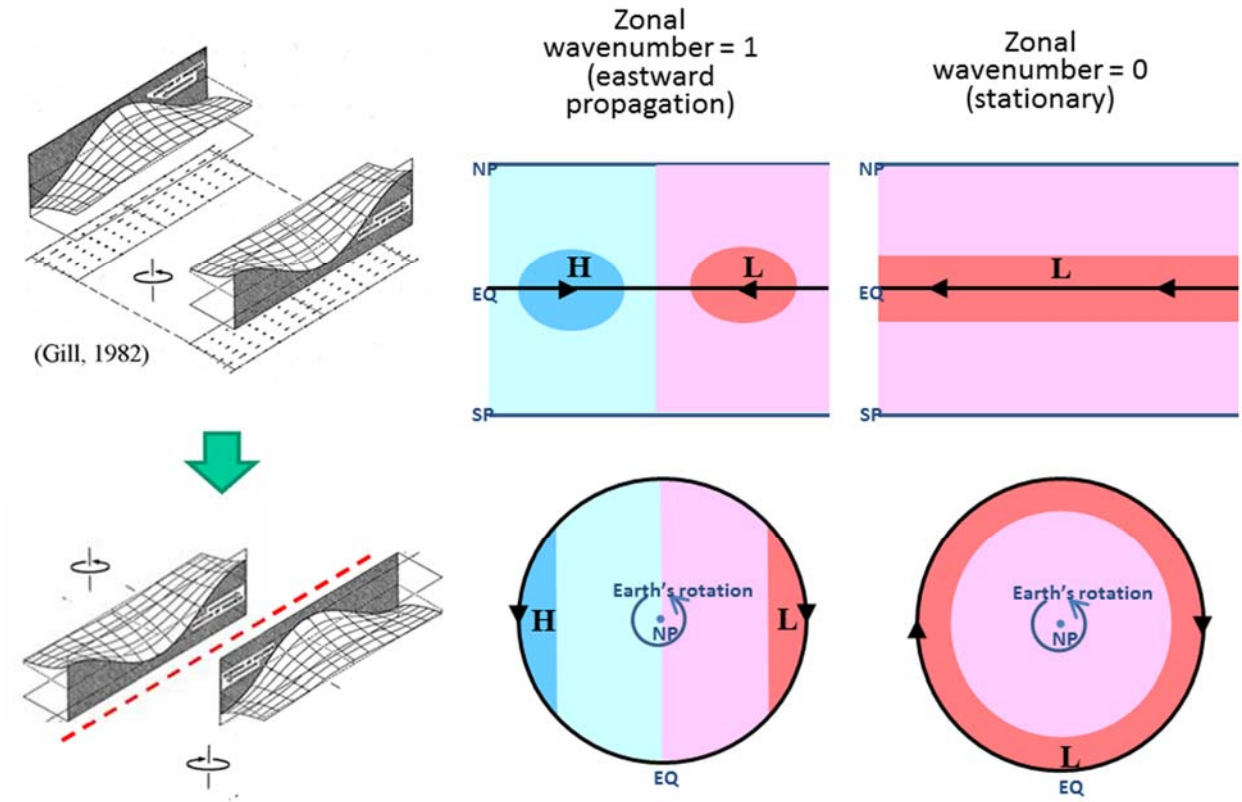

Fig. 5.7 Coastal (left) and equatorial (middle and right) Kelvin waves: the coastal cases for the both hemispheres are combined in the equatorial case just like the equator as a cost (Gill, 1982). For the equatorial Kelvin waves, equatorial and polar views of pressure and wind patterns for zonal wavenumber $k \cdot 2\pi a = 0$ (see Shigehisa, 1983, for derivation) and 1 are shown.

with $\tilde{v} \equiv 0$ (if exist) may not have been included. Matsuno (1966) noticed it, and obtained an additional category of wave satisfying

$$\hat{\omega} = \frac{kN}{(m^2 + 1/4H^2)^{1/2}}; \quad \frac{\hat{\omega}}{k}\tilde{u} = \tilde{\phi} \propto e^{-y^2/2\lambda^2}, \tag{5.19}$$

by restarting from the original equation system (5.1), (5.2) and (5.7) with putting $\tilde{v} \equiv 0$[44]. Such an additional solution is expected also from the mathematical completeness of orthonormality of the Hermite polynomials, and is labeled by $n = -1$ which is satisfying (5.14). The dispersion relation in (5.19) is non-inertial gravity-wavelike, but includes only one root propagating eastward ($\hat{c} = \hat{\omega}/k = \sqrt{gh} > 0$). The meridional profiles of $\tilde{u}$ and $\tilde{\phi}$ are like a Gaussian function centered on the equator with *e*-folding width $\sqrt{2}\lambda = \sqrt{2\hat{c}/\beta}$. The polarization relation is obtained as $\tilde{u} \approx -(l/k)\tilde{v} \approx -i(l/\beta y)\tilde{\phi}$, which is just geostrophic and completely different from gravity waves. These features are mathematically common to so-called Kelvin waves propagating over the ocean surface along a coastline (always seeing it in the right/left-hand side in the northern/southern hemisphere), and the wave given by (5.19) is called the *equatorial Kelvin wave* (Fig. 5.7). Namely, the equator with changing sign of the Coriolis parameter plays a role of coast trapping this special mode in the both sides. In the lower stratosphere the most dominant modes with zonal wavenumbers 1 or 2 in the equatorial circumference (i.e., zonal wavelengths of 40,000 or 20,000 km; see Section 5.4) have been called also as the *Wallace-Kousky waves* after their discoverers (Wallace

[44]The other root $\hat{\omega} = -kN(m^2 + 1/4H^2)^{-1/2}$ leading an inappropriate result $|\tilde{\phi}| \to \infty$ for $|y| \to \infty$ is omitted from solutions.

and Kousky, 1968), and in the upper stratosphere and mesosphere the period is shorter and the vertical wavelength is longer (Hirota, 1978). In the troposphere the equatorial parts of the most dominant intraseasonal variations (Madden and Julian, 1971; see Section 6.4) are constructed by equatorial Kelvin waves with periods and zonal wavelengths of some tens of days and some thousands of kilometers, and similar or shorter ones are observed also as tropopausal gaps (Shimizu and Tsuda, 1997).

These two special categories, the mixed Rossby-gravity and equatorial Kelvin waves, are collectively called the *equatorial waves*. They have been studied well observationally related to many types of interannual and intraseasonal variations (Sections 5.3−4 and 6.4) which are phenomena not only special for the tropics butt also impactful for the global climate. Advances of high-resolution observation networks and numerical models have contributed the establishment of wave dynamics and its successful applications to understand those phenomena. An important concept of the wave dynamics is *group velocity* given generally by

$$\overline{\boldsymbol{u}} + \frac{\partial \widehat{\omega}}{\partial \boldsymbol{k}}, \tag{5.20}$$

which is introduced as a progression velocity of the whole *wave packet* localized spatially and spectrally, and gives that of wave energy and momentum (exactly speaking, wave action). If we observe wave parameters and determine their types (dispersion and polarization relations), we may understand/predict their progressions/impacts by calculating the group velocity (5.20).

Since 1990s more several times of intense tropo-stratospheric observations mainly over Indo-Pacific regions around the maritime continent by radiosondes and/or wind profilers have revealed that waves with periods longer than a few days observed mainly in the zonal wind ($|u'| \gg |v'|$) are due to eastward propagating equatorial Kelvin waves mentioned above, whereas waves shorter than a few days usually with elliptic polarizations ($|u'| \sim |v'|$) are mainly westward-propagating mixed Rossby-gravity or inertio-gravity waves. These are superposed and organized into a transient localized structure, which appears as so-called hierarchical structure of a (super) cloud cluster (Section 6.4).

5.2. Zonal-vertical (Walker) circulation

The actual tropical diabatic heating is quite different from zonal symmetry, due to land-sea contrast and variations also on land (by topography, physiography, vegetation, etc.) and on sea (mainly by wind-driven currents), and the circulation is also different from the zonal-mean Hadley circulation. In particular, the land distribution of African and American continents and the Indonesian maritime continent (Section 4.4) and weak geostrophic balance in the vicinity of the equator (cf. Section 4.2) may induce a steady zonal circulation, in addition to the meridional Hadley circulation and seasonally reversing monsoons. For example, westward pressure gradient force between relatively low surface pressure over the maritime continent and high surface pressure in the central Pacific drives stronger easterly trade wind in the equatorial western Pacific. This strong wind makes the warm ocean-surface water thicker in the western side, as well as poleward Ekman transport and resulting so-called *equatorial upwelling* of the cold deep water over the central-to-eastern equatorial Pacific. Over the sea surface the easterly transports water vapor more westward, and enhance the upward motion (convective cloud activity) over the maritime continent, which feeds back to the westward pressure gradient and easterly. Therefore a steady circulation is generated between the maritime

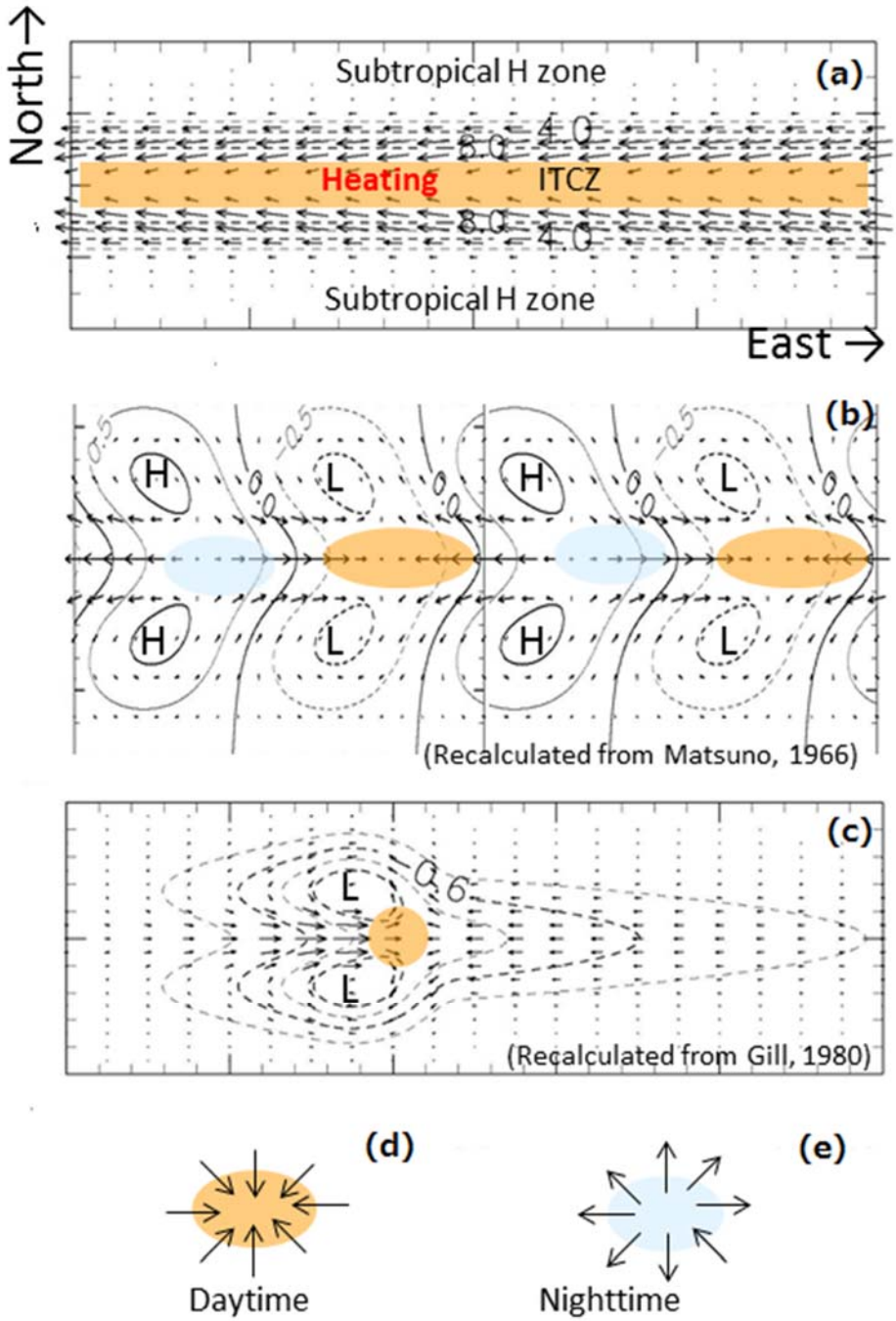

Fig. 5.8 Equatorially forced motions. (a) zonally homogeneous Hadley circulation-ITCZ-trade wind system (Section 4.3) obtained independently from Kosaka and Matsuda, 2005); (b)−(c) Matsuno (1966) - Gill (1980) patterns (see text), corresponding to real and maritime continents, and intraseasonal variations (Section 6.4); (d)−(e) diurnal-cycles sea-land breeze circulations (Section 6.1).

continent and the Pacific, which was called the *Walker circulation* by Bjerknes (1969), “since it can be shown to be an important part of the mechanism of Walker's "Southern Oscillation"” (cf. Section 5.3). Sir Gilbert Walker published many papers on interannual variations of the world climate including monsoons during his 20-year stay in the British Indian Meteorological Department, but he himself did show mainly pressure patterns and not the zonal circulation itself.

Exactly speaking, as discussed in Section 4.3, the distribution of heating/cooling throughout the troposphere is necessary to calculate any circulation, but the essential features of almost steady equatorial circulations may be

explained mainly by the boundary layer situations, of which mainly evaporation and moisture convergence maintain a convective system. Although those are a result of various interactions in the boundary layer and in Earth's surface, we may consider an external diabatic heating for the simplest problem. Furthermore we may assume that the steadiness is maintained by turbulent drag, such as the Rayleigh damping (4.12) and the Newtonian cooling (3.6). Then we replace $\partial/\partial t$ or $-i\omega$ in the wave equations in Section 5.1 with a simple drag coefficient $\alpha\ (>0)$[45], and omit the mean flow $\overline{u}$ for simplicity. Thus (5.10) is modified as

$$\frac{d^2\tilde{v}}{dy^2}+\left[-\left(m^2+\frac{1}{4H^2}\right)\frac{\alpha^2+\beta^2y^2}{N^2}-k^2+\frac{ik\beta}{\alpha}\right]\tilde{v}=-\tilde{Q}.$$

We may substitute expansions of $\tilde{v}$ and $\tilde{Q}$ by the orthonormal function series $H_n(y/\lambda)$, and obtain the factors of $\tilde{v}_n$ from those of $\tilde{Q}_n$ given arbitrarily. Note that above equation does not involve the (most important) Kelvin wave component ($n=-1$), which must be determined from similar expansions for the polarization relationships.

Matsuno (1966) and Gill (1980) calculated such circulations induced by steady heat sources Q aligned and isolated on the equator, respectively (Fig. 5.8). Gill modeled the *Indonesian maritime continent*[46] on infinitely broad Earth. Matsuno's cyclic specification corresponds to the case of neighboring continents affecting each other, or one continent on spherical Earth. Both obtained basically same results: the so-called *Matsuno-Gill pattern* with Kelvin-wavelike zonal wind along the equator and twin Rossby-wavelike vortices in the both subtropics. Around a heating source (convergence) a zonal ridge with westerly and a trough with easterly appear in the west and east, respectively, and twin cyclonic vortices in the both northern and southern sides of the westerly ridge. Matsuno's results involved also cooling (divergence), around which all the features are completely symmetric to those around the heating. Results around Gill's isolated heating source are zonally not symmetric; the eastern-side easterly is about three times broader longitudinally than the western-side westerly, and the latter is about three times stronger than the former (which is actually observed as a westerly burst). Gill speculated that circulations in the meridional and zonal cross-sections around the heat source correspond to those observed as the Hadley and Walker circulations (Fig. 5.9).

The same calculation may be applied also for an extreme (zonally homogeneous) case $k\to 0$, by which the Hadley circulation is obtained for an equatorially symmetric heating (Fig. 5.8(a); Kosaka and Matsuda, 2005). At the equator the horizontal wind vanishes, because the zero zonal wavenumber modes of Kelvin and Rossby waves (easterly and westerly) are canceled each other. In the both sides of this (the northern and southern subtropics) at the bottom the both waves have easterlies and the Rossby component makes weak equatorward flows (the Hadley cells) just observed as the trade winds in the actual tropical lower atmosphere. These features can be understood (as described by Gill) as the zonally elongated extremity of the Matsuno-Gill pattern.

The vertical structure of the Kelvin waves ($\hat{\omega}>0$) near the equator is expected inclined eastward ($k/m<0$), because the vertical group velocity (5.20) (without vertical mean flow)

$$W\equiv\frac{\partial\hat{\omega}}{\partial m}=-\frac{m\hat{\omega}}{m^2+1/4H^2}\approx-\frac{\hat{\omega}}{m}\quad\text{(opposite to phase velocity)}^{47}\qquad(5.21)$$

must be positive, that is, $m<0$. However, the dispersion relation (5.19) implies $|m|\propto N$, which is very small

[45]More correctly describing, the time derivative and the wave frequency are deleted ($\partial/\partial t=0,\ \omega=0$), and then the inhomogeneous (external forcing) terms are added as $(G_x',\ G_x',\ Q')\to-\alpha\,(u',\ v',\ \phi')+(0,\ 0,\ Q)$.
[46]Ramage (1968) first called so, mainly based on thunderstorm frequency distribution (only covering the whole equatorial circumference at that time) with a striking peak in this region, comparable to the other peaks in real continents of Africa and South America.
[47]This feature is common to the gravity waves.

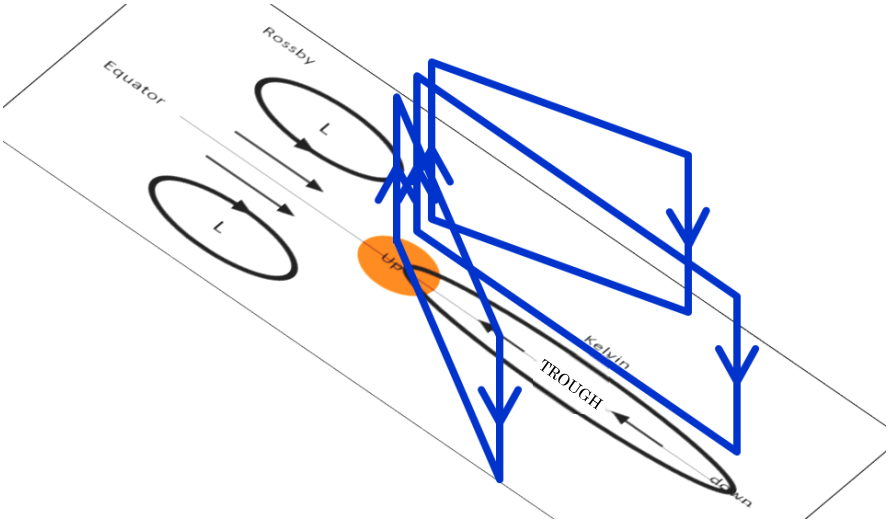

Fig. 5.9 The Hadley and Walker circulations associated with the Matsuno-Gill pattern.

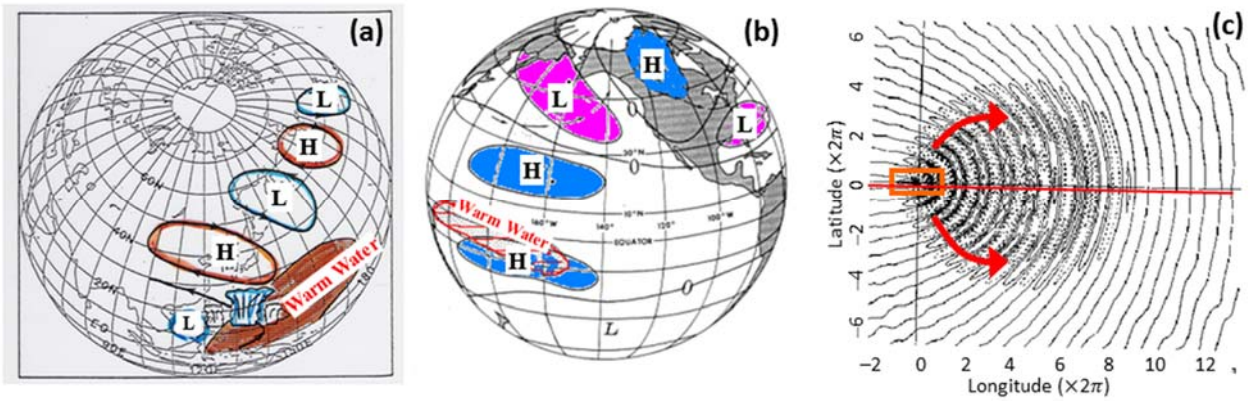

Fig. 5.10 (a) The Pacific-Japan (PJ) (Nitta, 1986) and (b) Pacific-North America (PNA) (Horel and Wallace, 1981) teleconnection patterns, and (c) a shallow-water Rossby wave propagation along a great circle (Hayashi, 1987).

(replacing θ by the equivalent potential temperature defined for moist atmosphere in Section 6.2; in particular $N = 0$ inside a cloud) in the tropical troposphere. Actually observed/analyzed Walker circulation cell has an almost vertical structure.

In summary the tropical circulation between intraseasonal and interannual scales is a superposition of the Hadley, Walker and monsoon circulations. By the Helmholtz theorem (Fug. 4.9 in Section 4.2) such a large-scale circulation may be separated into a non-divergent flow described by the streamfunction ψ and a irrotational field described by the velocity potential χ:

$$u = -\frac{\partial \psi}{\partial y} + \frac{\partial \chi}{\partial x}, \qquad v = \frac{\partial \psi}{\partial x} + \frac{\partial \chi}{\partial y}. \tag{5.22}$$

Taking the horizontal divergence from (5.22) to omit the geostrophic component ($\psi \sim \phi$, of which the zonal mean gives $\overline{u}$):

$$\frac{\partial u}{\partial x} + \frac{\partial v}{\partial y} = \frac{\partial^2 \chi}{\partial x^2} + \frac{\partial^2 \chi}{\partial y^2}, \tag{5.23}$$

we may obtain the potential flow perpendicular to contours of χ, which involves the Hadley, Walker and monsoon circulations (e.g., Krishnamurti, 1971; Krishnamurti et al., 1973; see Figs. 4.14 (a) and (b)). In the northern winter

the northern-hemispheric Hadley cell is reinforced by the 'astronomical' monsoon (Section 4.4), and in the lower troposphere they and the Walker circulation are all flown into the southern-hemispheric side of the maritime continent to make very active rainy season and upper-tropospheric divergence there. In the northern summer the Walker circulation centered at the Indonesian maritime continent has the same direction as a part of the summer 'geographical' monsoon centered at the Tibetan plateau, as well as the southern-Hadley cell reinforced by the 'astronomical' monsoon, and very strong divergence appears in the Tibetan upper troposphere.

The twin cells generated in the both subtropical sides of the Matsuno-Gill pattern are due to Rossby waves which are trapped modes near the equator by the given boundary condition. If we abandon this condition, there are other modes of Rossby waves propagating globally along any great circles (Hoskins and Karoly, 1981; Simmons et al., 1983; Hayashi and Matsuno, 1984), which transfer signals of tropical climate anomalies (Fig. 5.10). The so-called *teleconnection* between climates of distant places were considered long ago by Walker and Bliss (1923, and many others) and then by Bjerknes (1969), and now is explained dynamically by the Rossby wave propagations. Through this mechanism tropically excited phenomena cause abnormal weather and climate all over the world (see the next section).

5.3. Atmosphere-ocean interaction: El Nino-southern oscillation (ENSO) and Indian-Ocean dipole mode (IOD)

As mentioned in the previous section, the Walker circulation (in the same direction as the trade wind) pushes warm surface Pacific water westward, which causes so-called *coastal upwelling* off the South America centered around Peru. Mainly this. as well as cold equatorward currents along coasts of the Americas, keeps quite appropriate (relatively cold) environment for planktons and fishes eating them, namely very good fishery sea area, usually from March to December. From December the westerly monsoon from the Indian Ocean to the maritime continent becomes much stronger than the Pacific trade wind, and relatively weakened coastal upwelling and cold currents make off-Peru water warmer and fishery taking a break. This had been called El Niño (meaning a boy baby) originally (at latest since early Spanish colonial era some hundreds years ago; phenomena themselves probably known since the Inca Empire era), because all godly Peruvian fishermen celebrated Christmas (the birthday of the Holy Baby Jesus). This 'original usual El Niño' recovers at latest until March, associated with the withdrawal of southern Indonesian rainy season. However, every few years, extremely warmer sea water and several abnormal weather such as torrential rainfalls come to this area rather earlier than December and continues often for a year. Because the cause is different (as described below) from the usual one, the abnormal one was distinguished initially and called El Niño-like phenomenon etc., but now only this abnormal one (and often including related abnormal weather) is called *El Niño*.

Independently, from studies on interannual variations of monsoon and correlated phenomena at the Indian Meteorological Department, the Director General Walker (1923) discovered the so-called *southern oscillation* that surface pressure anomalies (from each long-duration means) at Darwin of Australia and Tahiti Island of the central Pacific have clear variations correlated negatively with each other at 2–5 year intervals. Almost half a century later, Bjerknes (1969) speculated the existence of so-called Walker circulation varying with the Darwin-Tahiti (and the whole Indo-Pacific) pressure anomalies, and all of them are related to El Niño (and opposite phase). In the eastern Pacific during the weaker Walker-circulation trade wind phase of the southern oscillation, the equatorial and coastal oceanic upwellings are reduced, the thermocline is deepened, and the sea surface temperature rises, that is referred

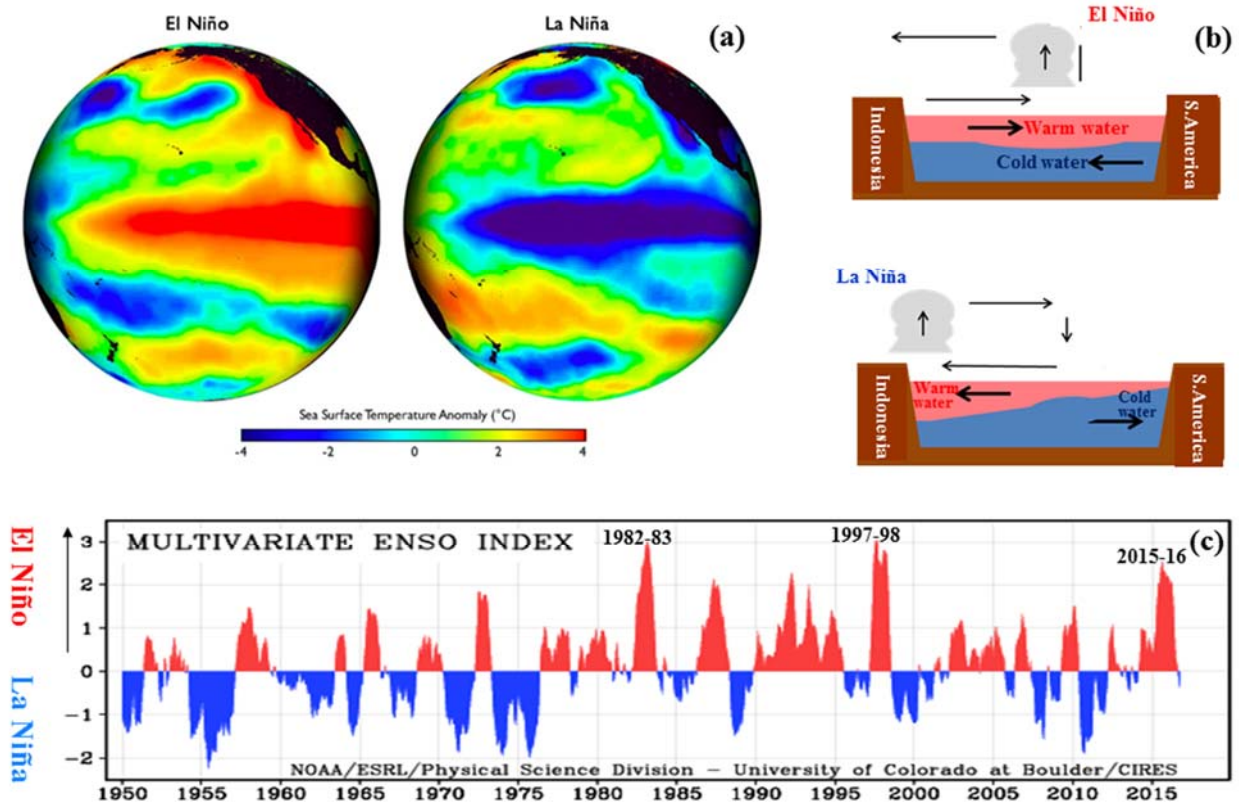

Fig. 5.11 El Niño and La Niña: (a) typical sea surface temperature distributions (Fiondella, 2009), (b) schematic zonal cross-sections of the equatorial Pacific and (c) 65-year variation of an index (http://www.esrl.noaa.gov/psd/enso/mei/).

to as El Niño. In the opposite phase, stronger trade wind induces stronger upwelling, shallower thermocline and cooler sea surface temperature in the eastern equatorial Pacific, whereas deeper thermocline and warmer surface water in the western Pacific and inland/surrounding seas of the maritime continent, that is (initially called the anti-El Niño but now taking another Spanish word on a girl baby) *La Niña*. The whole cycle of these events is called the *El Niño-southern oscillation (ENSO)*.

ENSO is, exactly speaking, not an 'oscillation' but is rather irregular interannual variation as the intervals (not 'periods') are changed in the range of 2-5 years (Fig. 5.11). It is like a global scale "see-saw" in atmospheric pressure and in the ocean thermocline[48]. The both phases El Niño and La Niña are the two 'stable' situations of this sea-saw, and must not be considered that one is normal and the other is abnormal. ENSO is a typically atmosphere-ocean coupled (interacting) phenomenon, and must not be considered which of atmosphere or ocean is the cause or the result. Anyway, associated with ENSO, the regional (the maritime continent, the Pacific, and the South America) climates such as rainfall and temperature are varying interannually (as seen only partly already in Fig. 4.17). Furthermore, the atmospheric anomalies may be propagated globally by (Rossby) waves, as shown later. Therefore, ENSO is one of the key issue to understand and predict interannual (a few-year scale) climate variability all over the world, and this is one of the major reasons why the tropical meteorology/climatology becomes a hot study subject.

In order to study this atmosphere-ocean coupled phenomenon, we may use (5.1), (5.2) and (5.7) for the

[48]Intervals of the South America, Africa and maritime continents (where the atmospheric updraft-convection centers are located in the La Niña phase) are roughly a quarter of the equatorial circumference. The central Pacific and the two true continents (updraft-convection in El Niño) have also similar intervals. In this meaning ENSO is alternative forced modes of zonal wavenumber four.

atmospheric process, and add another similar equation system for the oceanic process. At first, let us sketch the simplest steady solution of this six-variable six-equation system. For the atmosphere, on one hand, we assume a (latent and/or sensible) heating source $Q'_{(\mathrm{atmosphere})}$ dependent on the oceanic surface temperature, and neglect mechanical forcing ($G'_{x(\mathrm{atmosphere})} = G'_{y(\mathrm{atmosphere})} = 0$) for simplicity. The steady atmospheric response is the Matsuno-Gill pattern obtained so far in the previous section. For the ocean, on the other hand, we neglect heating ($Q'_{(\mathrm{ocean})} = 0$), and assume a mechanical forcing $\left(G'_{x(\mathrm{ocean})},\ G'_{y(\mathrm{ocean})}\right) \equiv +\alpha'\left(u'_{(\mathrm{atmosphere})}, v'_{(\mathrm{atmosphere})}\right)$ due to wind stress[49]. We also assume that the final steady ocean situation is adjusted as a completely flat ocean surface ($h' \to 0$), and we have

$$\begin{aligned} u'_{(\mathrm{ocean})} &\approx \frac{G_y{}'_{(\mathrm{ocean})}}{\beta y} = \frac{\alpha'}{\beta y} \cdot v'_{(\mathrm{atmosphere})}, \\ v'_{(\mathrm{ocean})} &\approx -\frac{G_x{}'_{(\mathrm{ocean})}}{\beta y} = -\frac{\alpha'}{\beta y} \cdot u'_{(\mathrm{atmosphere})}, \end{aligned} \tag{5.24}$$

which is similar to the meridional flow in the steady forced meridional circulation (4.20). (5.24) shows the sea water moves to the right-/left-hand side of wind targeting direction in the northern/southern hemisphere ($y > 0$ / $y < 0$).[50]

In the La Niña phase with convection center over the maritime continent, there are generated twin anticyclones in the northern and southern sides of a divergence over the central equatorial Pacific (as calculated by Matsuno), which intensify the both subtropical high pressure zones and a convergence ($v'_{(\mathrm{atmosphere})} \lessgtr 0$ for $y \gtrless 0$) at the equator off the South American coast, whereas the ocean water is transported westward ($u'_{(\mathrm{ocean})} < 0$) for the both hemispheres as in (5.24) and, to compensate it, the coastal upwelling is generated. Near the equator, due to intensified trade wind ($u'_{(\mathrm{atmosphere})} < 0$) transports the ocean water poleward ($v'_{(\mathrm{ocean})} \gtrless 0$ for $y \gtrless 0$), which is compensated by the equatorial upwelling. By these processes relatively cooler water region is elongated from the South American coast westward along the equator, and the surface warm water is transported and accumulated (as so-called *warm water pool*) in the western end of the Pacific. Therefore these processes feed back to maintain the Matsuno-Gill pattern for La Niña stably.

In the El Niño phase with convection center over the central Pacific, the Matsuno-Gill pattern in the opposite sense to the La Niña phase is maintained similarly. Therefore the both La Niña and El Niño situations may be maintained stably as steady solutions. If we want to study transience between La Niña and El Niño, we need to solve time-dependent equations with nonlinearity and dissipation. Even in this case we may assume that the atmosphere respond quickly to the sea surface temperature through $Q'_{(\mathrm{atmosphere})}$, and generate a Matsuno-Gill pattern. We may solve the time-dependent nonlinear dissipative oceanic equations for $\left(G'_{x(\mathrm{ocean})},\ G'_{y(\mathrm{ocean})}\right)$ given by the

[49]Because the forcing by wind for ocean is the counteraction of the forcing (friction) by ocean for wind, the sign becomes opposite between atmosphere and ocean. Note that the friction is neglected in comparison with heating in the atmospheric equations (and heating is neglected in the oceanic equations).

[50]More exactly speaking, the forcing $\left(G'_{x(\mathrm{ocean})},\ G'_{y(\mathrm{ocean})}\right)$ is the internal friction (stress gradient) dependent on the depth in the oceanic boundary layer, and its boundary value at the surface is given by the wind stress as in (5.24). Then the exact steady solution for the vertical profile (hodograph) of ocean current $\left(u'_{(\mathrm{ocean})}, v'_{(\mathrm{ocean})}\right)$ throughout the boundary layer is the so-called *Ekman spiral*, and its surface direction is 45º of the right-/left-hand side of wind. Even in this case the mass transport throughout the so-called *Ekman layer* is just as in (5.24) (which is used in Fig. 4.18). The atmospheric Ekman layer (which appears only when the Coriolis parameter is sufficiently large away from the equator) is briefly mentioned in Section 6.3.

atmospheric Matsuno-Gill Pattern. The direct integration of such equations can be done only numerically, and operational prediction results by world's various institutions are obtained for example at a website belonging to Columbia University of US: http://iri.columbia.edu/our-expertise/climate/forecasts/enso/current/ as well as that of each original institution. For semi-analytical or theoretical studies, some simplified equations to predict temperature changes are proposed, as described below.

A simplified equation to model the oceanic temperature change is

$$\frac{\partial T'}{\partial t} = -au' + bh' - cT'; \qquad a, b, c > 0, \tag{5.25}$$

where the three terms in the righthand side are the zonal advection (a: zonal temperature gradient), the warming due to deepening h' of the surface layer, and the dissipation expressed by the Newtonian cooling. From (5.25) T' determines $Q' \approx +\alpha' T'$, for which the atmospheric Matsuno-Gill response is calculated to determine oceanic u' and h'. 'Slow' variations of u' and h' are due to oceanic Kelvin and Rossby waves, which are neutral (not developed) solutions of the oceanic equations. However, Philander et al. (1982) showed that, coupled with the atmosphere, they may be unstable and self-developed. When the last two terms of (5.25) are dominant: $h' \approx (c/b)T'$, an ocean warm anomaly ($T' > 0$) makes atmospheric heating ($Q' > 0$) to generate (Matsuno-Gill pattern-like) atmospheric convergence, which makes oceanic forcing G' to generate oceanic (Kelvin wave and) convergence. In this case the oceanic (Kelvin wavelike) eastward current and the atmospheric (Rossby twin vortices') westerly are in the same direction, and the coupled warm water-active convection (cloud) system is developed rapidly. If this coupling development mechanism works actually, the wind convergence of atmosphere with small inertia must be sustained long enough to keep a positive correlation to induce the current convergence of ocean with large inertia. Key processes are small-scale dynamics and thermodynamics in the ocean surface layer to respond atmospheric forcing, and oceanic waves to extend local variations for broader area. In the latter process each equatorial wave is restricted in the propagation direction, and the oceanic waves cannot propagate beyond coasts.

It is possible that a wave is reflected as another type of wave. For example westward propagating Rossby wave reaching at the western coast is reflected as eastward propagating Kelvin wave. When a coupled 'warm' anomaly propagates eastward, an opposite (cold) anomaly will be emitted as a Rossby wave, which is reflected as an again reversed (warm, the same as the original) anomaly as a Kelvin wave. To express these processes, the third term of (5.25) is separated into a response directly dependent on $T'(t)$ and another one $T'(t-\tau)$ due to wave round-tripped for a time delay τ. The second term of (5.25) is expressed by a linear term dependent on T' and (when h' is amplified) nonlinear term dependent on T'^3. The first (advection) term is mainly dependent on T'. Therefore a revised equation may be written as

$$\frac{\partial T'}{\partial t} = -b'T'(t-\tau) + c'_1 T' - c'_2 T'^3; \qquad b > c'_1 > 0, \qquad c'_2 > 0, \tag{5.26}$$

which resembles a 'delayed oscillator' (Battisti and Hilst, 1989). If a steady state appears after a sufficiently long time ($t \gg \tau$, $\partial/\partial t \approx 0$), (5.26) gives (a trivial solution $T' \approx 0$ and) a pair of solution:

$$T' \approx \pm\sqrt{(c'_1 - b')/c'_2}, \equiv \pm T_0,$$

corresponding to La Niña and El Niño. Substituting a perturbation to the steady solution: $T' - T_0 \equiv \epsilon e^{-i\omega t}$ into (5.26) and taking the imaginary part of terms of the order of ϵ, we obtain $\omega \approx b' \sin \omega\tau$, from which we may study

the stability.

The tropically excited climate anomalies such as ENSO may affect globally by the Rossby wave-teleconnection mechanism mentioned in the end of previous section. An often observed teleconnection is the *Pacific-North America (PNA) pattern* in northern winter transferring El Niño-induced anomalies and causing abnormal weather over US (Horel and Wallace, 1981). Another one is the *Pacific-Japan (PJ) pattern* in northern summer (Nitta, 1986) and in northern winter (Chen, 2002). On the contrary extratropical situations may affect and interact with the tropical phenomena by similar mechanisms. For example, interannual anomalies of pressure (and so-called polar vortex under the geostrophic balance) in the northern high latitudes (called the *arctic oscillation (AO)*; Thompson and Wallace, 1998) may propagate equatorward, and modify the ENSO effects in the mid latitudes.

As mentioned in the previous section, the northern summer monsoon forced by the Tibetan plateau is considered to be connected with the Walker circulation, and hence also directly or indirectly with ENSO (e.g., Lukas et al., 1996; Webster et al., 1998). As the discovery of the southern oscillation by Walker (1923), ENSO is interacted directly with and the onset, activity and withdrawal of monsoons, and many studies are still in progress. Indirect connections are through the Indonesian throughflow from the Pacific to the Indian Ocean (e.g., Gordon, 2005), which is an important part of the global ocean circulation (see Fig. 4.8) and is known to be varied sensitively with wind variations such as monsoons and intraseasonal variations (Section 6.4).

Observations of ENSO with sufficient coverage and reliability have been continued from 1950s. Definitions of El Niño and La Niña are slightly different between countries (national operational agencies), institutions and investigators, and details are out of the scope of this mainly theoretical textbook. According to Japan Meteorological Agency (http://ds.data.jma.go.jp/tcc/tcc/products/elnino/index.html), El Niño periods occurred in 1951/52, 1953, 1957/58, 1963/64, 1965/66, 1968−70, 1972/73, 1976/77, 1982/83, 1986/88, 1991/92, 1997/98, 2002/03, 2009/10 and 2014−16, and among them the three biggest events were 1982/83, 1997/98 and 2014−16. La Niña periods occurred in 1949/50, 1954−56, 1964/65, 1967/68, 1970−72, 1973/74, 1975/76, 1984/85, 1988/89, 1995/96, 1998−2000, 2005/06, 2007/08 and 2010/11 (see Fig. 5.11(c)). Remarkable varieties of events have been suggested, for example the *El Niño Modoki*[51], in which the western Pacific resembles El Niño but the eastern not (Ashok et al., 2007).

A phenomenon similar to the Pacific ENSO has been observed as the *Indian Ocean dipole mode (IOD)* (Saji et al., 1999). In the 'positive IOD' phase the sea surface water is anomalously cooling/warming in the eastern/western equatorial Indian Ocean, and in the 'negative IOD' phase everything is opposite. For the western maritime continent rainfall correlations with both ENSO and IOD have seasonality and locality. In the western (Indian Ocean) coast of the middle (equatorial) Sumatera rainfall is correlated with IOD rather than ENSO (Fig. 5.12(b)). The rainy season onset comes later (earlier) in El Niño (La Niña) years than the average at many stations of the southern-hemispheric side (see lower panels of Fig. 4.17; Hamada et al., 2002), and in the northwestern Jawa drought in the dry season (May−October) occurs in conjunction with simultaneous development of positive IOD and El Niño, whereas wet conditions tend to appear in negative IOD with or without La Niña (Fig. 5.12(c); Hamada et al., 2012). Large-scale divergence (convergence) and lower (higher) atmospheric water vapor content tend to suppress (induce) rainfall in northwestern Jawa during the dry seasons of positive (negative) IOD years with cooler (warmer) sea surface temperature. However, such a clear correlation is not seen in the rainy season, and the rainfall amount throughout a

[51] 'Modoki' is a Japanese word, meaning '…oid', '-like', etc., namely resembling but different.

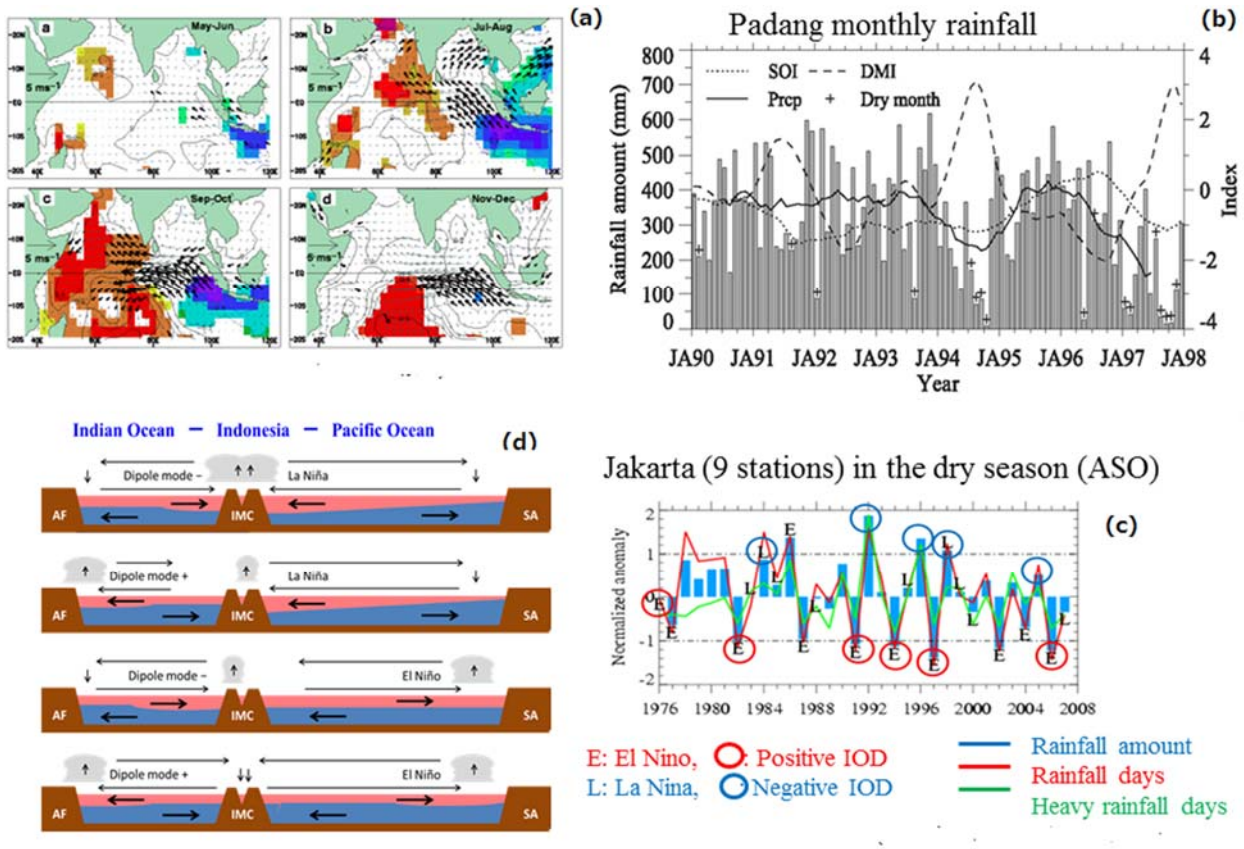

Fig. 5.12 (a) The Indian ocean dipole mode (IOD) (Saji et al., 1999), and its and ENSO's correlations with (b) monthly rainfall in Padang (Hamada et al., 2008) and (c) dry-season (August-October) rainfall in Jakarta (Hamada et al., 2012). (d) Schematic figure of the maritime continent and surrounding oceans with combination of IOD and ENSO (Yamanaka, 2016).

rainy season is not dependent upon the length of the rainy season (between onset and withdrawal) in many areas (Haylock and McBride, 2001; Hamada et al., 2002; McBride et al., 2003). Such low correlations may be due to anomalous Walker circulation patterns on the Indian Ocean side and steep mountains barriers there (Chang et al., 2004a), and due to more direct influence by the cold monsoon surges from the northern mid latitudes (Tangang et al., 2008; Hamada et al., 2012). For the eastern maritime continent (roughly to the east of central Kalimantan mountains) correlations with ENSO are relatively stronger (Aldrian and Susanto, 2003; Kubota et al., 2011; Lestari et al., 2016), due to monsoons as well as direct effects of water temperature of the Pacific.

5.4. Wave-mean flow interaction: Quasi-biennial oscillation (QBO) and semi-annual oscillation (SAO)

The pioneering tropical balloon observations by van Bemmelen (1913) at Batavia (now Jakarta) in the early 20th century noticed already the lower-stratospheric zonal wind variations non-synchronous with the tropospheric seasonal cycle (cf. right top panel of Fig. 3.4). Almost half a century later, Reed et al. (1961) and Veryard and Ebdon (1961) independently discovered that the equatorial lower-stratospheric zonal wind has a *quasi-biennial oscillation (QBO)* with features that successive easterly/westerly regimes appear above 30 km altitude every about 24 to 30 months, propagate downward by about 1 km/month without loss of amplitude, and disappear rapidly below 23 km (Fig. 5.13). This oscillation is zonally symmetric, and also symmetric about the equator with a maximum amplitude of about 20 m/s and a half-width of about 12º. Because of the zonal symmetricity, the mean meridional circulation is very small, and the temperature field satisfy the thermal wind balance (4.11) (or its L'Hospital rule version) with the

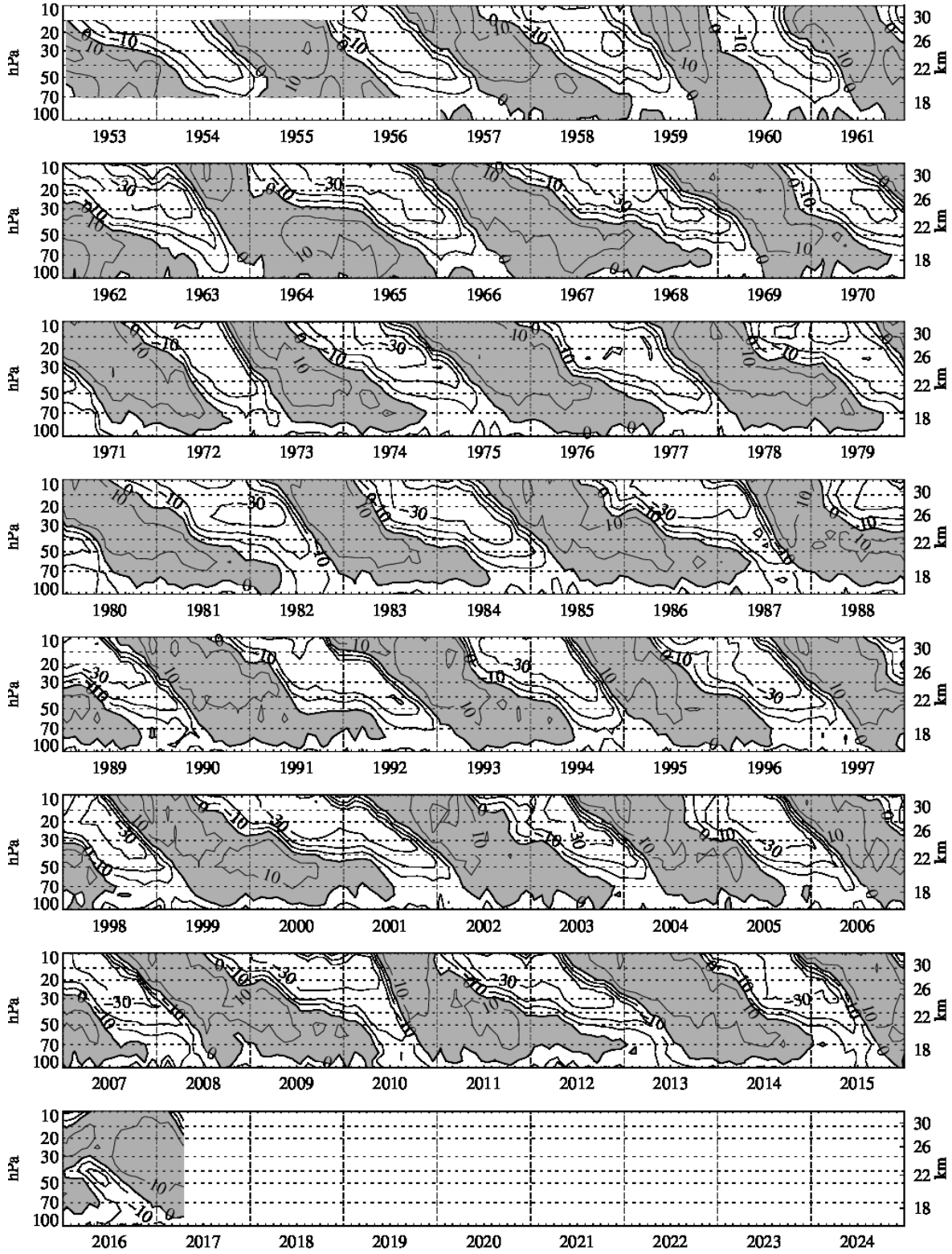

Fig. 5.13 Monthly mean zonal winds (10 m/s intervals; westerlies shaded) at Canton (Jan 1953-Aug 1967), Maledve (Sep 1967-Dec 1975) and Singapore (Jan 1976-). (updated from Naujokat, 1986; http://www.geo.fu-berlin.de/en/met/ag/strat/produkte/qbo/)

zonal wind. From the observed magnitude of vertical shear of the mean zonal wind at the equator is ~5 m/s/km, the temperature perturbation amplitude over the meridional width ~1200 km is estimated as ~3 K. From the L'Hospital version concerning the second derivative of temperature with the opposite sign to the temperature at the equator, the westerly and easterly shear zones have warm and cold equatorial temperature anomalies, respectively.

This phenomenon shows periodic behavior not associated with a periodic forcing, and becomes a big problem in atmospheric dynamics. Quantitatively the approximate biennial periodicity and the downward propagation without loss of amplitude must be explained. The occurrence of zonally symmetric westerly (superrotation; cf. Section 4.1) at the equator is also a mystery, and any plausible angular momentum supply and accumulation mechanisms (if due to any wave, what type of wave is sufficiently responsible) must be considered to explain the westerly phase of the oscillation.

The essential explanation was given as the wave-mean flow interaction theory by Lindzen and Holton (1968), Holton and Lindzen (1972), Plumb and McEwan (1978), and others. We start from a simplified version of the mean zonal momentum equation (4.2) or potential vorticity equation (4.27):

$$\frac{\partial \overline{u}}{\partial t} = \frac{1}{\rho_0}\frac{\partial \overline{E}_z}{\partial z} = -\frac{1}{\rho_0}\frac{\partial \rho_0 \overline{u'w'}}{\partial z}, \tag{5.27}$$

in which the righthand-side (gradient of the Reynolds stress; cf. Section 6.1) is now regarded as the divergence of wave momentum flux. As a perturbation theory (asymptotic expansion) $\overline{u}$ in (5.27) should be a second order quantity concerning the wave amplitude[52].

Above equation is identified with the wave action conservation law in the wave mechanics of general physics (Andrews and McIntyre, 1976):

$$\frac{\partial A}{\partial t} = -\frac{\partial B}{\partial z}; \quad A = \frac{E}{\widehat{\omega}}, \quad B = AW, \tag{5.28}$$

where A is the wave action density, B is the vertical wave-action flux, E is the energy density, and W is the vertical group velocity (the vertical component of (5.20); for gravity and Kelvin waves it is (5.21))[53]. kA and kB are called the wave momentum and the wave momentum flux, respectively. Because $kB = \rho_0 \overline{u'w'}$ is obtained from gravity wave solutions (inertio-gravity waves in Section 5.1 at the equator), we may write[54]

$$\frac{\partial}{\partial t}(\rho_0 \overline{u} - kA) = 0. \tag{5.29}$$

From (5.28) we have $kB = kAW = kEW/\widehat{\omega}$, and may calculate A, as well as $kB = \rho_0 \overline{u'w'}$, from wave solutions. It may be shown that A directs to the same direction as $\widehat{\omega}$.

From (5.21) waves with smaller $|\widehat{\omega}|$ have slower group velocity $|W|$ and stay there for longer duration, therefore they are more easily affected by damping such as viscosity and/or Newtonian cooling (even if the simplified equation does not incorporate them explicitly). From the dispersion relation (5.16) waves with smaller $|\widehat{\omega}|$ have larger $|m|$, i.e., shorter vertical wavelengths and larger vertical gradients (shear and/or lapse rate), therefore local instabilities and *wavebreaking* occur more easily. From (5.11), if the horizontal propagation is in the same direction as the mean flow, in particular

$$\text{if} \quad \omega \to \omega\overline{u}, \quad i.e., c \to \overline{u}; \quad \text{then} \quad \widehat{\omega} \to 0, \quad W \to 0 \text{ and } |m| \to \infty \tag{5.30}$$

---

[52]To express this clearly, the mean flow is often written as $\overline{u}^{(2)}$.

[53]The second formula of (5.28) is the same form as the energy of photon in quantum mechanics: $E = h\nu$, where ν is frequency (of electromagnetic wave; see Chapter 1), and h is the Planck constant (with dimension of action). In this meaning (5.28) is often called the *photon analogy*.

[54]It is *not* always that $kA = \rho_0 \overline{u}$, because waves may transmit the media without any interactions (breaking, damping or modulations) and the wave momentum may not be changed to a real momentum of the mean field. In this meaning kA is often called the *pseudomomentum*. (5.29) also implies that c $(= \omega/k)$ may be changed (*self-accelerated*) by nonlinear interactions, if $\overline{u}$ is changed (Fritts and Dunkerton, 1984; Tanaka and Yoshizawa, 1985).

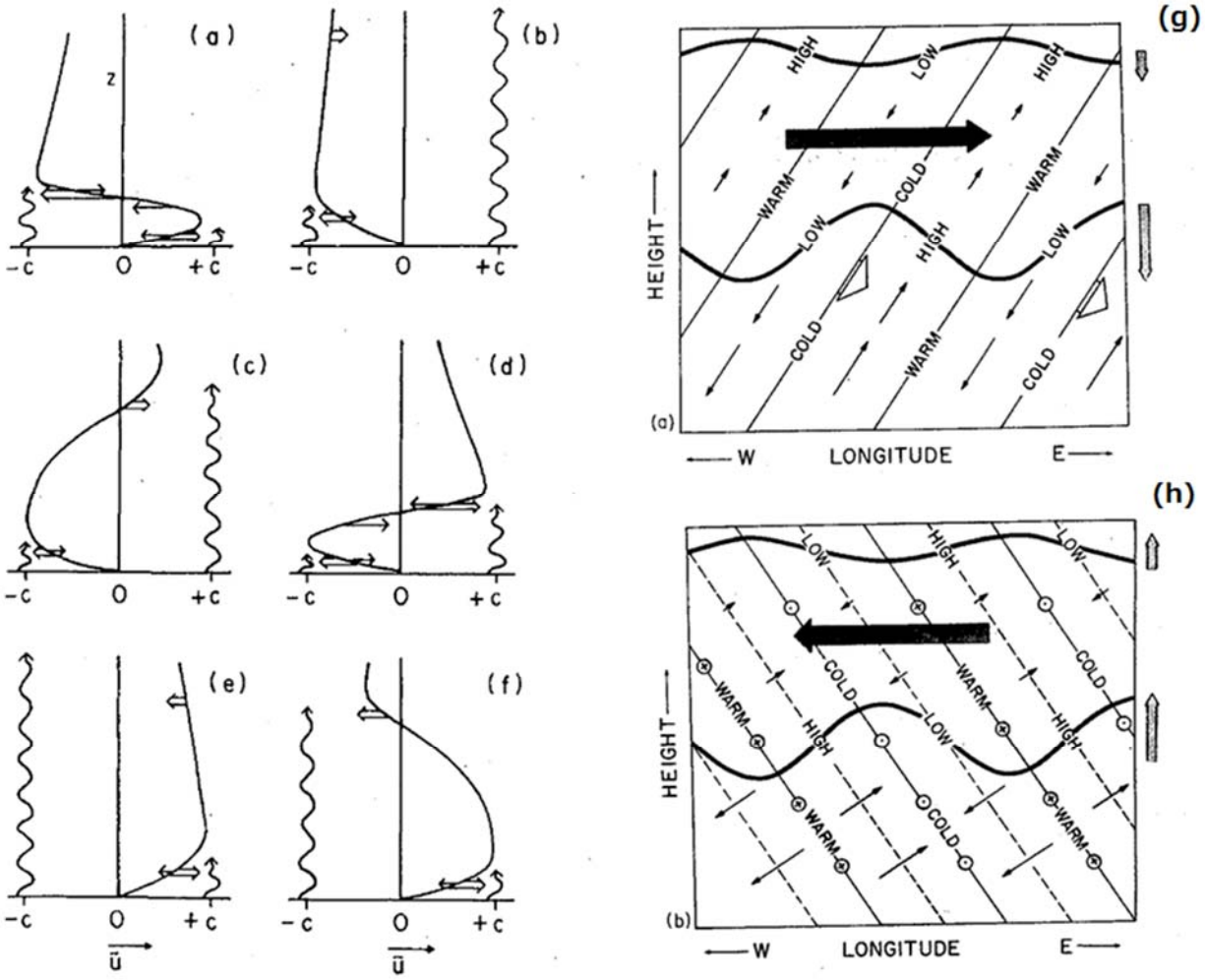

Fig. 5.14 (a)–(f) The QBO-cycle mechanism suggested by the laboratory experiments by Plumb and McEwan (1978): wavy arrows are east- and west-ward waves; double and single straight arrows are wave- and viscosity-driven acceleration (Plumb, 1984). Longitude-height structures of (g) Kelvin along the equator) and (h) mixed Rossby-gravity (along a latitude north of the equator) waves and their latitudinally integrated accelerations (thick horizontal arrows) are also shown (Andrews et al., 1987).

and waves are expected to break. If the media is almost without dissipation and almost homogeneous horizontally, waves conserve ω, k and c; but if there is a mean vertical shear (even weak), there may be the so-called '*critical level*' at which (5.30) is satisfied. Exact theoretical consideration show that (as long as the mean field is stable) gravity waves cannot transmit through the critical level with a significant amplitude and within a finite time, and namely they are substantially absorbed there (Booker and Bretherton, 1967).[55]

For waves propagating horizontally in the direction opposite to the mean flow, there are no such situations. As an earliest study Eliassen and Palm (1961) showed for gravity waves in a non-dissipating atmosphere

$$\frac{\partial}{\partial z}\rho_0\overline{u'w'} = 0 \quad \text{for} \quad \hat{\omega} \neq 0, \tag{5.31}$$

then (5.27) implies $\partial\overline{u}/\partial t = 0$, that is, there are no change (no acceleration nor deceleration) of the mean flow

[55]For the inertio-gravity waves with $f \neq 0$, the critical level is exactly not at $\hat{\omega} = 0$ but at $|\hat{\omega}| = |f|$ (Jones, 1967; Yamanaka and Tanaka, 1984). However, in particular in the tropics where $|f|$ is small, the wavebreaking and mean flow interaction will start sufficiently before any effect of f appears.

except at the critical level. This (as well as similar ones for other waves) is called the *non-acceleration theorem*. For example, in the westerly (eastward; $\overline{u} > 0$) the westward waves ($c < 0$) from the bottom propagate upward very quickly and transport the westward momentum ($kA < 0$) to the upper altitudes, whereas the eastward waves ($c > 0$) may encounter their critical levels somewhere and release the eastward momentum ($kA > 0$) there with decreasing the momentum flux ($\partial kB/\partial z < 0$) and accelerating the mean flow ($\partial \overline{u}/\partial t > 0$). During breaking the wave amplitude may be limited so as to keep a marginal state (which is called the wave *saturation*), and we may parameterize the eddy diffusivity K so as to realize a decaying factor $K\partial^2/\partial z^2 \approx -Km^2$ just for keeping the saturation amplitude (Lindzen, 1981). (5.31) also implies amplification of waves to compensate the density decrease, which is more effective (more easily to break) for the waves propagating to the mean flow direction, but is not negligible also for oppositely propagating waves arriving near the top. The last process mentioned above makes the opposite (easterly, i.e., westward) acceleration there.

Once easterly ($\overline{u} < 0$) is generated near the top, it plays a role of critical levels for westward waves ($c < 0$). Then the processes opposite to those mentioned above are started, and continued until the easterly layer arrives at the bottom. Just after the westward waves complete to accelerate the easterly in the lower altitudes, and eastward waves start again the westerly acceleration from the top. The QBO is just repeating these processes (Fig. 5.14). Both observational studies and theoretical models confirmed that energetically upward propagating equatorial Kelvin waves supply westerly momentum (i.e., u' and w' are positively correlated so that $\overline{u'w'} > 0$) probably enough to produce at least major part of the westerly phase of the QBO. However, although the mixed Rossby–gravity waves may provide a significant fraction of the westward momentum necessary to drive the QBO, contribution of mid-latitude Rossby waves and equatorial westward-propagating inertio-gravity waves is inevitably necessary.

Such origins of momenta are closely related to the generation mechanisms of equatorial and other waves maintaining the QBO. Rapid advances of spatially-temporally high-resolution and continuous observations, (e.g., Tsuda et al., 1994a, b, 2000; Sato et al., 1994, 1999; Ogino et al., 1995, 2016), as well as numerical modelling (e.g., Horinouchi and Yoden, 1996; Horinouchi et al., 2002, 2003), revealed clear tropical maximum of stratospheric gravity-wave activity in particular over the Indonesian maritime continent, where the tropospheric convective clouds also take maximum[56]. Momentum flux of such gravity waves have been requested to simulate the stratospheric dynamics such as equatorial quasi-biennial oscillations (Sato et al., 1999; Kawatani et al., 2010a, b). Effects of global warming on the QBO (e.g., Kawatani and Hamilton, 2013) and very recent abnormal behavior of the QBO (e.g., Osprey et al., 2016) are also studied in view of variabilities of related waves.

Above the QBO region, observations in the low latitudes are quite limited, by each small number of satellites (mainly thermal-wind estimations), lidars, VHF radars (above the middle mesosphere), large plastic balloons (below the stratopause) and rocketsondes (until around 2000). In the upper stratosphere-lower mesosphere (35−60 km altitudes) around the stratopause and in the upper mesosphere-lower thermosphere (70−90 km altitudes) around the mesopause, there are semiannual oscillations (SAOs) of anti-phase with each other (Reed, 1965; Hirota, 1978). Their generation mechanisms are considered essentially similar to the QBO, but by faster (longer-vertical wavelength)

[56]Because the sea-land circulation as the most dominant mode over the maritime continent is a horizontal convection, that is a superimposition of upward and downward propagating internal gravity waves, they may be modified if the background wind is changed. The diurnal cycle migration of convergence-cloud zone implies also generation of gravity waves of both landward and seaward propagations. See Yamanaka (2016) and Yamanaka et al. (2017).

eastward Kelvin waves (Hirota, 1979) and winter mid-latitude westward Rossby waves (Dunkerton, 1979, 1982), as well as inertio-gravity waves. Probably because these waves are originally from the lower atmosphere, the SAOs are modulated by the QBO and meridional circulations (e.g., Garcia and Sassi, 1999). In the much higher region (90−110 km altitudes) easterlies are dominant throughout a year, which are considered due to effects by diurnal thermal tides generated in the stratospheric ozone layer (Miyahara, 1981). Tides are dominant and important phenomena in the thermosphere including (Kato, 1980). Tides are also generated by water vapor absorption of infrared radiation in the troposphere, and appear as semidiurnal variability of surface atmospheric pressure. The global-vertical structures of diurnal tides are also studied, in particular on their excitation/amplification in the tropics (e.g., Sakazaki et al., 2012).

Exercise 5

Knowing the Matsuno's theoretical solution for equatorial waves:

$$\phi_n = e^{-\frac{1}{2}y^2} H_n(y)$$

$$\begin{pmatrix} v \\ u \\ \phi \end{pmatrix}_{-1} = \begin{pmatrix} 0 \\ \phi_0 \\ \phi_0 \end{pmatrix} \qquad \begin{pmatrix} v \\ u \\ \phi \end{pmatrix}_{ol} = \begin{pmatrix} 2i(\omega_{ol}+k)\phi_0 \\ \phi_1 \\ \phi_1 \end{pmatrix}$$

$$\begin{pmatrix} v \\ u \\ \phi \end{pmatrix}_{nl} = \begin{pmatrix} i(\omega_{nl}{}^2 - k^2)\phi_n \\ \frac{1}{2}(\omega_{nl}-k)\phi_{n+1} + n(\omega_{nl}+k)\phi_{n-1} \\ \frac{1}{2}(\omega_{nl}-k)\phi_{n+1} - n(\omega_{nl}+k)\phi_{n-1} \end{pmatrix}$$

and the Hermit polynomials:

$$H_0(\eta) = 1, \quad H_1(\eta) = 2\eta, \quad H_2(\eta) = 4\eta^2 - 2, \quad H_3(\eta) = 8\eta^3 - 12\eta, \quad H_4(\eta) = 16\eta^4 - 48\eta^2 + 12,$$
$$H_5(\eta) = 32\eta^5 - 160\eta^3 + 120\eta, \quad H_6(\eta) = 64\eta^6 - 480\eta^4 + 720\eta^2 - 120, \quad H_7(\eta) = 128\eta^7 - 1344\eta^5 + 3360\eta^3 - 1680\eta, \quad \cdots.$$

Please try to plot a pressure distribution ϕ for various wave modes.

Answers:
For example you can use "EXCEL".

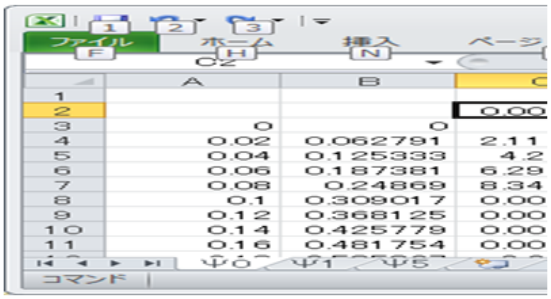

	A	B	C
1			
2			0.00
3	0	0	
4	0.02	0.062791	2.11
5	0.04	0.125333	4.2
6	0.06	0.187381	6.29
7	0.08	0.24869	8.34
8	0.1	0.309017	0.00
9	0.12	0.368125	0.00
10	0.14	0.425779	0.00
11	0.16	0.481754	0.00

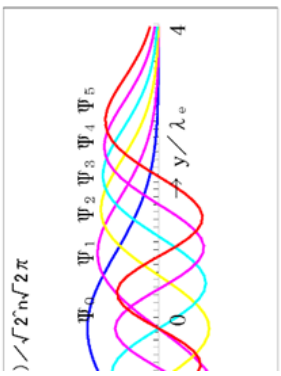

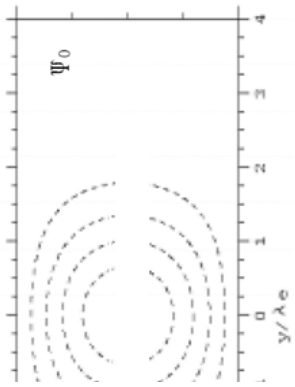

6. Convection: Why can't we predict rainfall?

The tropical atmosphere is heated strongly at the bottom (more exactly speaking during daytime; although the daytime insolation is larger than day and night infrared cooling, the net overheating is much weaker than daytime heating and is almost zero as shown later in Fig. 6.3(a)). In such a fluid heated at the bottom in the presence of gravity may have so-called convective instability, and the result is in general relatively small-scale convection of which the horizontal scale is similar to the vertical scale, that is the order of 10 km (Section 6.2). In addition even the tropical atmosphere is rather stable without latent heating by the moist process. This involves a paradox that convection is generated by cloud, whereas cloud is generated by convection. Therefore, we shall consider at first a stable (horizontally forced) convection between sea and land (Section 6.1) (see Fig. 1(a)), and then cumulus convection (Section 6.2) (Fig. 1(b)) and its self-organized structures (due to the second-kind instability) as tropical cyclones (Section 6.3) and intraseasonal variations (ISVs) (Section 6.4).

The governing equations in this chapter are almost common to those for the equatorial waves. (5.1)−(5.5), but now they are not always restricted by the hydrostatic, linear and dry approximations:

$$\frac{\overline{D}u'}{Dt} + u'\frac{\partial u'}{\partial x} + v'\left(\frac{\partial \overline{u}}{\partial y} + \frac{\partial u'}{\partial y} - f\right) + w'\left(\frac{\partial \overline{u}}{\partial z} + \frac{\partial u'}{\partial z}\right) + \frac{\partial \phi'}{\partial x} = K'\boldsymbol{\nabla}^2 u', \tag{6.1}$$

$$\frac{\overline{D}v'}{Dt} + u'\left(\frac{\partial v'}{\partial x} + f\right) + v'\frac{\partial v'}{\partial y} + w'\frac{\partial v'}{\partial z} + \frac{\partial \phi'}{\partial y} = K'\boldsymbol{\nabla}^2 v', \tag{6.2}$$

$$\frac{\overline{D}w'}{Dt} + u'\frac{\partial w'}{\partial x} + v'\frac{\partial w'}{\partial y} + w'\frac{\partial w'}{\partial z} + \frac{\partial \phi'}{\partial z} = \frac{R}{H}T' + K'\boldsymbol{\nabla}^2 w', \tag{6.3}$$

$$\frac{\overline{D}T'}{Dt} + u'\frac{\partial T'}{\partial x} + v'\frac{\partial T'}{\partial y} + w'\left(\Gamma + \frac{d\overline{T}}{dz} + \frac{\partial T'}{\partial z}\right) = K\boldsymbol{\nabla}^2 T' + \frac{L}{C_p}s, \tag{6.4}$$

$$\frac{\partial u'}{\partial x} + \frac{\partial v'}{\partial y} + \frac{1}{\rho_0}\frac{\partial \rho_0 w'}{\partial z} = 0, \tag{6.5}$$

$$\frac{\overline{D}r}{Dt} + u'\frac{\partial r}{\partial x} + v'\frac{\partial r}{\partial y} + w'\frac{\partial r}{\partial z} = K''\boldsymbol{\nabla}^2 r - s. \tag{6.6}$$

In this chapter we often neglect the variation of ρ_0 in the continuity equation (6.5) such as

$$\frac{\partial u'}{\partial x} + \frac{\partial v'}{\partial y} + \frac{\partial w'}{\partial z} = 0, \tag{6.7}$$

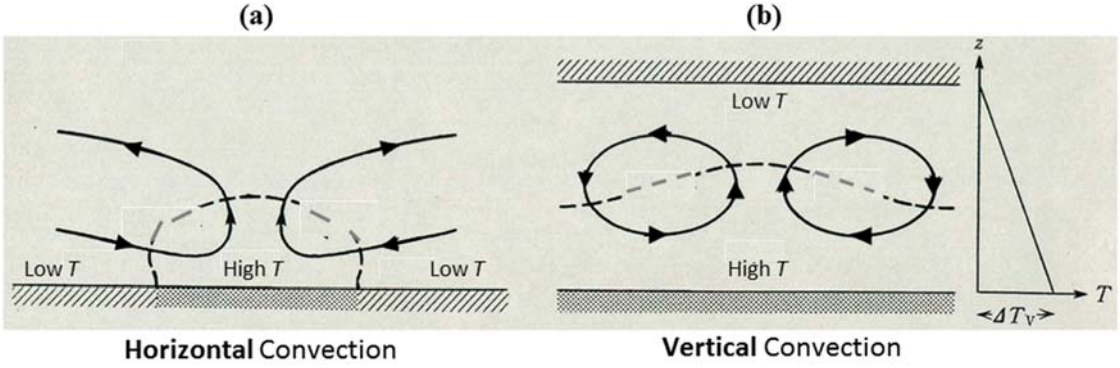

Fig. 6.1 Schematic comparison between (a) forced horizontal and (b) unstable vertical convections (modified from Ogura, 1997).

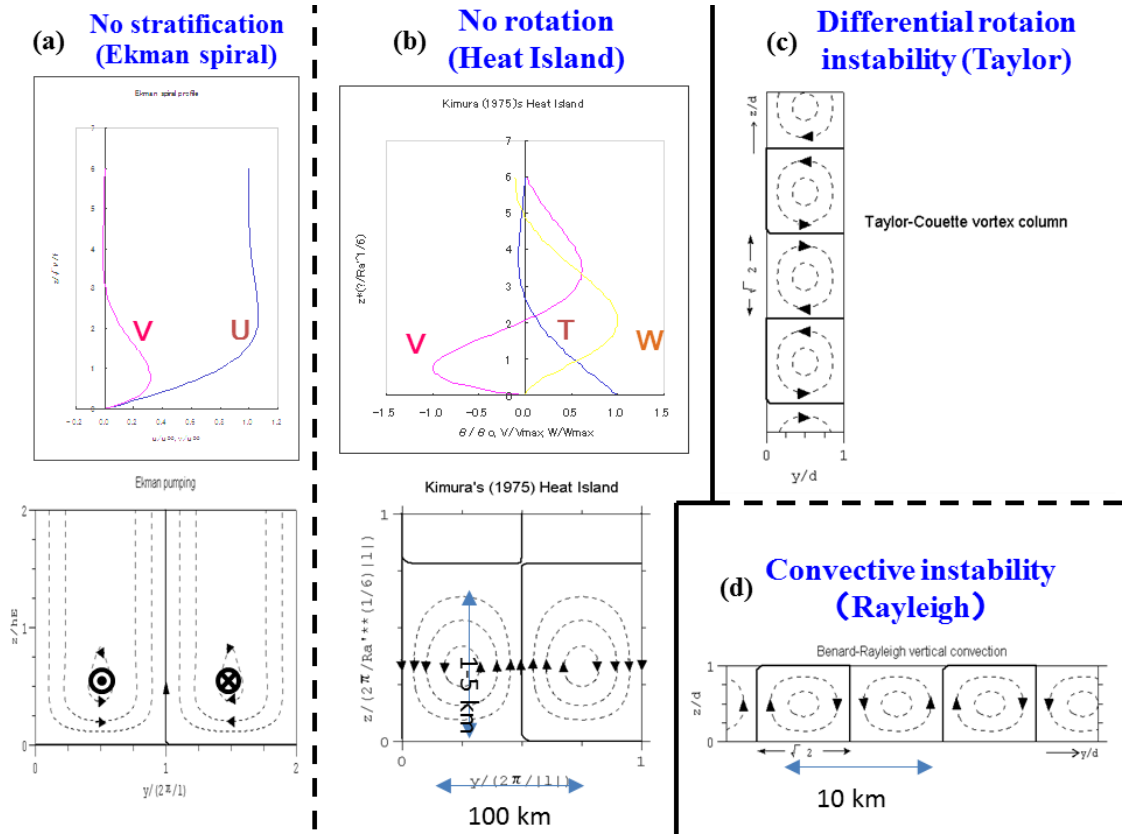

Fig. 6.2 Major solutions of the governing equation (6.9) for convection: (a) the Ekman spiral for no stratification; (b) heat-island (perpetual sea or land breeze) for no rotation; (c) Taylor's differential rotation instability; and (d) Rayleigh's convective instability.

in spite of keeping the buoyancy term in the vertical momentum equation (6.3), which is called the *Boussinesq approximation*. Under this approximation and the mean field varying only vertically, $\partial(6.1)/\partial z - \partial(6.3)/\partial x$ gives an equation for the meridional vorticity:

$$\eta' \equiv \frac{\partial u'}{\partial z} - \frac{\partial w'}{\partial x}, \tag{6.8}$$

as

$$\frac{\overline{D}\eta'}{Dt} + u'\frac{\partial \eta'}{\partial x} + v'\frac{\partial \eta'}{\partial y} + w'\left(\frac{d^2\overline{u}}{dz^2} + \frac{\partial \eta'}{\partial z}\right) = -\frac{R}{H}\frac{\partial T'}{\partial x} + \frac{\partial v'}{\partial y}\left(\frac{d\overline{u}}{dz} + \eta'\right) - \left[\frac{\partial v'}{\partial z}\left(\frac{\partial u'}{\partial y} - f\right) - \frac{\partial v'}{\partial x}\frac{\partial w'}{\partial y}\right] + K'\nabla^2\eta', \tag{6.9}$$

The left-hand side is the temporal variation of rotation (clockwise toward the rotation axis (y direction), as observed from the $-y$ direction) of air parcel in the xz-plane, and the right-hand side is its cause: the first term is the buoyancy torque due to a temperature gradient in the x direction (perpendicular to the rotation axis), the second term is the angular momentum conservation (rotation radius decrease) with convergence in the xz-plane (due to the velocity gradient along the rotation axis), the third term is 'tilting' (rotation axis direction change) of the rotations around the other (z and x) directions (these two terms do not appear if the rotation is two dimensional, that is homogeneous along the rotation axis), and the last term is the viscous dissipation. Major solutions of (6.9) are shown in Fig. 6.2.

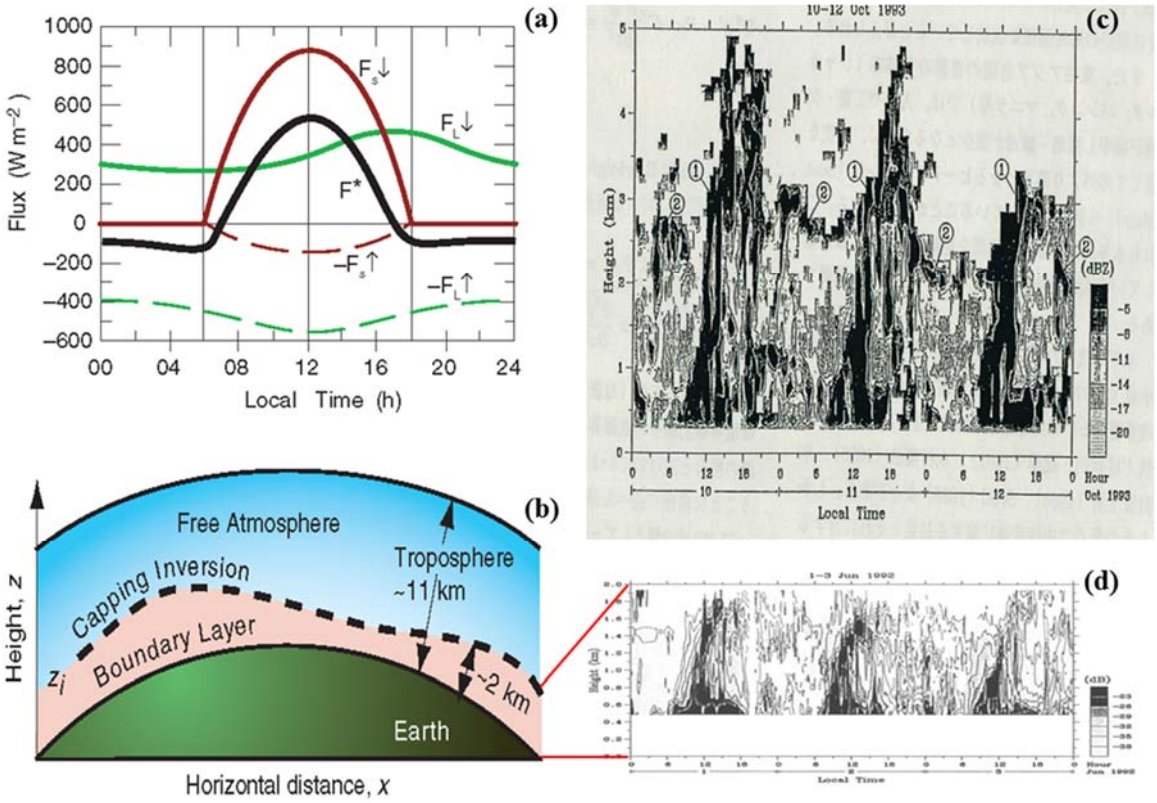

Fig. 6.3 Schematic view of (a) radiation budget (net flux (*) given by the sum of up- (↑) / down- (↓) ward fluxes of short- (S; from Sun) and long- (L; from ground) wavelengths) and (b) structure of the atmospheric boundary layer (Stull, 2006, not restricted for the tropics), and wind profiler echo (turbulence intensity and/or stratification stability) observation for three days in (c) the tropics (near Jakarta, Indonesia; Hashiguchi et al., 1995a) and (d) the extratropics (near Kyoto, Japan; Hashiguchi et al., 1995c).

Temporal variation of the integration of motion along a closed circuit in the plane of (in particular, as in Section 6.1, forced horizontal) convection becomes the integration of $\overline{D}\eta'/Dt$ over the area surrounded by the circuit (e.g., an example in Section 4.1 of Holton, 1992). This is called the *circulation theorem*, corresponding to the integration form of the vorticity equation (6.9).

6.1. Sea-land breeze circulation (Horizontal convection)

(i) Heat island (Steady local circulation):

At first let us consider a simple *horizontal convection* (Fig. 6.1(a)) forced by to a temperature gradient at the bottom under a stable stratification as parameterized by a real value of the Väisälä-Brunt frequency (4.19). For simplicity we assume two-dimensional ($v' \equiv 0,\ \partial/\partial y = 0$), no mean wind ($\overline{u}$=0), no moisture ($r \equiv 0$) and the Boussinesq approximation (6.7), we define a streamfunction ψ' such that

$$u' \equiv \frac{\partial \psi'}{\partial z},\quad w' \equiv -\frac{\partial \psi'}{\partial x};\quad \eta' = \frac{\partial^2 \psi'}{\partial x^2} + \frac{\partial^2 \psi'}{\partial z^2} = \boldsymbol{\nabla}^2 \psi', \tag{6.10}$$

then the vorticity and thermodynamic equations (6.9) and (6.4) become

$$\left(\frac{\partial}{\partial t} - K'\boldsymbol{\nabla}^2\right)\boldsymbol{\nabla}^2\psi' = \frac{\partial(\psi', \boldsymbol{\nabla}^2\psi')}{\partial(x,z)} - \frac{R}{H}\frac{\partial T'}{\partial x}, \tag{6.11}$$

$$\left(\frac{\partial}{\partial t} - K\boldsymbol{\nabla}^2\right)T' = \frac{\partial(\psi', T')}{\partial(x,z)} + \frac{H}{R}N^2\frac{\partial \psi'}{\partial x}. \tag{6.12}$$

These two equations are mathematically closed for two dependent variables ψ' and T'. For a horizontal convection considered here, on one hand, the horizontal temperature gradient of the second term in the right-hand side of (6.11) is always given by a bottom boundary condition (shown later in (6.14)). Thus, even if the temperature gradient is very weak, a very weak convection is generated, and if no gradient given, no convection generated. On the other hand, for a vertical (unstable or Bénard-Rayleigh) convection mentioned in the next subsection, the horizontal temperature gradient is generated automatically as a result of occurrence of convection, but the given (unstable) vertical temperature gradient HN^2/R (< 0, N: imaginary) should be large enough to exceed the viscosity (and heat conduction).

Some of the horizontal convection follow almost completely the temporal and spatial scales of forcing, and the others are spatially restricted within a boundary layer/region (narrower than the whole scales of forcing), temporally delayed and filtered in wavenumbers and frequencies. The former examples are found around a 'megacity' such as Jakarta, Bangkok and Manila (called '*heat island*') due to paved ground, many tall concrete buildings, car exhaust, air conditioners, industries, etc. making there warmer than its surrounding suburb-country area, which is considered mainly in this subsection. For the latter category is found along a coastline between broad sea and land surfaces (as considered in the next subsection). The meridional circulations and monsoons (Sections 4.3−5) with the forcing-circulation balance (4.20) are similar to the first category rather than the second category.

For a steady ($\partial/\partial t = 0$) and sufficiently weak (negligible nonlinear terms) situation of the heat island, (6.11) and (6.12) may be immediately reduced to an equation only for one variable. Assuming furthermore that the viscosity and diffusion are dominant in the vertical direction ($\boldsymbol{\nabla}^2 \approx \partial^2/\partial z^2$), the equation for T' becomes

$$\frac{\partial^6 T'}{\partial z^6} + Ra' \cdot k^4 \frac{\partial^2 T'}{\partial x^2} = 0, \quad Ra' \equiv \frac{N^2/k^4}{K'K}, \tag{6.13}$$

where k is taken from (the wavenumber of spatially cyclic heating in) an appropriate boundary condition:

$$T' = \Delta T \cos kx, \qquad u' = w' = 0 \ \left(\frac{\partial^2 T'}{\partial z^2} = \frac{\partial^3 T'}{\partial z^3} = 0\right) \qquad \text{at} \quad z = 0; \tag{6.14}$$

$$T',\ u',\ v' \to 0 \ \left(\frac{\partial^2 T'}{\partial z^2}, \frac{\partial^3 T'}{\partial z^3} \to 0\right) \qquad \text{at} \quad z \to \infty. \tag{6.15}$$

Substituting

$$T'(x, z) = \tilde{T}(z) \cdot \cos kx, \tag{6.16}$$

(6.13) is reduced to an ordinary differential equations only for z, and its solution may be obtained as

$$\tilde{T}(z) = \frac{1}{2} e^{-Ra'^{1/6} kz} + \frac{1}{\sqrt{3}} e^{-\frac{1}{2} Ra'^{1/6} kz} \cdot \cos\left(\frac{\sqrt{3}}{2} Ra'^{1/6} kz - \frac{\pi}{6}\right) \tag{6.17}$$

(Kimura, 1975). The solutions for T', u' and v' obtained by (6.17) , (6.16) and (6.10) are plotted in Fig. 6.2(b). The vertical scale of the local circulation becomes $Ra'^{-1/6}$ times of the horizontal scale. For a typical value $k \sim 2\pi/60$ km $\sim 10^{-4}$ m^{-1}, $N \sim 2\pi/10$ min $\sim 10^{-2}$ s^{-1} (corresponding to $d\overline{\theta}/dz \sim$ 3 K/km) and $K \sim K' \sim$ 10 m^2/s, we obtain $Ra' \sim 10^{10}$, which implies that the ratio of horizontal/vertical scales $\sim$ 50 times. Because the height of boundary layer on land in the tropics seems to be higher than the extratropics (2−5 km) (Hashiguchi et al., 1995a,b,c), the horizontal scale of the local circulation is expected to be 100−300 km.

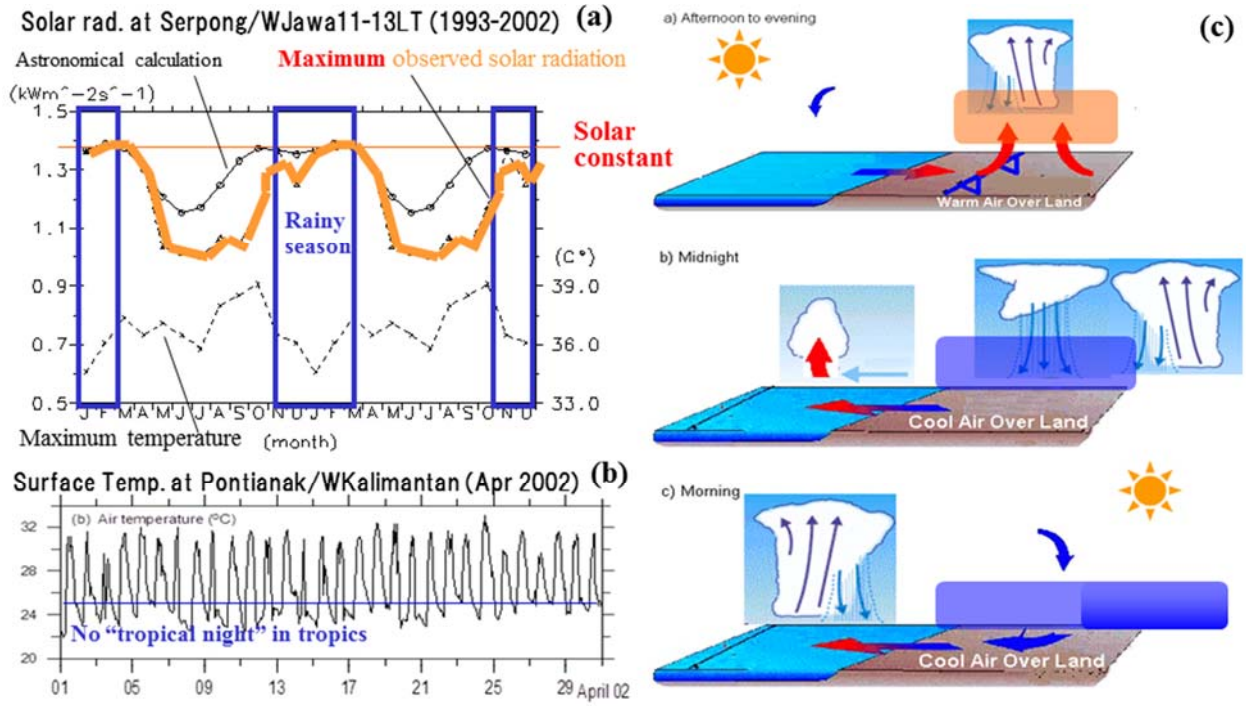

Fig. 6.4 Diurnal cycle mechanism. (a) Repeated two cycles of monthly maximum insolation (in a clear condition just before noon) at Serpong, West Jawa in 1993−2002, showing the annual maximum identified with the rainy season (Araki et al., 2007). (b) Hourly temperature at Pontianak, West Kalimantan in April 2002, showing every daily minimum lower than 25ºC (Wu et al., 2008a). (c) Schematic model for the 'sprinkler-like' cooling the ground and surface atmosphere during midnight and morning (Wu et al., 2009b).

(ii) Sea-land (and Mountain-valley) breeze circulation:

As have been mentioned on the annual-cycle monsoons (Section 4.4), there are sea-land differences across the coastlines of oceans (and large lakes like Victoria in central Africa) on the surface insolation heating and infrared cooling, of which the (tropically much stronger) diurnal-cycle atmospheric response is the *sea-land breeze circulation*. Probably the first detailed study on this circulation in the tropics was done at Batavia (Jakarta) by van Bemmelen (1922). The solar heating in J or $\overline{Q}$ is through complex processes of the parasol effect, land/ocean surface and atmospheric boundary-layers (e.g., Hartmann, 1994; Stull, 1988), but its variability is mainly dependent on its value calculated by the astronomical formula (cf. Fig. 6.4(a)−(b)):

$$I_s = \begin{cases} I_{s0}\left(\dfrac{\overline{d}}{d}\right)^2 (\sin\varphi\sin\delta + \cos\varphi\cos\delta\cos h) & \text{for daytime } (-h_0 \le h \le h_0) \\ 0 & \text{for nighttime} \end{cases} \tag{6.18}$$

where the solar declination angle δ and the Sun-Earth distance squared $\left(\overline{d}/d\right)^2$ concern the seasonal cycle through a diurnal integration of (6.18), as have been shown in Section 4.1.[57] In the daytime the cross-coastal temperature and pressure gradients (hotter and lower on land) induce a *sea breeze*, and its convergence with moisture transport generate strong convective clouds at a distance of the order of 100 km inland in the tropics[58]. The sea breeze lower than 2−5 km on land in the tropics (Hashiguchi et al., 1995a, b, c; thicker than the extratropics and the marine

[57]By this forcing the tides with global phase structures are also generated, just similar to the 'astronomical monsoon' in case of annual-cycle forcing.
[58]Development of a distinct boundary (called the sea breeze front in the extratropics) between cooler maritime air and the continental warmer air and its movement from the cost to inland do not always appear in the tropics. *Gust front* by an individual convective cloud is much clearer (cf. Section 6.2).

atmosphere considered in Sections 5.2 and 5.3) and the upper "return" current construct a circulation, and a strong vertical shear between them may cause a Kelvin-Helmholtz instability (Hadi et al., 2000).

At night, the land cools more rapidly than the sea and a *land breeze* develops. The nighttime cooling is mainly due to the emission of infrared radiation and thus clear sky condition is preferred in the extratropics, but is due to 'sprinkler effect' associated with strong rainfall from the convective cloud developed in the afternoon and thus dominant in the rainy season in the tropics (Wu et al, 2008a; Yamanaka, 2016) (Fig. 6.4(c)). In the morning and evening the surface wind direction is reversed between onshore and offshore, but the reversal time and feature vary depending on the mean wind (averaged for 24 hours), latitude and coastal geography. In the extratropics, as inertio-gravity wavelike characteristics (to be mentioned later), the Coriolis force induces an along-shore wind component, and rotates the wind direction clockwise/anticlockwise in the northern/southern hemisphere. Furthermore, another differential daytime insolation and nighttime cooling appear on the sloping terrain between mountain and valley (relatively strong and weak, respectively), inducing a *valley and mountain breeze circulation*. In the tropics, as will be mentioned later in the next subsection (iii), many areas have coastlines near mountains, and both sea-land and mountain-valley breezes are additive, which is a reason why the diurnal cycle is dominant there.

Theoretically we consider a local circulation forced by a periodical heating on the land ($x > 0$), and add a heating term $(R/H)\dot{Q}$ in the right-hand side of the thermodynamic equation (6.4). For simplicity we assume quasi-two-dimensional ($\partial/\partial y = 0$, but $v' \neq 0$), constant mean wind ($\partial\overline{u}/\partial z$=0), no moisture ($r \equiv 0$), $K' = K$ and the Boussinesq approximation (6.7), we define a streamfunction ψ' as (6.10). Then (6.11) and (6.12) for the previous problem are replaced by

$$\left(\frac{\partial}{\partial t} + \overline{u}\frac{\partial}{\partial x} - K\boldsymbol{\nabla}^2\right)\boldsymbol{\nabla}^2\psi' = f\frac{\partial v'}{\partial z} - \frac{R}{H}\frac{\partial T'}{\partial x}, \tag{6.19}$$

$$\left(\frac{\partial}{\partial t} + \overline{u}\frac{\partial}{\partial x} - K\boldsymbol{\nabla}^2\right)v' = -f\frac{\partial \psi'}{\partial z}, \tag{6.20}$$

$$\left(\frac{\partial}{\partial t} + \overline{u}\frac{\partial}{\partial x} - K\boldsymbol{\nabla}^2\right)T' = \frac{H}{R}N^2\frac{\partial \psi'}{\partial x} + \frac{H}{R}\dot{Q}. \tag{6.21}$$

Note that, if the flow v' along the coastline satisfies a thermal wind balance (4.11) with the temperature gradient $\partial T'/\partial x$ across the coastline, (6.19) may give a trivial solution $\psi' \equiv 0$ with no circulation.

Substituting $\frac{\partial}{\partial z}$(6.20) and $\frac{\partial}{\partial x}$(6.21) into $\left(\frac{\partial}{\partial t} + \overline{u}\frac{\partial}{\partial x} - K\boldsymbol{\nabla}^2\right)$(6.19), we have a single equation for ψ':

$$\left[\left(\frac{\partial}{\partial t} + \overline{u}\frac{\partial}{\partial x} - K\boldsymbol{\nabla}^2\right)^2\boldsymbol{\nabla}^2 + N^2\frac{\partial^2}{\partial x^2} + f^2\frac{\partial^2}{\partial z^2}\right]\psi' = -\frac{\partial \dot{Q}}{\partial x}. \tag{6.22}$$

Here the spatial scale is smaller than the case considered in (5.8), and all the factors may be regarded as constants. Thus we substitute

$$(\psi', \dot{Q}) = (\tilde{\psi}, \tilde{Q})e^{i(kx+mz-\omega t)}, \tag{6.23}$$

into (6.22), and obtain, using (5.9),

$$[\{(\hat{\omega} + iK(k^2+m^2))^2 - N^2\}k^2 + \{(\hat{\omega} + iK(k^2+m^2))^2 - f^2\}m^2]\tilde{\psi} = -ik\tilde{Q}. \tag{6.24}$$

If K is sufficiently large and N, $|f|$ and $|\tilde{Q}|$ are all not so large, then we may assume an imaginary part ω_i of ω, and (6.24) gives

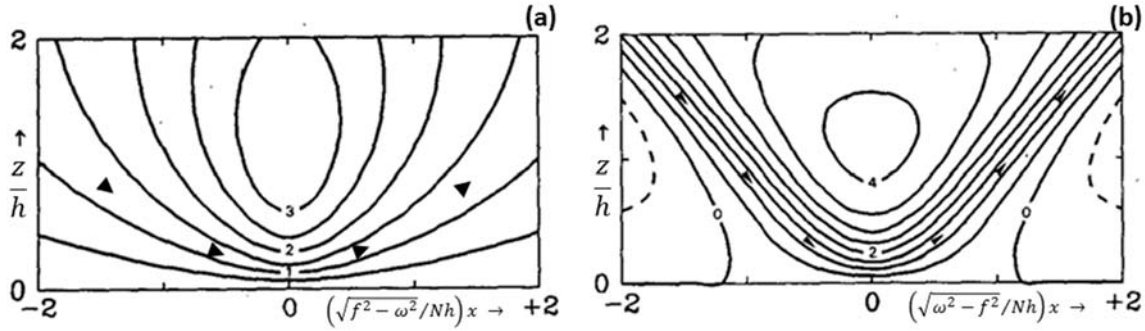

Fig. 6.5 Streamlines $\psi'/(h^2\omega)$ (h: a vertical scale; $\omega \equiv 2\pi/1\text{day}$) as solutions of (6.22) in the vertical plane perpendicular to the coastline ($x > 0, z = 0$: land surface; $x < 0, z = 0$: sea surface) under no mean flow ($\overline{u} = 0,\ \widehat{\omega} = \omega$) for (a) the extratropics ($|\varphi| > 30^\circ,\ |f| > |\widehat{\omega}|$) at 'noon' ($\omega t = \pi/2$) and (b) the tropics ($|\varphi| < 30^\circ,\ |f| < |\widehat{\omega}|$) at 'sunset' ($\omega t = \pi$) (Rotunno, 1983).

$$\omega_i = -K(k^2 + m^2), \quad \text{i.e.,}\ \ \psi' \propto e^{-i\omega t} \propto e^{\omega_i t} = e^{-K(k^2+m^2)t},$$

which corresponds to a damping motion due to viscosity/diffusion. If K and $|f|$ are both large, and the situation is steady and horizontally uniform ($\omega = 0,\ k = 0$), then we assume a complex vertical wavenumber $m \equiv m_r + im_i$, and (6.24) becomes

$$K^2m^4 + f^2 \approx 0, \quad \text{i.e.,}\ \ {m_r}^2 \approx {m_i}^2 \ \text{ and } \ 2m_rm_i \approx \frac{f}{K}, \quad \text{i.e.,}\ \ m \approx (-1+i)\sqrt{\frac{|f|}{2K}}$$

(other roots are inappropriate), which gives (under boundary conditions: $(u', v') = 0$ at $z = 0$ and $(u', v') \to (u_\infty, 0)$ fat $z \to \infty$) so-called *Ekman's spiral hodograph*:

$$(u' - u_\infty,\ v') \approx u_\infty e^{-\frac{z}{\delta_E}}\left(-\cos\frac{z}{\delta_E}, \sin\frac{z}{\delta_E}\right), \quad \delta_E \equiv -\frac{1}{m_r} = \frac{1}{m_i} = \sqrt{\frac{2K}{|f|}}. \tag{6.25}$$

This result does not include any thermal conditions such as the heating $\dot{Q}$ (although N-dependency might be included in K), but δ_E is a good approximation for the boundary layer top in the extratropics (δ_E~1.4 km for K~10^2 m^2/s and $|f|$~10^{-4} s^{-1}). However, it can hardly be applied in the tropics, where $|f|$ is small and $\dot{Q}$ is essentially important due to large moisture and strong heating.

When K is small, (6.24) becomes

$$[(\widehat{\omega}^2 - N^2)k^2 + (\widehat{\omega}^2 - f^2)m^2]\tilde{\psi} = -ik\tilde{Q}. \tag{6.26}$$

If the heating $\tilde{Q}$ is omitted, the (free) solution must satisfy the inside of the left-hand side bracket being zero, which is just the dispersion relation for the inertio-gravity waves (5.16) (for $l = 0$ and $|\widehat{\omega}|$ not neglected for N). This is why the wind direction rotates clockwise/anticlockwise in the northern/southern hemisphere. As mentioned for the Hadley circulation (Section 4.3), the horizontal convection may be given by a superimposition of upward and downward propagating internal waves, which in total satisfy the bottom boundary condition of zero vertical velocity (Fig. 2.7). Thus, as mentioned in Section 5.1, any disturbances (including those forced by $\tilde{Q}$) satisfying $|f| < |\widehat{\omega}| < N$, may be propagating vertically, and the other modes must be decaying vertically (upward, if the heating sources are at the bottom) (Rotunno, 1983) (Fig. 6.5). For the sea-land breeze circulation the heating $\tilde{Q}$ is originated from the insolation (6.18) with the diurnal cycle, of which the frequency $\omega = 2\pi/1$ solar day $= 2\pi/24$ h $= 7.272\times10^{-5}$ s^{-1}. Because the Coriolis parameter (without using the β-plane approximation (4.7)) is given by $f = 2\Omega \sin\varphi$, where

$\Omega = 2\pi/1$ sidereal day = $2\pi/(24\ \text{h}\times 365/366) = 7.292\times 10^{-5}\ \text{s}^{-1}$, the diurnal cycle frequency should satisfy $|\hat{\omega}| > |f|$ approximately for $|\varphi| < 30^{\circ}$, if $\overline{u}$ is sufficiently weak. Therefore, it is expected that the sea-land breeze circulation must be dominant in the tropics.

It is known, in addition to the shear layer between the surface sea wind and the return flow mentioned before, that a *sea-breeze front* exists as the rather clear-cut leading edge of the sea-wind region, at which convective clouds associated with showers, thunders and gusts are often organized (although a smaller-scale gust front with individual cloud is also remarkable). In the coasts near steep mountains a land- (or mountain-) breeze front with similar features is also observed, which appears typically during torrential rainfalls in the IMC (e.g., Wu et al., 2007). The horizontal scale λ_d of the sea-land breeze circulation cells and the migrations of such frontal structures may be given essentially by the dispersion relation of internal gravity waves (e.g., Rotunno, 1983; Niino, 1987): from (6.26) or (5.16)

$$\lambda_d \approx \frac{2\pi}{|k|}. = \sqrt{\frac{N^2-\hat{\omega}^2}{\hat{\omega}^2 - f^2}}\frac{2\pi}{|m|} \approx \frac{N}{|\hat{\omega}|}h_d \approx \frac{\sqrt{gh}}{\tau}, \tag{6.27}$$

where h_d is the height of the sea-land breeze circulation cell and $\tau = 2\pi/1$ day. Observationally $\sqrt{gh} \sim$ 5−10 km/h ≈1−3 m/s (one order slower than that for the large-scale equatorial waves), $h_d \sim$ 2−5 km, and λ_d ~100−300 km (see the next subsection (iii)).

More realistic intermediate cases include the both aspects mentioned above (e.g., Niino, 1987). If the forcing is not vertically wavy like (6.23) but limited at the bottom like the steady heat island case mentioned in the previous subsection (i), the vertical extension is controlled also with viscosity/diffusivity as $\propto Ra'^{-1/6} \propto K^{1/3}$ in (6.13) or as $\delta_{\mathrm{E}} \propto K^{1/2}$ in (6.25). 'Roll' structures (associated with banded clouds actually) due to convective and shear instabilities generated locally at around the sea-breeze front are also studied theoretically (Asai, 1970, 1972; partly mentioned in the end of Section 6.2(i)). Realistic nonlinear numerical studies on the sea-land breeze circulations were pioneered by Filipino meteorologist Estoque (1962), who considered Manila Bay at about 15ºN with Coriolis force and background wind. Sun and Orlanski (1981a, b) showed both linear analytical and nonlinear numerical solutions for the sea-land breeze circulations which are gravity-wavelike and dependent on the Coriolis force. Some studies without the Coriolis force (e.g., Fovell, 2005) may be applicable also for the equatorial tropics, which will be mentioned briefly again the next section. Recent high-resolution models simulating the equatorial sea-land breeze circulations show various differences from the extratropics (Saito et al., 2001; Wu et al., 2003; Sasaki et al., 2004; Arakawa and Kitoh, 2005; Hara et al., 2009; Sato et al, 2009) (see Figs 6.4(c), 6.6−6.9), More details and other aspects of the diurnal-cycle sea-land (and mountain-valley) breeze circulations are mentioned in several mesoscale and boundary-layer meteorology textbooks (e.g., Stull, 1988; Lin, 2007), although most descriptions are on the extra- or sub-tropics.

Because the sea-land circulation is a superimposition of upward and downward propagating internal gravity waves, the former may be regarded as a source of the latter, in particular those propagating until the middle and upper atmospheres (cf. Section 5.4). Their propagations are modified if the background wind is changed. Actually the amplitude distributions of gravity waves in the lower stratosphere (Fig. 5.4(h)−(i)) resemble those of convective activity and their cause (solar radiation) (Fig. 4.6(a)). Local instability and turbulence generation has been also observed at the cloud top (e.g., Mega et al., 2010, 2012). The spectral features of cloud top temperature

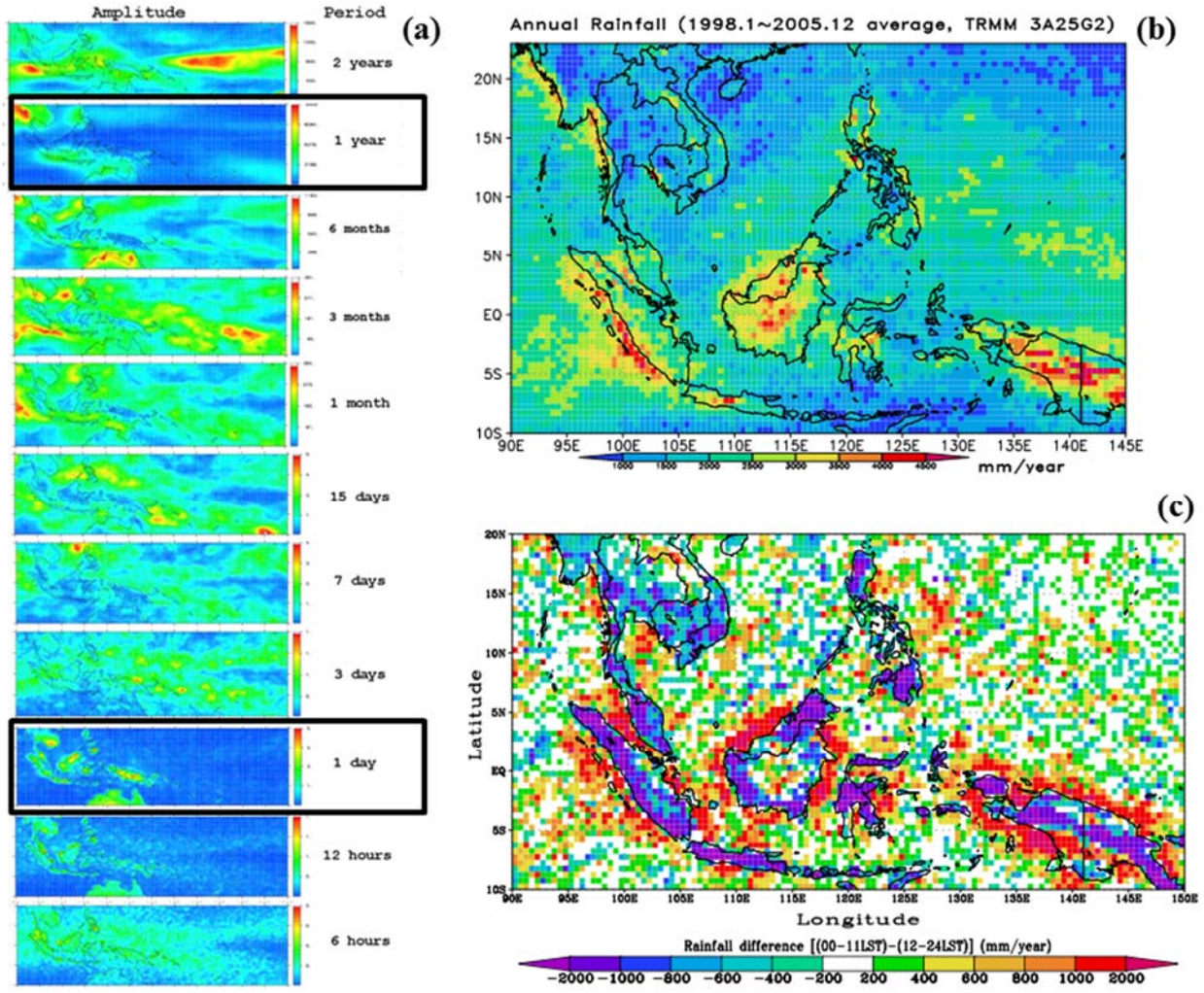

Fig. 6.6 Geographical distributions of (a) power spectral densities of 6 h–2 year components of cloud top temperature variations analyzed from 14-year hourly Geostationary Meteorological Satellites (GMS) – infrared (IR) data (Yamanaka, 2016), and (b) annual amount and (c) AM-PM difference of 3-year TRMM-PR rainfall data over the Indonesian maritime continent (Mori et al., 2004)

(corresponding to height of cloud convection) are also similar to so-called universal shapes of gravity waves (e.g., Gage and Nastrom, 1985; Nastrom and Gage, 1985; Hashiguchi et al., 1997). Generations of gravity waves from cloud systems actually observed over the IMC and their emissions to the whole middle atmosphere have been simulated by numerical models (e.g., Horinouchi and Yoden, 1996; Horinouchi et al., 2002, 2003). Momentum flux of such gravity waves have been requested to simulate the stratospheric dynamics such as equatorial quasi-biennial oscillations (Sato et al., 1999; Kawatani et al., 2010a, b), which implies also a link between climates in the troposphere and stratosphere (e.g., Kawatani and Hamilton, 2013). Furthermore the global-vertical structures of diurnal tides are also studied, in particular on their excitation/amplification in the tropics (e.g., Sakazaki et al., 2012, 2015).

(iii) Diurnal cycle dominancy in the IMC and other regions

Because the IMC is not a continent but an archipelago, it has very long coastlines surrounding large/small islands, where the diurnal-cycle sea-land breeze circulations with convective activity are generated (see, e.g., Johnson, 2011; Yamanaka, 2016). The atmosphere has high humidity (which is conditionally unstable as mentioned in the next subsection), and convective clouds are generated on land in the afternoon until evening, as shown in Fig. 6.6 (Houze

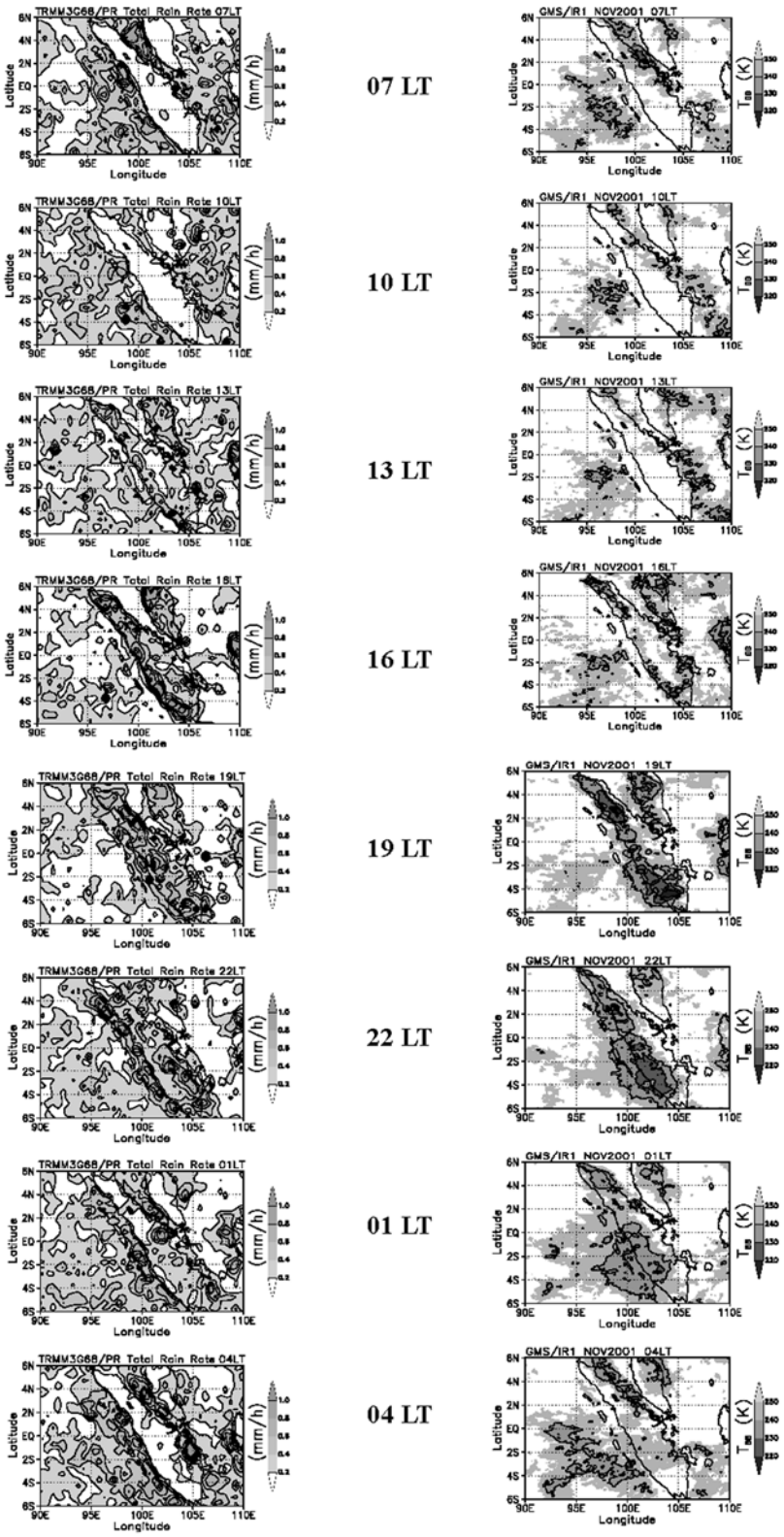

Fig. 6.7 Diurnal cycles of TRMM (on a Sun-nonsynchronous low-Earth orbit) rainfall averaged for 1998-2000 and GMS cloud top temperature averaged for November 2001. Modified from Mori et al. (2004). For GMS data also see Sakurai et al. (2005).

et al., 1981; Hendon and Woodberry, 1993; Nitta and Sekine, 1994; Hashiguchi et al., 1995; Sugimoto et al., 2000; Yang and Slingo, 2001; Ohsawa et al., 2001; Kubota and Nitta, 2001; Renggono et al., 2001; Hadi et al., 2002; Murata

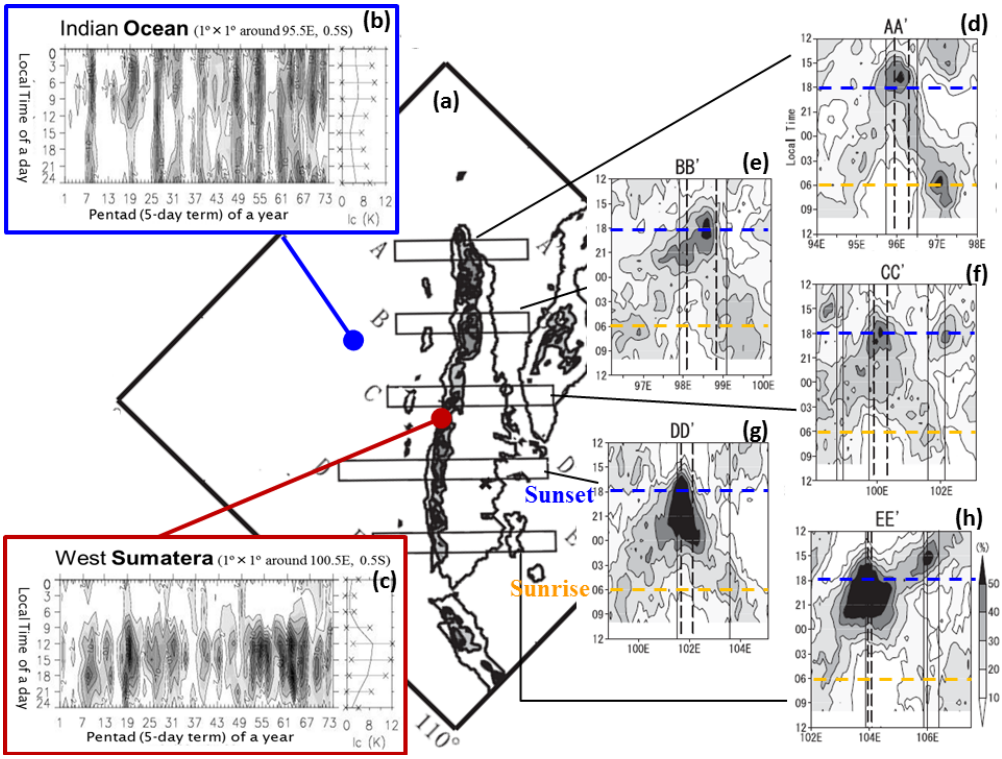

Fig. 6.8 Diurnal cycles of cloud top temperature (a) around Sumatera, shown by seasonal-local time variations on (b) the Indian-Ocean and (c) and western coast inland (Sakurai et al., 2005) and (d)-(h) five zonal-local time variations (Hamada et al., 2008).

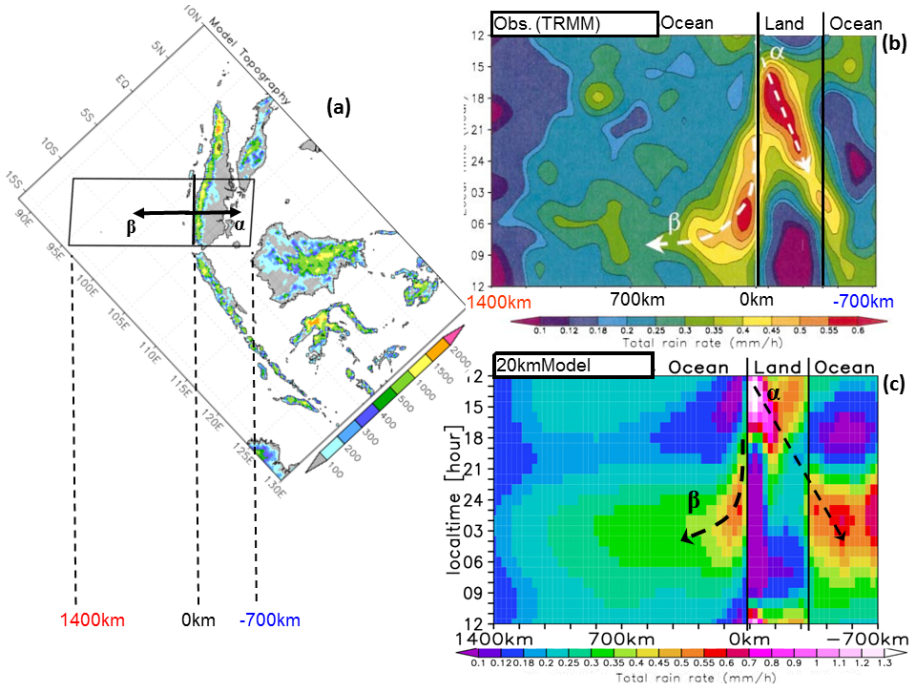

Fig. 6.9 Zonal-local time variations of diurnal-cycle rainfall migrations (a) along a section of Sumatera (b) observed by TRMM (Mori et al., 2004) and (c) analyzed from a global high-resolution numerical model (Arakawa and Kitoh, 2005).

et al., 2002; Sorooshian et al., 2002; Wu et al., 2003; Mori et al., 2004; Sakurai et al., 2005; Araki et al., 2006; Tabata et al., 2011b; and many othres). The diurnal cycles over the IMC are dominant even in the rainy season (austral summer in Jawa and Bali), because rainfall-induced sprinkler-like land cooling reverses the trans-coastal temperature

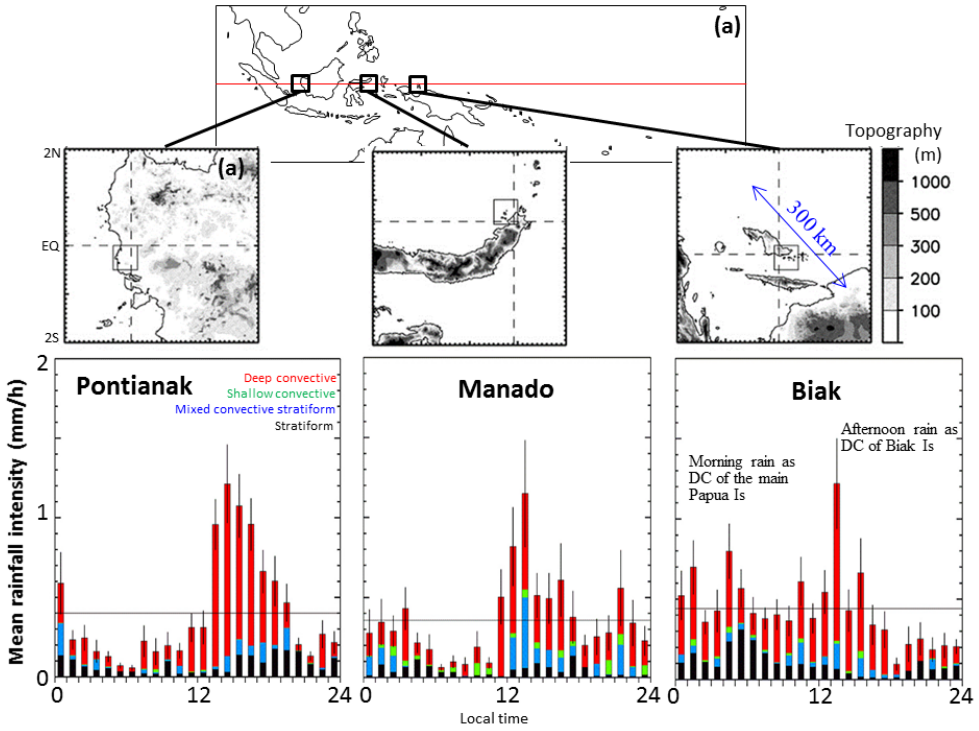

Fig. 6.10 Diurnal cycles of rainfall intensity observed by wind profilers at Pontianak (Kalimantan), Manado (Sulawesi) and Biak (near Papua) (Tabata et al., 2011b). Rainfall is classified as stratiform (black), mixed stratiform/convective (blue), shallow convective (green) and deep convective (red) types. A small island Biak has afternoon and dawn (main-island sea-side) peaks.

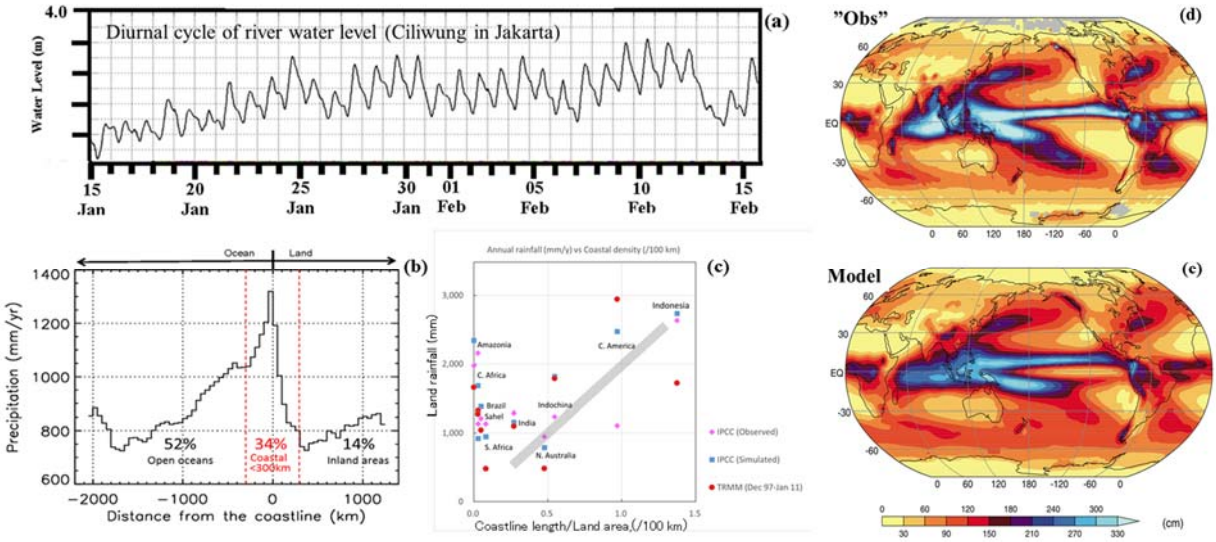

Fig. 6.11 (a) Diurnal cycle observed at a river in west Jawa (Sulistyowati et al., 2014), (b) rainfall as a function of the coastal distance over the tropics observed by TRMM (Ogino et al., 2016) and (c) regional rainfall as a function of the coastal 'density' (= length/area in 100 km resolution) over the tropics (modified from Yamanaka, 2016) calculated based on TRMM observations and calculated from (d) observation and (e) model of IPCC (2007).

gradient before sunrise (Fig. 6.4(c)), and subsequent clear sky on land until around noon provides solar heating dependent on season (Wu et al., 2008a).

In the western coast of Sumatera as one of the most recarkable places of the diurnal cycle (Mori et al., 2004), a convective rainfall peak appears near the coastline in the daytime and migrates toward inland until the evening (see Figs. 6.7−6.9). Another equally convective-stratiform rainfall peak starts from the coastline and migrates offshore

until the morning. Each rainfall peak migration has a distance up to 400 km and a speed around 10 m/s. The diurnal cycles are almost unique causes of surface winds stronger than 10 m/s (shown later in Figs. 6.15(a) and (d)) in the IMC almost free from cyclones (except for a rare case as shown later in Fig. 6.19). Although a local wind called "Sumatras" has been known (e.g., Scott, 1956; Nieuwolt, 1968; Chen et al., 2014), probably partially due to steep mountains (up to 3,800 m), strong winds appear near active convective clouds usually in local evening with diurnal cycle. Seasonal and meridional variations of the diurnal cycle in Sumatera associated with the ITCZ displacement have been analyzed (Sakurai et al., 2005).

As shown in Figs. 6.8(b) and (c) very clearly, the most dominant mode is changed to the diurnal cycle near the coastline, from ISVs on the open ocean (see Section 6.4, including interactions of the two categories). Theoretically the horizontal scale of the diurnal-cycle sea-land breeze circulation in the low latitudes may be estimated by (6.27) as λ_d ~100−300 km. Observed values of λ_d in the IMC are 100 km or more (Wu et al., 2003, 2008a, 2009b; Mori et al., 2004; see Figs. 6.7−6.9), and the rainfall is concentrated in a distance within about 300 km (both on the land and sea sides) from the coastline (Ogino et al., 2016; see Fig. 6.11(b) later). Thus the land with clear diurnal cycle must be larger than 100 km, which has been suggested by earlier studies (e.g., Kubota and Nitta, 2001). In case of adjacent small and large islands (the former located inside the coastal area of the latter), the smaller one (such as Siberut in the west of Sumatera, and Biak in the northwest of Papua as shown in the right of Fig. 6.10) a little complex feature appears due to the diurnal cycles of the both islands (Wu et al., 2008b; Tabata et al., 2011b; Kamimera et al., 2012). In narrow straits such as Melaka (Malacca; between Sumatera and Malay) and Makassar (between Kalimantan and Sulawesi) the diurnal cycles of the both islands are interfered and sometimes seem to propagate from one island to the other (e.g., Ichikawa and Yasunari, 2007; Wu et al., 2009a; Fujita et al., 2011). They correspond to the confluence of wind known in particular in the Melaka Strait (e.g., Ramage, 1971; Fujita et al., 2010).

The diurnal cycles over the IMC are excited by solar radiation every day and developed almost spontaneously by processes mentioned above. Therefore, as well as their amplifications at maxima (two times a year) of solar heating and moisture transport by monsoon and/or ISVs, any suppression processes may induce their temporal/spatial variability. Larger-scale may concern such amplification and suppression, as considered since earlier studies around the IMC (e.g., Houze et al., 1981; Johnson and Priegnitz, 1981; Johnson and Kriete, 1982). Western coast predominance in comparison to eastern coast (in Sumatera and Kalimantan, as well as Malay, Indochina Peninsula and Indian Subcontinent) has been reported (cf. Figs. 6.6−6.7) and discussed in view of prevailing winds and/or gravity-wave propagations to enhance a circulation cell on the western side and suppress the other one on the eastern side (e.g., Murata et al., 2002; Mori et al., 2004; Xie et al., 2006; Wu et al., 2009a, b).

Horizontally quasi-continuous observations of rainfall over tropics with a space-borne precipitation radar on the Tropical Rainfall Measurement Mission (TRMM) launched in November 1997 have revealed that the diurnal-cycle rainfalls along the maritime-continent coastlines are heavier on the sea side (called the *coastal heavy rainband*, or CHeR) than on the land side (Mori et al., 2004, 2011; Wu et al., 2008a, 2009b). Prior to them several observational (e.g., Chang et al., 2004a) and numerical (e.g., Ogura and Yoshizaki, 1988) studies noticed substantially similar phenomena of convective activities and considered mainly orography (mountain range) effects on monsoons. After starting TRMM other studies for various areas in tropics (e.g., Xie et al., 2006) also noticed what we call CHeR, and studied mainly the orographic effect. Mechanisms generating the sea-side dominance have been shown numerically

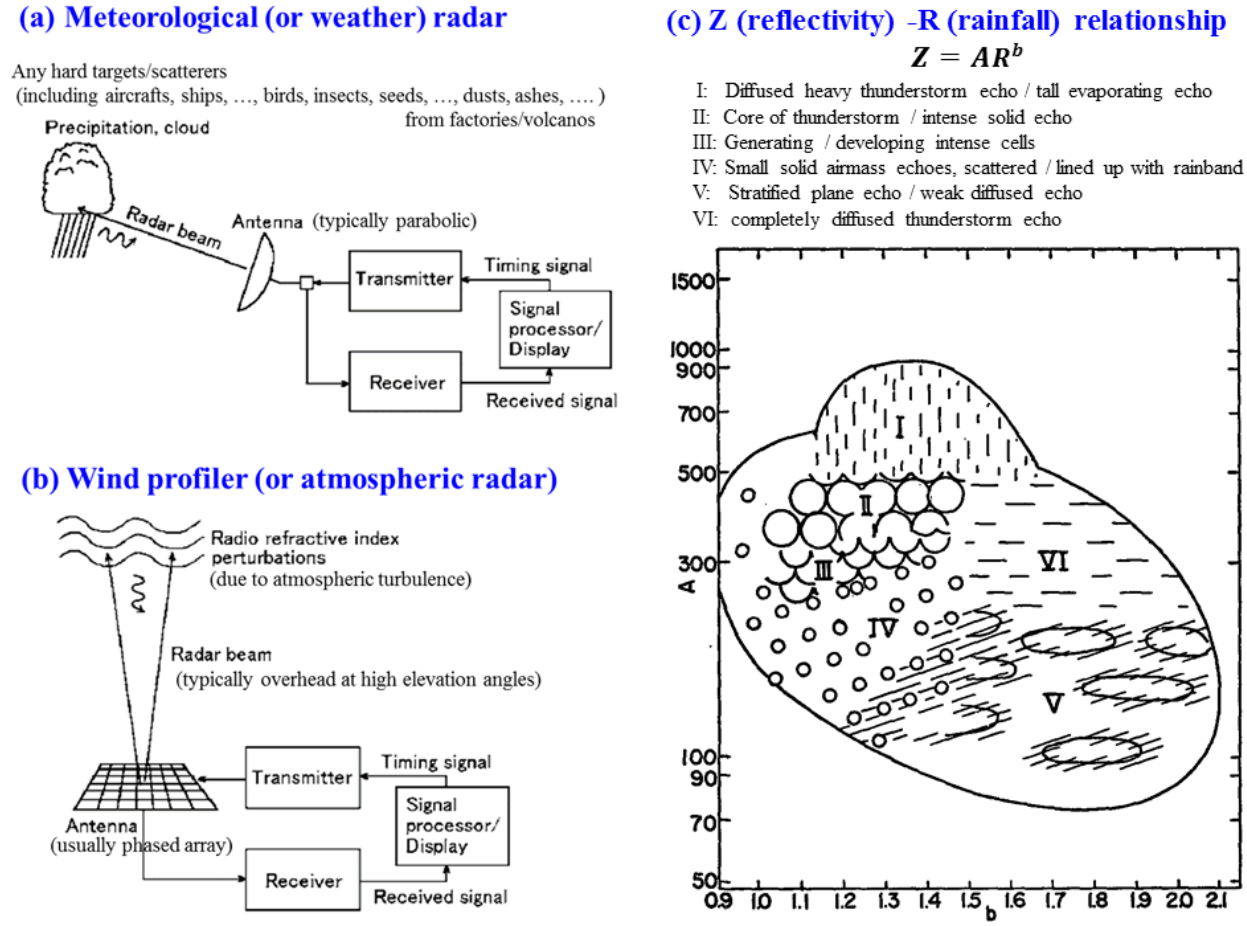

Fig. 6.12 Principles of (a) meteorological radar and (b) wind profiler (Fukao and Hamazu, 2014), and (c) the so-called Z-R relationship for meteorological radars (Fujiwara, 1965).

(Wu et al., 2008, 2009b) by nocturnal outflow (land breeze) and seaward migration of land clouds. It is shown very recently (Ogino et al., 2016) that tropical rainfall may be approximately expressed in general by a function of the coastal distance with dominance on the sea side.

The success of TRMM (including many other results which cannot be mention in this article) showed not only the scientific importance of such smaller-scale diurnal cycle, but also the technical necessity of radar remote sensing facilities (cf. Fig. 6.12) to cover the tropics for both scientific and operational objectives. Some subtropical southeast Asian countries (e.g., Malaysia, Thailand and Philippines) installed meteorological radars relatively earlier, mainly to watch typhoons. The central maritime continent – Indonesia started to install advanced operational radars since 2006, after a long history from (each few) intermittently operated old radars and research-use wind profilers (mainly on atmospheric vertical coupling; see Hashiguchi et al., 1995a; Fukao, 2006) and meteorological Doppler radars (Yamanaka et al., 2008, 2017) and now reach 40 stations covering almost the whole archipelago (Fig. 6.13).

Complex shaped coastlines such as bays and peninsulas generate convergence/divergence and other interactions of local flows. In particular in the western coasts of Sumatera Island, Indochina Peninsula (Myanmar-Thailand-Malay) and Indian Subcontinent, steep slopes of mountains (Barisan, Arakan-Tenasserim, and Western Ghāts) are located within a few hundred kilometers of the coast, sea breezes and terrain effects appear in combination. It has been known (e.g., Sorooshian et al., 2002; Mapes et al., 2003a, b; Warner et al., 2003) over the Central America that

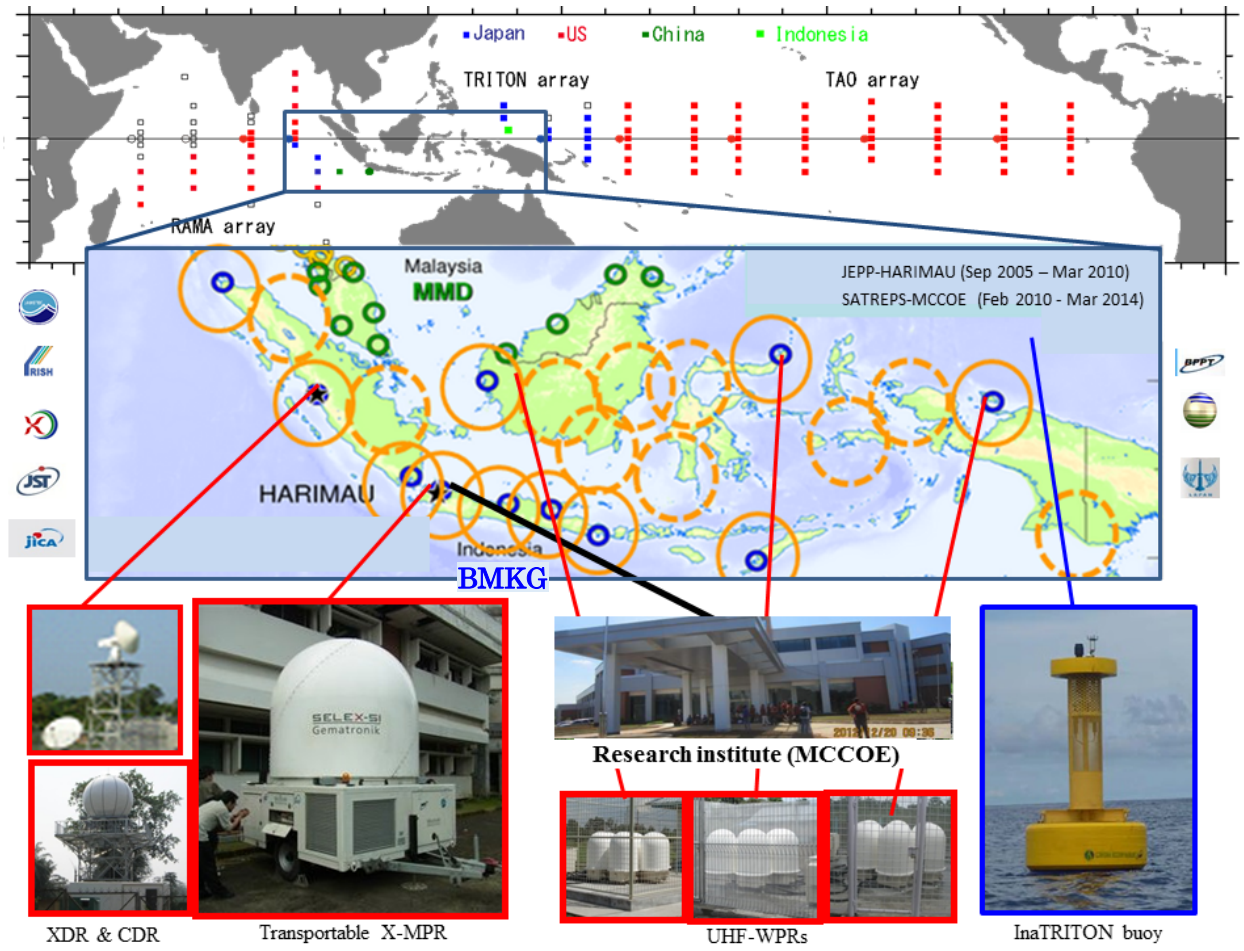

Fig. 6.13 Observation networks used in JEPP-HARIMAU (2005-2010) and SATREPS-MCCOE (2010-2014) projects (Yamanaka et al., 2008, 2017), collaborating international buoy arrays (upper map) and Indonesian operational radars (lower map; around 2010).

sea and upslope winds produce strong low-level convergence and convective rainfall over slopes of mountains (Sierra Madre de Chiapas) from afternoon to evening, and that land and katabatic winds produce convergence and convection over the offshore in particular of bay-like portions of the coastline (such as the Gulf of Panama).

The dominance of diurnal cycles suggests that the hydrologic cycle is very quick over the IMC. It has been observed and understood well (since Wu et al., 2003; Mori et al., 2004) that rainfall comparable to the annual amount (both on the sea and land sides of the coastlines) and water vapor transport by sea winds are clearly following the diurnal cycle. A recent study (Sulistyowati et al., 2014) has shown a diurnal cycle of river water level (Fig. 6.11(a)), that is, water transport from land to sea, which must be balanced with sea-wind water-vapor transport, if the water budget is closed in a river basin, a coastal sea just outside the river mouth and the atmosphere over them. This hypothesis is not so bad, because all of river flow, sea-land breeze circulation and raincloud migration are approximately perpendicular to the coastline, and also because the water is conserved by so-called cold trap mechanism at the top of tall convective clouds near the very low-temperature tropopause (often around –80°C or cooler; see e.g., Holton et al., 1995) which also follow the diurnal cycle. Although quantitative evidence has not yet been sufficient, if the evaporation from sea surface and evapotranspiration from land surface also follow the diurnal cycle, this hypothesis should hold. By this very quick water cycle, the water is almost conserved, whereas the (sensible and latent) heat transport from the earth's surface to the whole troposphere is effective enough to satisfy the

global energy budget.

Concerning interannual variations of rainfall correlated strongly (at least partly) with ENSO/IOD (Section 5.3), we may consider amplitude modulations of the diurnal cycle associated with variations of SST. Because the sea-land breeze circulations are directly enforced by the land-sea temperature difference (e.g., Estoque, 1962; Rotunno, 1983; Niino, 1987), cooler SST in El Niño and/or positive dipole mode may induce weaker land breeze and suppress sea-side rainfall in the early morning than in La Niña and/or negative dipole mode. Complex topography of coastlines, land surfaces and ocean bottoms may induce highly inhomogeneous regionality of correlations between atmosphere and ocean interacting each other. Relationship with ISVs and the diurnal cycle may be also similar (cf. Section 6.4). Serious flood events were caused by the diurnal cycles amplified by La Niña/negative IOD, transequatorial boreal winter monsoons (cold surges from Siberia) and ISVs (Wu et al., 2007, 2013), although the general relationship among the diurnal cycle, ISV, monsoon and ENSO/IOD is still a target for future studies.

It is the diurnal-cycle rainfalls along the world's longest coastlines associated with many large islands of the IMC that generate the equatorial rainfall peak controlling the global climate (see Fig. 6.11(c)). The rainfall concentration is about 2,000 mm/year for a "coastline density" 10^{-2} km^{-1} (corresponding to 102 km coastline around 10^4 km^2 area), which is consistent with the coastal peak 1,300 mm/year in Fig. 6.11(b) and also with the equatorial rainfall peak 2,000 mm/year in the middle panel of Fig. 4.6, considering that the total tropical coastline length (almost in the IMC) is almost equivalent to the equatorial circumference (40,000 km). Although it has been explained often directly by the warmest seawater surrounding the IMC, rainfall over the open ocean is less than over the islands in the IMC (cf. Qian, 2008). Indeed the solid land is heated easier than the liquid sea, but convective precipitating clouds generated over the true continents (Africa and South America) are less active than over the IMC as seen in Figs. 6.11(d)−(e) obtained from IPCC (2007) for example. Instead the diurnal cycles generated around the longest coastlines of the IMC are essential to generate the largest rainfall there. For each heavy rainfall condition produced by large-scale phenomena such as ENSO/IOD (Section 5.3), monsoon surges (Section 4.4) or ISVs (Section 6.4), only some areas have actual heavy rainfalls (Wu et al., 2007, 2013), but an integration over the long coastlines may achieve the world's largest annual rainfall amount over the IMC.

The relationships (shown in Figs. 6.11(b)−(c)) indicating importance of the local diurnal cycles imply that a climate model needs to resolve the equatorial coastlines with a scale sufficiently smaller than 100 km. Actually, recent global models have satisfied such high resolutions (e.g., Neale and Slingo, 2003; Arakawa and Kitoh, 2005; Hara et al., 2009; Satoh et al., 2008; Sato et al., 2009; Love et al., 2011). Their downscaling and regional model applications are also progressed for usual diurnal cycles (Wu et al., 2003, 2008a, 2009a, b) and extreme rainfalls making floods (Trilaksono et al., 2011, 2012).

6.2. Conditional instability and clouds (Vertical convection)

(i) Convective (Rayleigh-Taylor) instability for dry atmosphere

The vertical convection is generated spontaneously by the convective instability ($N^2 < 0$). Although in the actual atmosphere it cannot be separated from the moist (cloud condensation) processes (Chapter 3), at first we shall consider purely dynamical processes of the dry convective instability. The simplest case is a linear steady problem of which the basic equation is essentially the same as (6.13) but here without neglecting the horizontal viscosity and

diffusion:

$$\nabla^6\psi' - Ra \cdot d^{-4}\frac{\partial^2\psi'}{\partial x^2} = 0, \quad Ra \equiv \frac{(-N^2)d^4}{K'K}, \quad N^2 < 0, \tag{6.28}$$

where Ra is non-dimensional and called the *Rayleigh number*, and d is the height of the unstable layer given in the boundary condition:

$$\frac{\partial u'}{\partial z} = w' = T' = 0 \ \left(\psi' = \frac{\partial^2\psi'}{\partial z^2} = \frac{\partial^4\psi'}{\partial z^4} = 0\right) \qquad \text{at} \quad z = 0, d. \tag{6.29}$$

Physical differences from the forced horizontal convection under stable stratification have been mentioned below (6.12) in the previous section.

Lord Rayleigh showed that a roll-type convection with an axis along the y-direction satisfying (6.29):

$$\psi' \propto \sin kx \sin\frac{n\pi}{d}z, \qquad n = 1, 2, 3, \cdots,$$

may be a solution of (6.28) under the following necessary condition:

$$Ra = \frac{[k^2 + (n\pi/d)^2]^3}{k^2/d^4} \geq \frac{27}{4}\pi^4 \equiv Ra_c \qquad \left(\text{equality at} \quad n = 1, \qquad kd = \frac{\pi}{\sqrt{2}} \ \equiv k_c d\right), \tag{6.30}$$

where Ra_c is called the critical Rayleigh number, k_c is called the critical wavenumber, and n is the number of rolls in the vertical direction. Therefore the convection of vertically one cell structure ($n = 1$) should be generated $Ra \geq Ra_c \approx 660$, and the horizontal size of the roll convection is $\pi/k_c = \sqrt{2} \approx 1.4$ times of the height d, as have been shown in Fig. 6.2(d). The other vertically multi-cell convections ($n \geq 2$) must be generated much larger (much unstable) Ra, for which always the one-cell ($n = 1$) has been developed earlier, thus they do not appear actually. The condition (6.30) is mathematically equivalent to a shear instability of flow between differentially rotating cylinders studied by G. I. Taylor (replacing the buoyancy torque in Rayleigh's problem by the centrifugal torque), and often called the *Rayleigh-Taylor instability*.

For a three-dimensional problem the solution becomes tetragon cells:

$$\psi' \propto \sin kx \sin ly \sin\frac{n\pi}{d}z, \qquad n = 1, 2, 3, \cdots,$$

and in the condition formula (6.30) the zonal wavenumber k is replaced by the horizontal wavenumber $\sqrt{k^2 + l^2}$. These are called the *Bénard-Rayleigh convections*[59]. Numerical and laboratory experiments have shown that the resulta are also dependent on the Prandtl number $Pr \equiv K'/K$. If Pr is $10^1 - 10^2$, two-dimensional rolls appearing for smaller Ra are took over by three-dimensional cells at beyond $Ra \sim 10^4$, and become turbulence at around $Ra \sim 10^5$. Among many studies, Lorenz (1963) studied a much simplified (truncated) problem consisting only of the amplitude (dependent only on *t*) of w' and horizontal and vertical variation parts of T' of a two-dimensional-roll mode of innumerable solutions of (6.11) and (6.12). He showed that, if Ra is sufficiently large, alternative oppositely-rotating rolls (which are steady if Ra is small) continue to replace each other nonperiodically. This *deterministic chaos* depicted an essential aspect of dynamics of fluid including the Earth's atmosphere, that is, a difficulty concerning meteorological forecasts and climatological predictions, and has been applied for many physical

[59]In 1900 Bénard discovered hexagonal cells generated in a thin fluid layer heated at the bottom. In 1916 Rayleigh proposed the convection theory and obtained the two-dimensional rolls. By many studies following them, the cell shape (hexagon or tetragon) is dependent on experimental conditions, and the original Bénard's experiments were governed mainly by surface tension.

and mathematical fields.

The convection theories mentioned above are still a major part of general fluid dynamics, but the unstable stratification $N^2 < 0$, i.e., $\partial\overline{\theta}/\partial z < 0$, i.e., $\partial\overline{T}/\partial z < -\Gamma$ appears very rarely in the actual atmosphere even in the tropical atmosphere heated very much by the insolation. Even if the thermal stratification is stable ($N^2 > 0$), there may be shear instabilities. If a vertical shear $\partial\overline{u}/\partial z$ exists, and the Richardson number Ri defined in (4.19) satisfies $0 < Ri < 1/4$ (Miles, 1961; Howard, 1961), strong roll-type disturbances (called 'cat's eye', and seen as 'billow clouds') are generated (the *Kelvin-Helmholtz instability*). If the shear is strong in case of unstable stratification (Ri is small negative), rolls with axis along the background flow $\overline{u}$ are predominant (Asai, 1970), which may explain cloud patterns over the Sea of Japan, the East China Sea and the Pacific Ocean during strong winter monsoons in the extratropics. Other (symmetric or baroclinic) shear instabilities with stable stratifications ($1/4 < Ri < 1$ or $Ri > 1$; cf. Section 4.2) are essentially important for the extratropical frontal and cyclonic disturbances, but not so in the tropical troposphere.

(ii) Conditional instability for moist atmosphere

It is the moist process that destabilize the atmosphere in particular in the tropics, although its inseparable relationship with convection is somewhat paradoxical, as so far mentioned in Sections 3.3 and 6.1. Cloud condensation with strong convection (upward motion) and resulting showery rainfall in very narrow area is much more dominant than the other manner of condensation (such as making a fog in extratropical sea surface or mountain slope) by almost static cooling and slow ascending of a broad area[60]. In a convection water vapor ascending with upward flow ($w' > 0$) starts condensation around an aerosol particle (*heterogeneous nuclearization*) when it reaches the lifting condensation level (Fig. 3.6). In this way liquid or solid cloud particles are formed in the gaseous atmosphere, through complex chemical and microphysical processes. Sum of them makes latent heat release in the thermodynamics for the atmosphere. In the IMC microphysical features such as raindrop size distributions and their seasonal/diurnal variations (Renggono et al., 2001, 2006; Kozu et al., 2006) and isotope ratios of rainwater indicating its origins (Ichiyanagi, 2007; Kurita et al., 2009; Fudeyasu et al., 2011; Suwarman et al., 2013) have also been observed. Importance of clouds in the tropics is far larger than in the extratropics. (cf. Fig. 4.9) since pressure field-controlling circulations generate clouds in the extratropics, whereas clouds produce circulations in the tropics. Thus the cumulus convections in the tropics are, in spite of their individual scales similar to the extratropics, not an issue of the mesoscale section but the central issue of the whole tropical meteorology.

The most basic description on the moist atmosphere has been given in Section 3.3. Substituting the saturated value r_s given by (2.7) into the specific humidity r of the equivalent potential temperature θ_e (the second equation of (3.10)) for a saturated air parcel, we have

$$\theta_e^* \equiv \theta \cdot \exp\left(\frac{Lr_s}{C_p T}\right) \text{ (saturated equivalent potential temperature)}, \tag{6.31}$$

of which the conservation ($\partial\theta_e^*/\partial z = 0$) leads to the moist (pseudo-)adiabatic lapse rate Γ_m as (3.11). When the

[60]This does *not* mean absence of stratiform cloud in the tropics. A matured cumulonimbus cloud is associated with an anvil extending over much broader area than the original cloud around the tropopause. Over the sea surface smog is generated in particular around the maritime continent by a forest fire in the El Nino (generally less rainfall) year. These two stratiform clouds contribute to rainfalls very little but to radiative energy budget considerably.

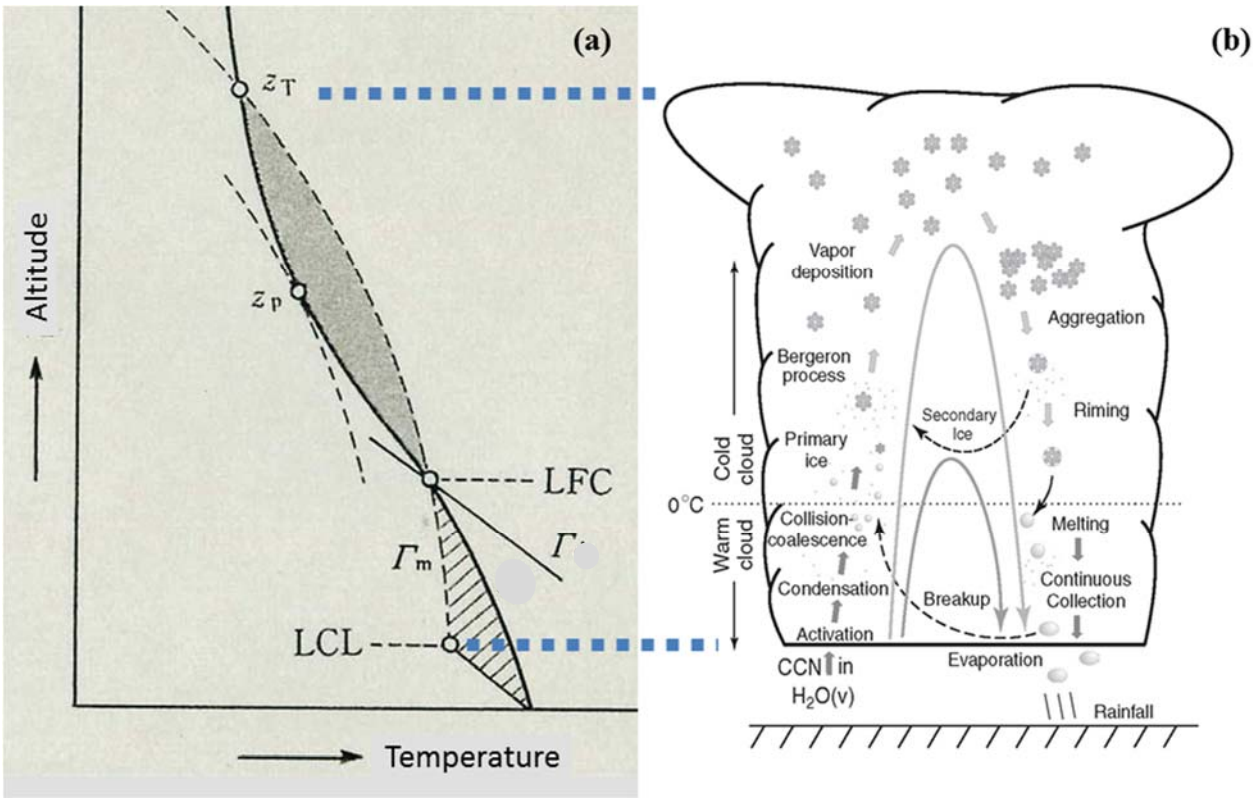

Fig. 6.14 Schematic pictures for typical convective cloud, concerning (a) temperature profile (thick curve) and (b) microphysical processes (Lamb, 2003).

vertical temperature gradient satisfies

$$-\Gamma < \frac{\partial T}{\partial z} < -\Gamma_{\mathrm{m}} \quad \left(i.e., \quad \frac{\partial \theta}{\partial z} > 0 \ \text{ and } \ \frac{\partial \theta_{\mathrm{e}}{}^{*}}{\partial z} < 0 \right), \tag{6.32}$$

then the atmosphere is unstable and generates (vertical) convection as mentioned in the previous section, if a parcel is saturated (in a cloud). If not (below, outside and above of the cloud), the atmosphere is stable. This situation is called the *conditional instability*.

In general the tropical lower and middle troposphere satisfies (6.32), and at the tropopause $\theta \approx \theta_{\mathrm{e}} \approx \theta_{\mathrm{e}}{}^{*} \approx \theta_{\mathrm{e}}(z=0)$ (the left-hand side panel of Fig. 3.6). Even in the tropics, however, $\theta_{\mathrm{e}} < \theta_{\mathrm{e}}{}^{*}$ for large regions in the troposphere, so that an air parcel moves upward only in case of any forcing as the dry (unsaturated) process with keeping θ (exactly speaking, the virtual potential temperature θ_{v} corresponding to the virtual temperature T_{v}), that is decreasing T by the dry adiabatic lapse rate Γ as in (3.7). If the forcing to lift up the air parcel is continued enough to reach an altitude called the *lifting condensation level (LCL)*, where the moisture satisfies the saturation ($r = r_{\mathrm{s}}$), then the condensation started and LCL becomes the cloud bottom. Furthermore, if the forcing is continued (because still T of the parcel at LCL is cooler than the surrounding atmospheric temperature), the parcel continues to move upward and condense the involved water vapor (to generate cloud droplets[61]) with keeping $\theta_{\mathrm{e}}{}^{*}$ (of the value at the LCL), that is decreasing T by the slower moist adiabatic lapse rate Γ_{m} as in (3.11), and may reach an altitude called the *level of free convection (LFC)*, where T of the parcel becomes equal to the surrounding atmospheric

[61]This process is irreversible and diabatic, because all the cloud droplets are assumed to be removed from the parcel (and fall to the ground as raindrops) with taking out a very small amount of heat, and is called *pseudoadiabatic*.

temperature decreasing upward steeper than Γ_{m} in the conditionally unstable situation (6.32). After that the parcel (warmer than the surrounding atmosphere) may move upward without forcing, until losing the buoyancy at an altitude (that is the cloud top) where T becomes equal to the surrounding temperature again. At the tropopause, above which the surrounding temperature gradient is changed rapidly to positive in the tropics, most of clouds must have the tops there or below. Similarly at the so-called *inversion layer* over the trade wind on the tropical ocean (Section 4.1) and also on the Indochina peninsula before the monsoon onset (Nodzu et al., 2006), lower convective clouds have tops.

The moist process producing the latent heat occurs only in the updraft area of a cloud, whereas the dry adiabatic process under rather stable stratification appears in the (broader) downdraft area surrounding the cloud even in the tropics. Considering this fact and the saturation and thermodynamic equations, (2.7) and (3.10), may be rewritten as

$$\left(\frac{\partial}{\partial t}+u\frac{\partial}{\partial x}+v\frac{\partial}{\partial y}\right)\theta+\Gamma_{\mathrm{e}}w\approx\frac{e^{(R/C_pH)z}}{C_p}(J+LS),$$
$$\text{where}\qquad \Gamma_{\mathrm{e}}\equiv\begin{cases}\theta\cdot\partial\ln\theta_{\mathrm{e}}{}^{*}/\partial z & \text{for}\quad r\geq r_{\mathrm{s}}\ \text{ and }\ w>0,\\ \partial\theta/\partial z & \text{for}\quad r<r_{\mathrm{s}}\ \text{ or }\ w\leq 0.\end{cases} \tag{6.33}$$

Γ_{e} is called the *equivalent static stability*. If there are no radiative heating nor additional moisture input, the righthand-side of the rewritten thermodynamic equation (6.33) becomes zero. If we replace (6.5) and (6.7) by (6.33) (and rewrite θ by T appropriately), we may solve the governing equations for moist convections by the mathematically same manner (without using r as a variable explicitly) as for dry convection mentioned in the previous subsection. Therefore the basic features of the cloud convections should be similar to those of the Bénard-Rayleigh convections described in the previous subsection: generation governed by the critical Rayleigh number, aspect-ratio (vertical/horizontal scales) of approximately unity, and so on. For the tropical troposphere the vertical scale is restricted by the tropopause height around 17 km, the horizontal scale of the whole convection (combining both updraft (cloud) and downdraft (clear) areas) should be similar. Corresponding to the fact that the latent heating occurs only in the updraft area, the value of Γ_{e} is larger in the downdraft area than in the updraft area. Thus the updraft (cloud) is narrower and stronger than the downdraft (clear area). Numerical calculations including nonlinear and dissipation terms have simulated realistic lifetimes from 10 min to 1 h. The criterion (6.32) is conditional, so that convections are not always generated even if (6.32) is satisfied. However, if convections are generated, they may extend beyond the initial (lower-tropospheric) conditionally unstable layer and reach at above the tropopause. For details of these features, see textbooks on dynamics of convective clouds (e.g., Houze, 1993; Emanuel, 1994; much simpler descriptions are also given in Section 9.5 of Holton, 1992).

The *convective available potential energy (CAPE)* provides a measure of the maximum kinetic energy for a convectively unstable parcel, assuming that water vapor and condensed water do not affect the buoyancy, and also that the parcel ascends without mixing with the environment ($K'=0$) and adjusts instantaneously to the local surrounding pressure ($\phi'=0$). The left-hand side of the vertical momentum equation (6.3) for such a parcel is expressed by the Lagrangian time derivative as in (2.1)–(2.3): $\frac{Dw\prime}{Dt}=\frac{Dz}{Dt}\frac{dw\prime}{dz}=w'\frac{dw\prime}{dz}=\frac{d}{dz}\frac{w\prime^2}{2}$, and the right-hand side is only the buoyancy term $(R/H)T'$ where $H=R\overline{T}/g$. Therefore,

$$\mathrm{CAPE}\equiv\left.\frac{w'^2}{2}\right|_{\max}=g\int_{z_{\mathrm{LFC}}}^{z_{\mathrm{T}}}\frac{T'}{\overline{T}}dz, \tag{6.34}$$

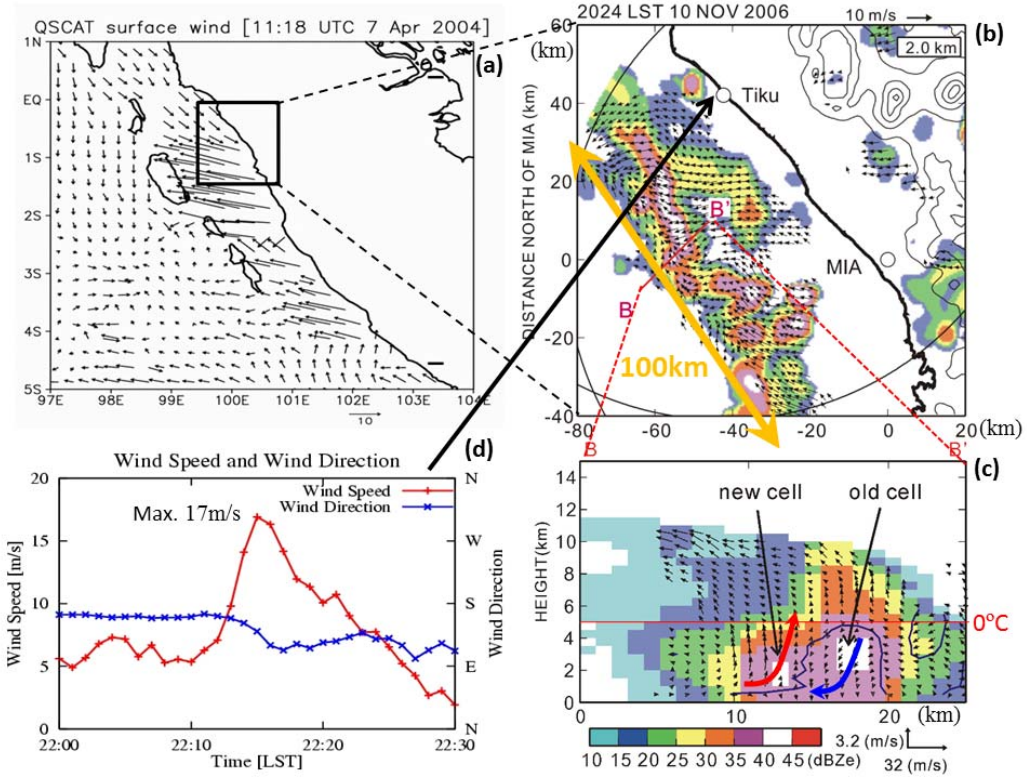

Fig. 6.15 Observations of development of a convective cloud system at (a) the western coast of Sumatera with other case of QuikSCAT sea-surface wind: (b) horizontal and (c) vertical displays of rainfalls (contours) and winds (arrows) observed with dual X-band Doppler radars installed at Tiku and MIA indicated in (b) (Sakurai et al., 2009, 2011), and (d) strong gust observed with surface anemometer (Kawashima et al., 2006, 2011).

where T' is given by the deviation of parcel temperature from the surrounding temperature $\overline{T}$, z_{LFC} is the altitude of LFC ($T' = 0$ there), and z_{T} is the other zero buoyancy level ($T' = 0$ again) around the tropopause (see the left panel of Fig. 3.6). For typical values $T' \approx$ 1–2 K between $z_{\mathrm{T}} - z_{\mathrm{LFC}} \approx$ 10–12 km over the tropical ocean, we have CAPE $\approx$ 500 m^2/s^2, which is smaller than the supercell (to be mentioned later) over the mid-latitude continent. Actually the scales of thundershowers (with graupels) and water spouts associated with cumulonimbus clouds observed in the maritime continent are generally smaller than thunderstorms (with hails) and tornadoes in the central US, although the generation frequency and total rainfall is larger in the former than in the latter.

Actual cloud is not vertically one-dimensional but three-dimensional, and ascending saturated air parcels inside the cloud may be mixed by the so-called *entrainment* of less moist or dry surrounding/outside air. Some cloud droplets are evaporated to maintain saturation of the parcels/clouds, and the latent 'cooling' due to evaporation reduces θ_{e} and w' of the parcels.[62] Therefore the CAPE (6.34) overestimates the actual kinetic energy.

The mesoscale convective cloud systems (in any latitudes) are primarily categorized into the single cell, the multicell, and the supercell storm (with lifetimes of roughly 0.5 h, many hours and much longer, respectively[63]), and their occurrences are mainly dependent on the vertical shear (roughly < 10, 10–20 and > 20 m/s, respectively, below 4 km altitude) (see e.g., Houze, 1993), which are not explained by the magnitude of CAPE. In the multicell storm, a *gust front* (with cold downdraft/outflow induced by raindrop evaporation) of the old cell makes the conditionally-

[62]For more discussions on the entrainment, see Subsection 9.5.4 of Holton (1992) (for details, e.g., Houze, 1993; Emanuel, 1994).
[63]For individual convective cell (cumulonimbus cloud) involved in a multicell the lifetime is similar to the single cell.

unstable surface air to ascend and generate the new cell. In the supercell the vertical shear makes the convection cell to tilt and slow development, which results in a very strong storm with tornadoes[64]. Vertical shears in speed and in direction affect the most unstable modes, such as preference of rolls aligned in the shear flow direction (Asai 1972). To the present author's knowledge, there has not been any report of a supercell in the tropics, probably because of no broad plains. In the maritime continent Kawashima et al. (2006, 2011) and Sakurai et al. (2009, 2011) reported Doppler radar observations of cumulonimbus systems in west Sumatera.

The ice phase (ice crystals, snowflakes, graupels and hails) involved in the cumulonimbus cloud produces a strong local electric field, thunder and lightening. It was based on the thunderstorm frequency that Ramage (1968) named the maritime continent. Concerning lightening, Hidayat and Ishii (1998) analyzed seasonal and diurnal variations around Jawa, Hamid et al. (2001) showed ENSO impacts over the IMC, Kodama et al. (2006) showed lightening activation due to stronger convective instability in dry (El Niño) phase, and Virts et al. (2013a, b) studied Madden-Julian oscillation (MJO; see Section 6.4) and diurnal cycles based on a global network. They are in general consistent with the convective cloud activities described in this article, but more studies are needed for the significance of vertical (atmosphere-ionosphere) coupling and for a practical application to warn local torrential rainfall. Atmospheric electricity including thunderstorms may be another process linking atmosphere vertically.

In summary in the explanation mentioned above the following two aspects are important. One is the necessity of any mechanism to lift the surface air (with large θ_e) to the LCL and the LFC. The other is the mechanisms to organize the convective clouds (expected to be individually small-scale and distributed homogeneously) into large-scale structures as observed actually in the tropics. In the extratropics the geostrophic wind-pressure field has an instability mechanism to generate the extratropical cyclone-front systems, which produce large-scale updraft areas. In the tropics there are in total three phenomena/mechanisms to cause the conditional instability effectively. The first one has been described in Section 6.1 as the diurnal-cycle sea-land breeze circulations forced near the coastlines. The other two are developed by multi-scale destabilization mechanisms interacted/coupled with (water vapor supply from) the warm ocean water. In the subtropics, on one hand, somewhat apart from the equator the Coriolis force may work to produce a strong vortex, which is the tropical cyclone to be mentioned in Section 6.3. In the vicinity of the equator, on the other hand, a Matsuno-Gill pattern organized over the open ocean with interacting each other, which is the intraseasonal variation (such as MJO) travelling eastward along the equator (Section 6.4).

6.3. Conditional instability of second kind (CISK) and tropical cyclones

Yanai et al. (1973) proposed an evaluation method of the large-scale effect of clouds in the tropics with insufficient number of observations. The thermodynamic equation (2.5) and the water vapor conservation equation (the second one of (2.4)) are integrated for a large-scale horizontal area:

$$\left(\frac{\partial \overline{T}}{\partial t}+\overline{u}\frac{\partial \overline{T}}{\partial x}+\overline{v}\frac{\partial \overline{T}}{\partial y}\right)+\overline{w}\left(\frac{\partial}{\partial z}+\Gamma\right)=\overline{Q_1}=\frac{\overline{J}+L\overline{s}}{C_p}-\frac{1}{\rho_0}\frac{\partial \rho_0\overline{T'w'}}{\partial z}, \tag{6.35}$$

$$\frac{L}{C_p}\left(\frac{\partial \overline{r}}{\partial t}+\overline{u}\frac{\partial \overline{r}}{\partial x}+\overline{v}\frac{\partial \overline{r}}{\partial y}+\overline{w}\frac{\partial \overline{r}}{\partial z}\right)=\overline{Q_2}=-\frac{L}{C_p}\left(\overline{s}+\frac{1}{\rho_0}\frac{\partial \rho_0\overline{r'w'}}{\partial z}\right), \tag{6.36}$$

[64]A line-shaped ensemble of multi- or super-cells is called the *squall line*, which moves in a different direction than the individual thunderstorms (similar to the equatorial supercluster; Section 6.4).

where $\overline{Q_1}$ and $\overline{Q_2}$ are the apparent heat source and moisture sink for the large-scale dynamics. Note $\overline{(\ )}$ and $(\ )'$ are *not* the zonal mean and disturbance, but the average for a regional (observed) area and an anomaly from this average. The moisture supply $\overline{S}$ from the outside (ocean and land) does not appear explicitly, and is involved implicitly in the net condensation amount $\overline{s}$. At first each left-hand side can be calculated based on the large-scale observations (an objective analysis) of $\overline{u}$, $\overline{v}$, $\overline{w}$, $\overline{T}$ and $\overline{r}$, which gives $\overline{Q_1}$ and $\overline{Q_2}$. Next the difference of each right-hand side of (6.35) and (6.36) becomes

$$\Delta\overline{Q} \equiv \left(\overline{Q_1} - \frac{\overline{J}}{C_p}\right) - \overline{Q_2} = -\frac{1}{C_p\rho_0}\frac{\partial}{\partial z}\rho_0\left(C_p\overline{T'w'} + L\overline{r'w'}\right) \approx -\frac{1}{C_p}\frac{\partial\overline{h'w'}}{\partial z}, \tag{6.37}$$

where h' is a perturbation of the *moist static energy*:[65]

$$h \equiv C_pT + \phi + Lr, \qquad dh \approx C_pT \cdot d\ln\theta_e. \tag{6.38}$$

Therefore the contribution by clouds $\partial\overline{h'w'}/\partial z$ can be evaluated from $\overline{Q_1}$, $\overline{Q_2}$ and the radiative heating $\overline{J}$ as another calculable quantity, without knowing $\overline{s}$.

In the moist (pseudo-)adiabatic process ($\theta_e =$ const.) h is approximately conserved, the integration of (6.37) in the cloud becomes

$$\int_{(\text{cloud bottom})}^{(\text{cloud top})} \Delta\overline{Q}\, dz \approx -\frac{1}{C_p}\left[\overline{h'w'}\right]_{(\text{cloud bottom})}^{(\text{cloud top})} \approx 0. \tag{6.39}$$

Observations confirmed (6.39), which implies that the effect of convective clouds is not negligible. Therefore the numerical model even for the large scale phenomena must express it ($\partial\overline{T'w'}/\partial$, etc. in the original equations) in the tropics. In order to overcome this issue, there are two strategies: parameterization and high resolution. The former is to express small (sub-grid) scale phenomena by an experimental/theoretical formula, whereas the latter is to improve (zoom up) the spatial resolution (and time step). In the cloud process these are not separable, because the microphysical and turbulent process cannot be observed practically and calculated explicitly, and any parameterizations are inevitably necessary. These are not only technical issues of numerical calculation, but also theoretical issues on why/how multiple scale phenomena from microphysics to large-scale dynamics appear in the tropical atmosphere.

The most popular large-scale phenomena in the (sub)tropics are the *tropical cyclones*, which are called *typhoons* in the northwestern Pacific and *hurricanes* in around the north America. They are intense vortical storms that develop over very warm surface water the tropical oceans (except for around the south America). Their typical radial scales are several hundred kilometers, but the horizontal scale of the region of most intense horizontal winds is typically only about 100 km in radius. Because the Coriolis force needs to sustain strong *gradient* (mainly geostrophic plus partly *cyclostrophic*) tangential winds (50−100 m/s) with strong radial pressure gradient due to very low central pressure, they appear in general in the latitudes higher than around 10º (Fig. 6.16). This structure may be described by equations similar to the zonal mean global circulation (4.2)−(4.6), if we consider the northern hemisphere ($f > 0$) and take x-coordinate in the clockwise tangential direction along the circular isobar (pressure contour line), y-coordinate in the outward radial direction and z-coordinate in the upward vertical direction[66]. In this case the

[65] h is the sum of the enthalpy $C_pT + Lr$ and the gravity potential energy ϕ, and also the sum of the dry static energy $C_pT + \phi$ and the latent heat Lr. When h is conserved, the integration of h from LFC to the cloud top is approximately equal to CAPE (6.34). Because h is approximately conserved when θ_e is conserved, h is used as an alternative to θ_e.

[66] This local Cartesian description of the cylindrical coordinate system is different from more popular one (x: outward, y: 'anti-clockwise' tangential; z: upward) but is better for considering the similarity to the equatorial global case.

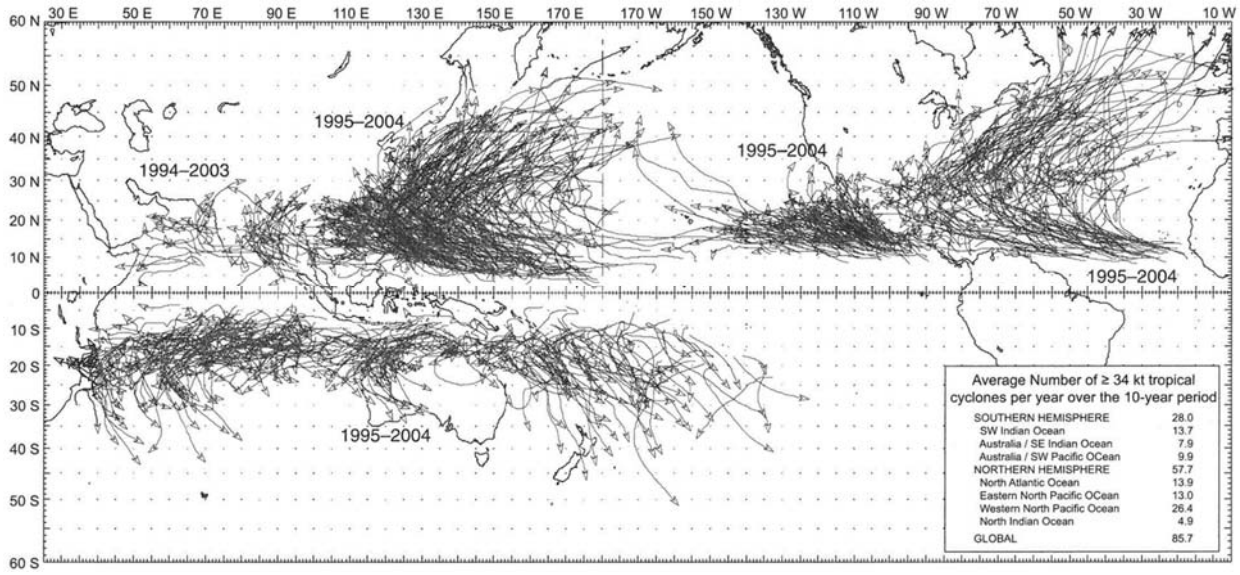

Fig. 6.16 Genesis locations and tracks of tropical cyclones (with winds ≥ 17 m/s) in 1995−2004 (Lin, 2007).

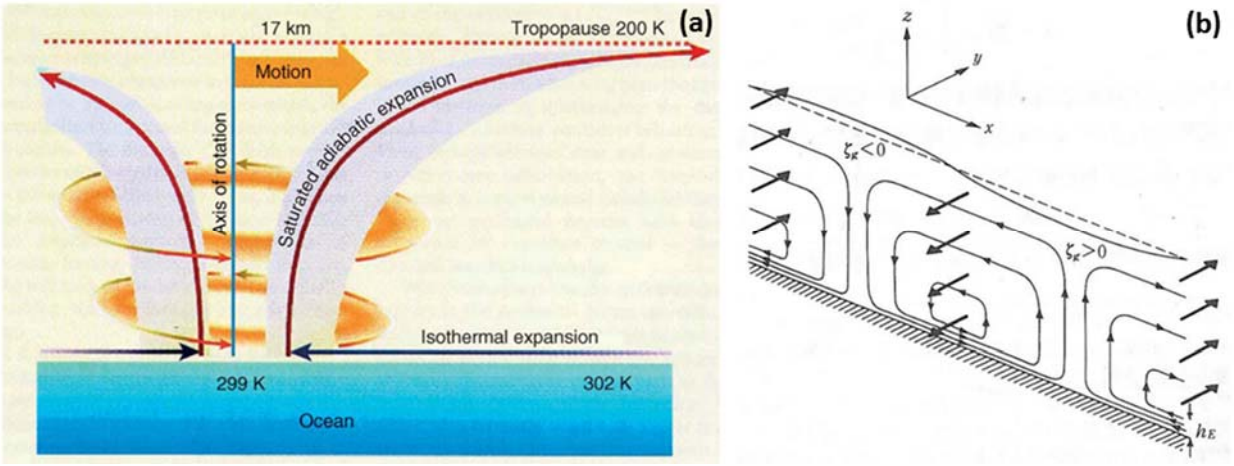

Fig. 6.17 Schematic figures of (a) the 'meridional' (secondary) circulation (Willoughby, 1999), and (b) the Ekman pumping (Pedlosky, 1979) of the tropical cyclone.

tangential wind is anti-clockwise ($\overline{u} < 0$) for the northern hemisphere ($y > 0$), and clockwise ($\overline{u} > 0$) for the southern hemisphere ($y < 0$). The Coriolis factor f should be replaced by $f + \overline{u}/y$ including the centrifugal force. Considering that the angular momentum $M = (f/2)y^2 + (-\overline{u})y$ is conserved, the tangential wind $\overline{u} = (f/2)y - M/y$ becomes a monotonically increasing (cyclonically decreasing) function of y, the cyclonic rotation ($\overline{u} < 0$) is limited for $y < \sqrt{2M/f}$. Actual typhoon suggests $\sqrt{2M/f} \sim$ a few hundreds of km. In order to settle M and $\overline{u}$ near the center as realistic values, f should be sufficiently large, which requests the latitude larger than about 10º.

The 'meridional' (radial-vertical) circulation ($\overline{v}$, $\overline{w}$) (Fig. 6.17(a)) may be considered by applying the case of Hadley circulation (4.20) or (4.23) (with replacing f by $f + \overline{u}/y$. In the boundary layer $\overline{u}$ has the opposite sign to both $f + \overline{u}/y$ and the x-direction friction $\overline{G}$, thus the radial wind must blow to the center ($\overline{v} < 0$). By the conservation of M, the centrifugal force $\overline{u}^2/y$ increases rapidly with approaching to the center ($y \to 0$), and exceed the y-direction pressure gradient completely, which implies that air cannot enter into the vicinity of the center ($\overline{v} \to 0$) if the acceleration term is not neglected, and the continuity equation (similar to (4.5) in the zonal-mean case) requests very large updraft $\overline{w} > 0$, which is sustained by very large $\overline{Q}$ due to the very active (very strongly latent

heating) convective clouds. Namely, reading the second formula of (4.20) inversely:

$$\overline{Q}\left(\approx \overline{Q_1}\right) \approx \Gamma \cdot \overline{w}, \tag{6.40}$$

we expect the temperature lapse rate Γ or the updraft $\overline{w}$ must be parameterized appropriately in order to construct a numerical model of typhoon/hurricane. Inside this no updraft (clouds) and the vorticity conservation ($\partial(-\overline{u})/\partial y =$ const.) requests decrease of $\overline{u}$ toward the center[67]. These structure in the vicinity of the tropical cyclone center is called the *eye*, and the very tall clouds surrounding it are called *eye wall* (Fig. 6.18).

A parameterization of Γ has been mentioned as the convective adjustment (Manabe and Strickler, 1964) in Section 3.2: if the calculated lapse rate $-\partial T/\partial z$ in an altitude region exceeds a critical value[68], it is rewritten by T satisfying $\theta_{\mathrm{e}} = \text{const.}$ and no change of the energy before and after the adjustment (therefore (6.39) holds automatically). This scheme is, however, cannot express the large-scale effect of cumulus clouds growing beyond the unstable layer top as pointed out in the previous section. Kuo (1974) proposed a formula similar to the Newtonian cooling (3.6)[69]:

$$\overline{Q} - \frac{\overline{J}}{C_p} \approx -\alpha\left(\overline{T} - \overline{T}_c\right) \quad \text{for} \quad z_{(\text{cloud bottom})} \le z \le z_{(\text{cloud top})}, \tag{6.41}$$

which makes relaxation to a standard temperature profile $\overline{T}_c$ in the cumulus (e.g., given by the moist pseudoadiabatic lapse rate based on θ_{e} at the cloud bottom (LCL)) by a finite time given by α^{-1}. This scheme can express the heating effect up to the cloud top (where actual $\overline{T}$ is identified with the value in the moist pseudoadiabatic profile) much higher than the initial unstable layer top. The relaxation time constant α has, however, very broad arbitrariness (even within the condition (6.39)).

Ooyama (1969) noted the updraft (moisture flux) inside a cloud over the convergence of moist air in the planetary boundary layer, and proposed another parameterization:

$$\overline{Q} - \frac{\overline{J}}{C_p} \approx \eta \cdot \frac{\rho_{(\text{boundary layer top})}}{\rho_0} \frac{\partial \overline{\theta}}{\partial z} \cdot \overline{w}_{(\text{boundary layer top})} \quad \text{for} \quad \overline{w}_{(\text{boundary layer top})} > 0 \tag{6.42}$$

In this case the non-dimensional parameter η is essentially important. Under the condition (6.39), if $\eta > 1$, then $\overline{w}_{(\text{inside cloud})} > \overline{w}_{(\text{boundary layer top})}$, implying the existence of entrainment effect due to mixing of outside air to the ascending air inside the cloud. $\overline{w}_{(\text{boundary layer top})}$ can be obtained by applying the wind-driven ocean equations (5.24) for the boundary layer-driven free-atmosphere (perturbation from the axi-symmetric field) in the present problem. Replacing the Coriolis factor βy by constant f for simplicity, making $\partial(\text{2nd eq})/\partial x - \partial(\text{1st eq})/\partial y$ of (5.24), we have

$$\frac{\partial v'_{(\text{free atmosphere})}}{\partial x} - \frac{\partial u'_{(\text{free atmosphere})}}{\partial y} \approx -\frac{\alpha'}{f}\left(\frac{\partial u'_{(\text{boundary layer})}}{\partial x} + \frac{\partial v'_{(\text{boundary layer})}}{\partial y}\right). \tag{6.43}$$

Because the inside of bracket in the right-hand side is the horizontal convergence in the boundary layer, (6.43) is rewritten by (5.5) as $+(\alpha'/\rho_0 f)\,\partial \rho_0 w'/\partial z$, which is approximated by $w'_{(\text{boundary layer top})}/$

[67]Ishihara et al. (1986) and Tabata et al. (1992) by meteorological Doppler radars and Shibagaki et al. (2003) and Teshiba et al. (2005) by wind profilers showed detailed structures of typhoon eyes, and Fudeyasu et al. (2008a) showed the origin of rainwater near a typhoon eye, although they were all in the mid latitudes (Japan).

[68]This is a measure of generation of convection, formulated for example to take a value between Γ_{m} and Γ as a function of the relative humidity r/r_s.

[69]A similar parametrization (usually with a different value of α) is applied also for $\overline{Q_2}$ concerning r.

(boundary layer depth), since $w' = 0$ at the bottom (sea surface). Because the left-hand side is the perturbation of vertical vorticity in the free atmosphere (of which the axi-symmetric component is given by a formula similar to (4.18)), the meaning of (6.43) is that the cyclonic/anticyclonic vorticity in the free atmosphere is on the up-/down-draft in the boundary layer (Fig. 6.17(b)), which is called *the Ekman pumping*.

By the Ekman pumping mechanism, the tropical cyclone as a very strong cyclonic vortex may be associated with many very strong updraft areas in the boundary layer. In the conditionally unstable atmospheric boundary layer over the tropical ocean, in particular over very warm water of the tropical western Pacific[70], the updrafts become cumulus convections developing beyond LFC and their released latent heat sustain (through $\overline{Q}$) the tropical cyclone-scale $\overline{w}$. This process is expressed, by x-averaging (6.43) and using (6.42), as

$$\overline{w}_{(\text{boundary layer top})} \approx -\frac{fd}{\alpha'}\overline{q}, \qquad \overline{w}_{(\text{vortex top})} \approx \eta \cdot \overline{w}_{(\text{vortex bottom})}, \tag{6.44}$$

where $d \approx \sqrt{K'/f}$ is the boundary layer depth (similar to the Ekman layer depth δ_{E} (6.25)), and the Rayleigh damping factor in (6.43) has been rewritten as $\alpha' \approx K'/d^2$ by the eddy diffusivity K'. Taking y-differentiation of the tangential momentum equation similar to (4.2)[71], using the axi-symmetric continuity equation similar to (4.5), and z-integrating from the free-atmosphere bottom (the boundary layer top) to the vortex top (height: H), we obtain

$$\frac{\partial \overline{q}}{\partial t} \approx -f\frac{\partial \overline{v}}{\partial y} = f\frac{\partial \overline{w}}{\partial z} \approx \frac{f}{H}[\overline{w}]^{(\text{vortex top})}_{(\text{boundary layer top})} \approx (\eta - 1)\frac{\sqrt{K'/f}}{H} f\overline{q}. \tag{6.45}$$

Therefore, if $\eta > 1$, the vorticity $\overline{q}$ increases in time, and the vortex is developed, and the inverse of the factor of $\overline{q}$ in the right-hand side, $H/\left[(\eta - 1)\sqrt{K'f}\right]$, is called the *spin up* time. The latent heat $\overline{Q}$ released by cumulus clouds make $\overline{w}$ (> 0) and (by the continuity) $\overline{v}$ (< 0) increase, by which air moved toward the center make (by conservation of M) the cyclonically rotating tangential wind $-\overline{u}$ and its gradient-balanced pressure gradient $\partial\overline{\phi}/\partial y$ increase (that is, the central minimum pressure deepen). The cyclonic development in this way is feedback to the enhancement of w', that is the cumulus cloud development at the beginning. This theoretical mechanism may explain the realistic development time scale and the dominant horizontal scale of actual typhoons and hurricanes, and Charney and Eliassen (1964) had named this mechanism as the *conditional instability of the second kind (CISK)*. An improvement considering an initial role of wave disturbance to make convergence and local instability has been also proposed (Hayashi, 1970; Lindzen, 1974).

Energetically speaking, the kinetic energy of a tropical cyclone is always dissipated in the boundary layer and supplied by the conversion of latent heat obtained by ocean surface evaporation, through the potential energy producing the 'meridional' circulation. Increasing the surface (mainly tangential) wind speed, the sea surface disturbance, evaporation and latent heat supply are enhanced much more, and the boundary-layer inflow $\overline{v}$, θ_{e} and a potential energy making feedback to the tangential wind $\overline{u}$ increase rapidly from outside to inside. This mechanism is called the *wind-induced surface heat exchange (WISHE)* (Emanuel, 1987; Neelin et al., 1987). In the narrow outward-sloping eyewall clouds throughout the troposphere, air may ascend without forcing, because both θ_{e} and M are conserved along the updraft, which is neutral in the meaning of the (conditional) symmetric stability mentioned in Section 4.3. Radial outflow exists in a rather thin layer near the tropopause, and rather weak downdraft

[70]Observations suggest that the tropical cyclones are generated/developed over the ocean surface water warmer than about 26.5ºC.
[71]We may neglect $\partial\overline{u}/\partial y$ (in comparison to f), $\partial\overline{u}/\partial z$ (by the nature of vortex tending to be parallel to the rotating axis; the Taylor-Proudmann theorem), and $\overline{G}$ (without considering any systematic distribution of clouds).

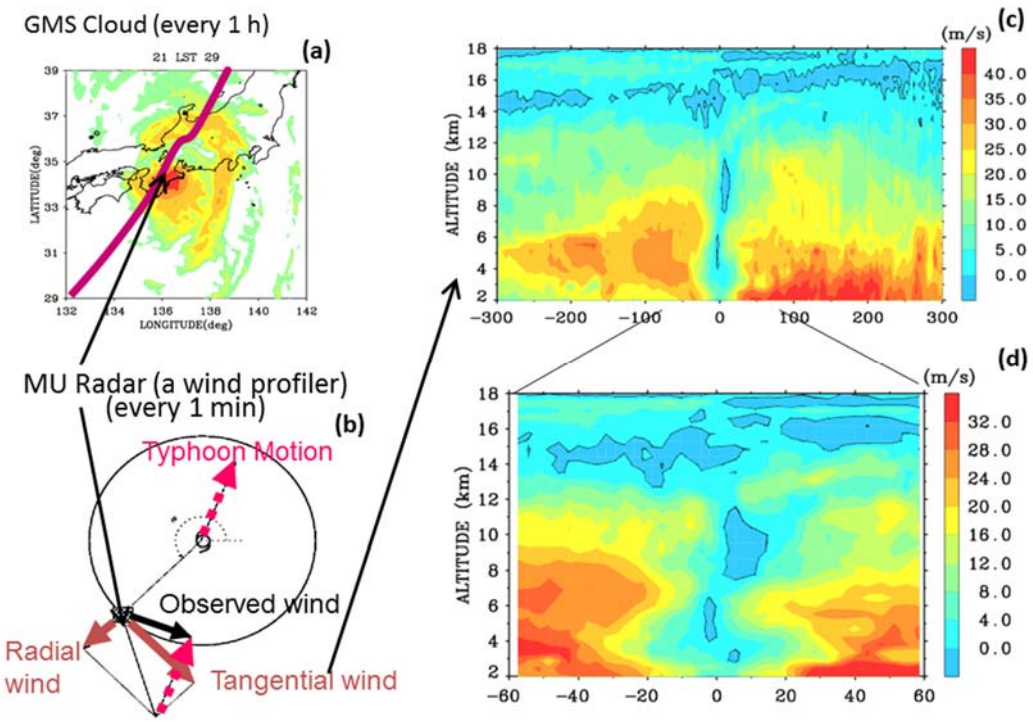

Fig. 6.18 Wind profiler (MU radar) observation of (a) a matured typhoon (T9426, Orchid) just passed by. (b) Subtraction of the moving velocity from the observed wind velocity, and decomposition between the radial and tangential wind components. (c) Pseudo-'meridional' cross-section (with radial distance exchanged from time series at the single observatory; positive is the foreside) of the tangential wind velocity and (d) its magnified one showing the 'eye' structure. After Shibagaki et al. (2003).

region is distributed broadly. With this structure the tropical cyclone is warmer than the surroundings, which is called the *warm core*.

Because the typhoons in Asia-Pacific countries, the hurricanes in north-central American countries and others (the cyclones in south Asian and southern Pacific countries) are still of the worst meteorological disasters, improvement of numerical prediction (and warning/informatics of the prediction products) of the tropical cyclones is one of the biggest issue in the meteorological operations, although almost real time tracking of the center and storm (torrential rain and/or violent wind) distribution of each cyclone has been achieved so much by the meteorological satellites and radars. The movement of tropical cyclone of mesoscale follows the large-scale wind field, so that the latter is quite important for prevention of the typhoon/hurricane disasters and have been improved very much during these decades. Prediction of development/decay of the tropical cyclone is just that of cumulus clouds, namely parameterization or high resolution as mentioned in the previous section. The physically most advanced parameterization was originated by Arakawa and Schubert (1974) who formulated the effect of subgrid-scale cumulus cloud activities by a function (types with the number of vertical levels) of the 'entrainment ratio' (corresponding to the cloud top height and η), and statistical features of each type of clouds under an energetical equilibrium.

For the weather forecast and disaster prevention each national operational agency defines categories of tropical storms, mainly based on the maximum wind speed near the center, and give a number or a name satisfying a definition. For example the Japan Meteorological Agency (and its leading Regional Specialized Meteorological Center Tokyo-Typhoon Center for the east Asia-Pacific region) defines a typhoon by its location in the northwestern Pacific and its maximum (10 min-averaged) wind stronger than 34 knot (≈ 17 m/s), and gives it a number restarting every year and an international name listed by WMO: http://www.jma.go.jp/jma/jma-eng/jma-center/rsmc-hp-pub-eg/tyname.html.

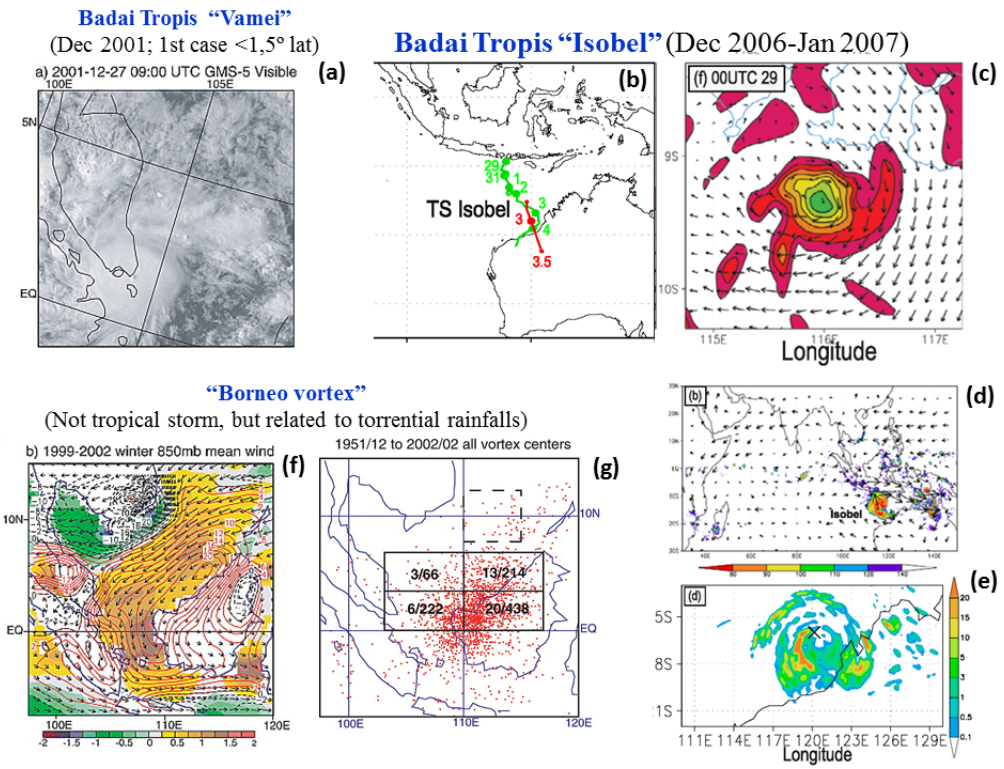

Fig. 6.19 Near-equatorial tropical cyclones: (a) *Vamel* (Chang et al., 2003), and (b)−(e) *Isobel* (Fudeyasu et al., 2008b). (f) − (g) Other sub-synoptic-scale vortical disturbances called "Borneo vortex" (Chang et al., 2003).

Details and differences in each country are mainly for disaster prevention rather than based on physics, and are not described in this text. Recently the increase and intensification of tropical storms interest the society, as a possible result by the global warming (e.g., Chan and Liu, 2004; Emanuel, 2005; Webster et al., 2005; Oouchi et al., 2006), although the societal vulnerability and damages are not dependent only on the physical characteristics of meteorological phenomena.

Because of the necessity of the Coriolis force, average annual occurrence of tropical cyclones inside the equatorial deformation radius (4.21) is only two (dispersed between zero and seven each year) on the northern (Philippine and Micronesian) side (during the past century; Kubota and Chan, 2009; Kubota et al., 2012; Kubota, 2012) and less than 1.5 on the southern (Australian) sides (for the last two decades of the last century; Hall et al., 2001). They are much rarer (as reported by Chang et al., 2003; Fig. 6.19(a))[72] and not so much developed over inland seas and islands of the IMC (called "*badai tropis*" in Indonesia-Malay language), which could be simulated by high-resolution (cumulus-resolving) numerical models (Fudeyasu et al., 2008b) (Figs. 6.19(b)−(e)). Because the ITCZ shifts annually but is not completely following a weak annual cycle of solar radiation (Fig. 4.5), and it concerns typhoon generation mainly in the northern subtropics (often northern than 20°N in boreal summer), otherwise it involves mainly ISVs (because southward shifts of the ITCZ are not so deep even in the austral summer). However, a few very strong typhoons (such as a case and a "super typhoon" Haiyan (Yolanda, T1330) in 2013, as well as

[72]There is another category of sub-synoptic-scale vortical disturbance (called the *Borneo vortex*, or *cold surge vortex*) appearing on around the South China Sea (e.g., Chang et al., 2003; Yokoi and Matsumoto, 2008; Tangang et al., 2008; Chen et al., 2015), considered to be developed by the stretching of vorticity due to updraft generated by latent heat release near the center and a rainband-like structure in the north east of the center. This category is related to, rather than a tropical cyclone, intensification of the cold (monsoon) surge (Section 4.4) and a cause of torrential rainfall in this area.

another one in 1912 almost just 100 years ago, and less strong ones such as reported by Holliday and Thompson, 1986, between them almost every about three decades) have been generated and developed very much along (for a few days a little southern than) 10°N (Kubota, 2014, private communications) . On the other hand, even near the South America with cool sea water, recent warming may produce a tropical cyclone (Pezza and Simmonds, 2005).

After landing the tropical cyclone decays gradually, because of losing the moisture supply and of increasing the friction at the bottom surface. This *spin down* process may be expressed by (6.45) with $\eta = 0$, and the decaying time scale is given by $H/\sqrt{K'f} \sim 1$ day. The frictional contrast between sea and land surfaces also makes low-level divergence and downdraft of upper air with large vorticity in the area with wind blowing from land to sea (e.g., in the western side for landing on a west-east coastline in the northern hemisphere), which makes a shift of the cyclone center as a cause of 'freak' tropical cyclone just before landing[73]. After decaying some tropical cyclones become extratropical cyclones and develop again. For further reading on the tropical cyclones see convection and cloud dynamics textbooks (e.g., Houze, 1993; Emanuel, 1994), and also a recent project overview (Moncrieff, et al., 2012).

6.4. Multiple-scale cloud clusters and intraseasonal variations (ISVs): Madden-Julian oscillation (MJO)

(i) Observations

Takayabu and Nitta (1993) classified the tropical cloud clusters organized over the tropical ocean into two categories: one is the tropical cyclones with vortical shape generated way from the equator and moving with the large-scale within a limited region (such as over the northwestern Pacific and east Asia) flow for one to few weeks until decaying, which have been described in the previous section; the other is the *intraseasonal variations* (ISVs) to be described in this section, which are generated just as the Matsuno-Gill pattern-like shape (Figs. 5.8 and 5.9) and moving always eastward along the equator over an ocean or occasionally through the oceans for weeks to two months. The most dominant mode of ISVs was observationally discovered by Madden and Julian (1971, 1972), and is called the Madden-Julian oscillation (MJO), Nakazawa (1988) showed the *hierarchical structure* of MJO with a *super cluster* (with horizontal scale $\gtrsim 10^3$ km) involving smaller-scale *clusters* (~ 10^2 km) of individual clouds ($\lesssim 10^1$ km), and that the smaller clusters move in a different (often opposite) direction from the super clusters (Fig. 6.20). As schematically shown in Fig. 6.21, the MJO super cluster starts developing with a surface low-pressure anomaly and boundary-layer moisture convergence over the Indian Ocean, warming and anomaly (Walker-like) circulation of the troposphere, and ascending of the tropopause. The system moves gradually eastward at about 5 m/s (~ 430 km/day, corresponding roughly to period of 1, 1.5, or 3 months for zonal wavenumber 3, 2 or 1, respectively) and becomes most active over the western Pacific. After reaching the central Pacific cooler than the western warm pool, the system gradually weakens, although occasionally anomaly continues to move more eastward around the globe (Takayabu et al., 1999). The MJO is like a Matsuno-Gill pattern consisting of equatorial Kelvin and Rossby waves (see Section 5.2), and its smaller hierarchies are likely to mixed-Rossby gravity or inertio-gravity waves.

Wheeler and Hendon (2004) originated the real-time multivariate MJO (RMM) index, based on a pair of empirical orthogonal functions (EOFs)[74] of the normalized daily anomalies of lower-/upper-level (850-/200-hPa) zonal wind and cloud top height (by outgoing longwave radiation). The principal components (RMM1 and 2,

[73]Even over the ocean a tropical cyclone trajectory becomes irregular by weak large-scale wind, and by interactions of two cyclones approaching each other. The latter is called the *Fujiwhara effect* (Fujiwhara, 1923).
[74]A comprehensive explanation (with simple examples) of the EOF analysis is given in Chapter 21 (pp.821−823) of Stull (2015).

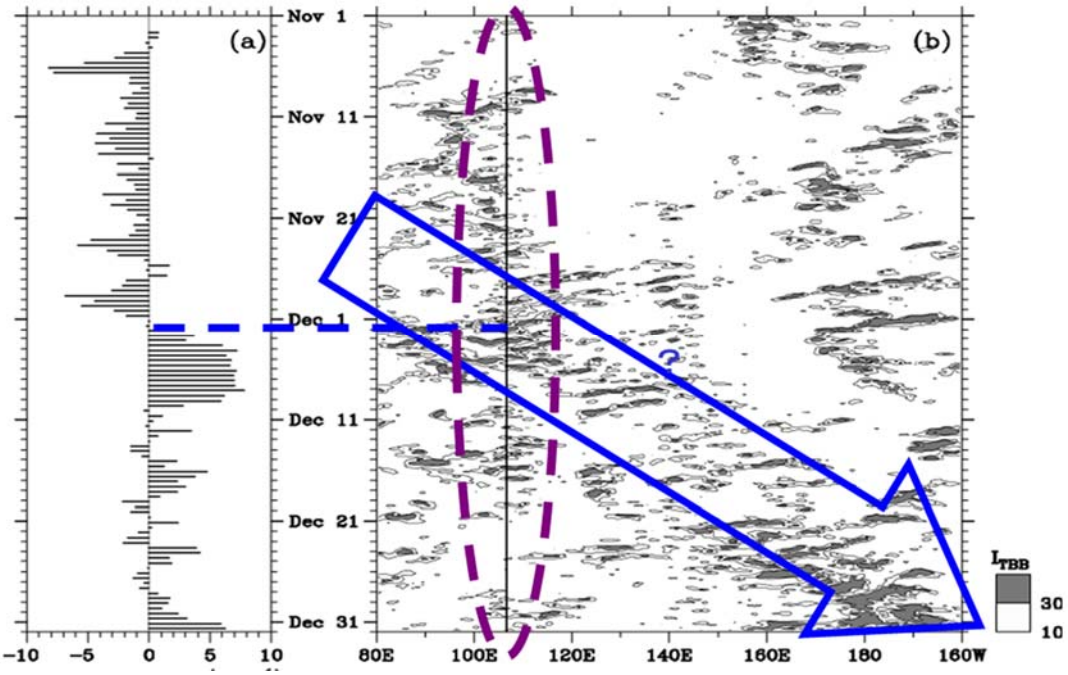

Fig. 6.20 An ISV passage detected by (a) wind profiler-observed (6ºS, 107ºE) semi-daily-mean lower-tropospheric zonal wind and (b) 3-hourly meteorological satellite-observed I_{TBB} = 250 K – black body temperature along 6ºS (Hashiguchi et al., 1995a). As found in earlier studies, there is an eastward moving supercluster (the large arrow) and smaller hierarchies moving different directions. In addition, near the Jawa Island (the vertical line at 107ºE in (b)) the diurnal cycles appeared clearly.

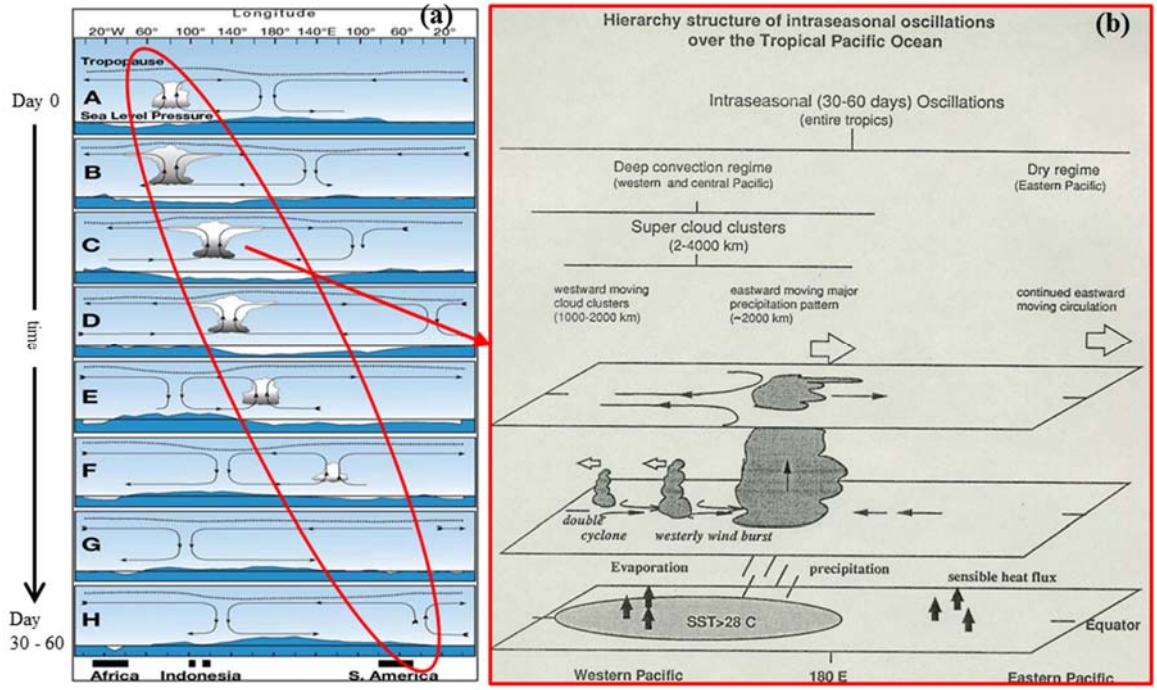

Fig. 6.21 Schematic figures of the Madden Julian oscillation (MJO): (a) eastward movement and longitudinal dependency (Madden and Julian, 1994) and (b) the internal hierarchical structure (Lau et al., 1989).

corresponding to temporal amplitude variations) of the first two leading functions (EOF1 and 2, corresponding to zonal convection distributions active near the IMC and *in*active over the Indian Ocean, respectively)[75] are calculated and plotted in the RMM1-RMM2 plane (Fig. 6.22(a)−(c)). The MJO amplitude is given by the distance from the

[75]The fact that the leading functions have not essentially changed since 1970s indicates the regularity of the MJO.

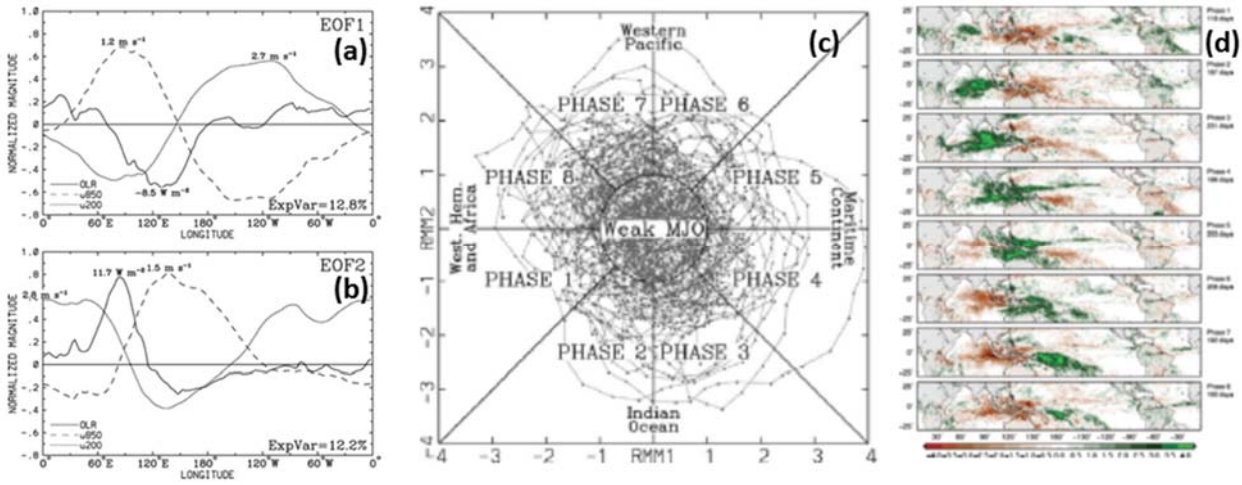

Fig. 6.22 (a)(b) The first two EOFs (see text) and (c) the real-time multivariate MJO (RMM) index space indicating eqastward movement of MJO (Wheeler and Hendon, 2004). (d) Composites of intraseasonal (30– 90 days) anomalies in TRMM precipitation (mm/day) during November–April of 1998–2012 based on the RMM index (Zhang, 2013).

origin, and if it is less than 1 (the amplitude less than the standard deviation), we define that MJO is weak. The MJO phases are defined (classified into 1–8) by the azimuthal location, which rotates usually anticlockwise. For example, if plotted near the bottom (RMM2 taking *mini*mum), the convection center is located over the Indian Ocean, which is defined as phases 2–3. When plotted in the right (RMM1 taking maximum), the convection center is located near the IMC, which is defined as phases 4–5. Composites of this analysis for the boreal winter (Fig. 6.22(d)) show clearly that the convection center starts over the Indian Ocean, passes through the IMC and into the western Pacific, although more eastward propagation (go-around) is less clear. For the boreal summer, the MJO moves also northward due to monsoon (Lawrence and Webster 2002), which cannot be shown in the Wheeler-Hendon RMM index concerning only zonal movement. However, this index is recognized most useful to express MJO status, and calculated/reported operationally every day by Australian Bureau of Meteorology: http://www.bom.gov.au/climate/mjo/, and other countries' agencies also use this.

The MJO is considered to interact atmospheric/climatological phenomena from the diurnal cycle to interannual variability (Moncrieff et al. 2012). The MJO influences on almost global weather and climate through tropical cyclone activities (e.g., Liebmann et al. 1994; Maloney and Hartmann 2001) (Section 6.3), variations of teleconnections (Fig. 5.10), monsoons (e.g., Yasunari, 1979; Takeda and Ikeyama, 1984; Lau and Chan, 1986; Hendon and Liebmann 1990; Wang and Rui, 1990; Sui and Lau, 1992; also see a book edited by Lau and Waliser, 2005) (Section 4.4), ENSO/IOD (e.g., Nitta and Motoki 1987; McPhaden, 1999) (Section 5.3), the Indonesian throughflow (e.g., Gordon, 2005).

Because the MJO is a movement of the tropical convection center from the Indian Ocean into the Pacific, it influences regional weather and climate greatly in particular over the IMC in between. The rainy season onset of the southern hemispheric part of the IMC (Section 4.4) is determined by an ISV (Hashiguchi et al., 1995a) (see Fig. 6.20), and through the rainy season rainfall over the IMC increases actually during the active/wet phase of the dominant mode (MJO) of ISVs (Murata et al., 2002, 2006; Shibagaki et al., 2006a, b; Seto et al., 2006; Johnson and Ciesielski, 2013; Marzuki et al., 2013), in particular on surrounding seas larger than on the large islands (Hidayat and Kizu, 2009) . Shorter hierarchy resembling mixed Rossby-gravity and/or inertio-gravity waves with periods of a few days also has been observed mainly near the eastern/western ends (Pacific and Indian Ocean sides) of the IMC (Takayabu

et al., 1996; Widiyatmi et al., 1999, 2001). The smaller-scale diurnal cycle rainfalls may be modified by larger-scale ISVs (Hashiguchi et al., 1995; Widiyatmi et al., 1999, 2001; Murata et al., 2002, 2006; Shibagaki et al., 2006; Rauniyar and Walsh, 2011; Kanamori et al., 2013; Peatman et al., 2014), seasonal cycle/monsoons (Hashiguchi et al., 1995; Renggono et al., 2001; Hamada et al., 2002; Okamoto et al., 2003; Sakurai et al., 2005; Xie et al., 2006; Araki et al., 2006; Koseki et al., 2013). Such modification/interaction may amplify diurnal cycles (Section 6.1) and cause heavy rainfalls in the western IMC (Wu et al., 2007, 2013).

Simultaneously the existence of the IMC influences the structure and movement of MJO quite largely. Based on satellite cloud cluster observations and objective analysis for about one year, Nitta et al. (1992) pointed out modification (such as propagation in the southern side of the equator) of the ISVs. Using more systematic analysis of longer-year data, essentially similar results are also confirmed recently by Zhang and Ling (2017). Mori et al. (2004), Wu et al. (2009b) and Ogino et al. (2016) have demonstrated the sea-side dominance of diurnal-cycle rainfall as CHeR (see Section 4), which is consistent with other evidence by Hidayat and Kizu (2009) that the ISV-correlated rainfall is also heavier than on the sea side. Locally roughly closed water cycle and a little opened energy release over the IMC are consistent with most of ISVs (super cloud clusters) decaying/modifying after landing the IMC. Cloud systems involved/maintained in an ISV migrating eastward over the Indian Ocean are decayed by almost complete consumption of water for rainfall in the local evening followed by clear atmosphere in the local morning. In this process the local rainfall keeps the diurnal cycle but its amount may be affected by moisture, stratification stability and wind field associated with the ISV. Therefore the diurnal cycle may be amplified by ISVs and, in longer time scale, by the annual cycle of the ITCZ (Sakurai et al., 2005; Wu et al., 2007, 2013).

The MJO/ISVs are phenomena mainly over the open ocean, and need special observations because there are no dense observations (islands themselves are not so many in particular over the Indian Ocean). The fully-operated (land, vessel, and space) scientific observation project focused on the MJO was started in 1992 over the western Pacific (Webster and Lukas, 1992; Nakazawa, 1995) and in 2006 over the Indian Ocean (Yoneyama et al., 2008, 2013).

(ii) Theoretical and numerical approaches

As mentioned in Chapter 5, there are various atmospheric waves in the tropical trade wind (easterly) zone. In the dawn of tropical meteorology based on physics and observations about half a century ago, studies on the stability of the axi-symmetric easterly to generate such *easterly wave* were done, following successful results on the mid-latitude westerly waves (baroclinic instability on the extratropical cyclones). However, the tropical atmosphere is *barotropic* (original meaning is ρ is a function only of p, and thus T is constant horizontally) and no vertical shear by the thermal-wind relation (4.11), that is, the dynamics becomes horizontal and two-dimensional. In this case the equatorial wave equation (5.9) may be written, with assuming $|m| \to 0$, $H \to \infty$ and $|\widehat{\omega}| \ll N$, and recovering the horizontal shear term $\partial\overline{u}/\partial y$,

$$\frac{d^2\tilde{v}}{dy^2} - \left(k^2 + \frac{k\tilde{\beta}}{\widehat{\omega}}\right)\tilde{v} = 0, \tag{6.46}$$

where

$$\tilde{\beta} \equiv \frac{d\overline{q}}{dy} = \beta - \frac{d^2\overline{u}}{dy^2} = \beta + \frac{1}{k}\frac{d^2\widehat{\omega}}{dy^2} \tag{6.47}$$

is the meridional gradient of the vertical vorticity and often called the *effective* β. (6.47) has a neutral solution (with a real ω) corresponding to the (barotropic) Rossby wave.

When $\beta = 0$, namely $\tilde{\beta} = -d^2\overline{u}/dy^2$, (6.46) becomes the so-called Rayleigh equation, which is the most basic one (for a shear instability) with a boundary condition:

$$\tilde{v}(y_1) = \tilde{v}(y_2) = 0 \tag{6.48}$$

in the hydrodynamic instability theor. Namely, we may solve an eigenvalue problem on $\hat{\omega} \equiv \hat{\omega}_r + i\omega_i$, and determine an instability if an eigenvalue satisfying $\omega_i > 0$ (that is, $|\tilde{v}| \to e^{+\omega_i t} \to \infty$ for $t \to \infty$). Another strategy is to obtain an integration theorem as follows: taking $\tilde{v}^* \cdot (1.89) - \tilde{v} \cdot (1.89)^*$:

$$\frac{d}{dy}\Im\left[\tilde{v}^* \frac{d\tilde{v}}{dy}\right] = -\omega_i \frac{k\tilde{\beta}}{|\hat{\omega}|^2}|\tilde{v}|^2,$$

where $(\ )^*$ is the complex conjugate, and $\Im[\ ]$ indicates the imaginary part, we integrate this for $y_1 \le y \le y_2$ under the boundary condition (6.48), and obtain

$$\omega_i k \int_{y_1}^{y_2} \tilde{\beta} \frac{|\tilde{v}|^2}{|\hat{\omega}|^2} dy = -\Im\left[\tilde{v}^* \frac{d\tilde{v}}{dy}\right]_{y=y_1}^{y=y_2} = \Im\left[\tilde{v} \frac{d\tilde{v}^*}{dy}\right]_{y=y_1}^{y=y_2} \equiv 0.$$

If an unstable solution ($\omega_i > 0$) exists, the ingration of the left-hand side must be zero, that is, the integrant changes the sign at any point of $y_1 \le y \le y_2$. Because $|\tilde{v}|^2/|\hat{\omega}|^2 > 0$, it is requested that $\tilde{\beta} = 0$, that is,

$$\frac{d^2\overline{u}}{dy^2} = \beta \qquad \text{somewhere} \quad y_1 < y < y_2, \tag{6.49}$$

which is called the *Kuo's theorem* on the *barotropic instability* (Kuo, 1949)[76]. Another form of this instability criterion is obtained by substituting $\tilde{v} \equiv \hat{\omega} V$ into (6.46) and (6.47):

$$\hat{\omega}\frac{d^2V}{dy^2} + 2\frac{d\hat{\omega}}{dy}\frac{dV}{dy} - k^2\left(\hat{\omega} + \frac{\beta}{k}\right)V = 0, \qquad V(y_1) = V(y_2) = 0,$$

taking the difference between this first equation multiplied with $\hat{\omega} V^*$ and its complex conjugate multiplied with $\hat{\omega}^* V$, and integrating the result for $y_1 \le y \le y_2$:

$$\overline{u}_{\min} - \frac{\beta}{2k^2} < c_r < \overline{u}_{\max}\,; \tag{6.50}$$

otherwise taking the sum of them and integrating the result, (in this case ${\omega_i}^2$ is constant and can be put out of the integral)

$$\left(c_r - \frac{\overline{u}_{\min} + \overline{u}_{\max}}{2}\right)^2 + {c_i}^2 \le \left(\frac{\overline{u}_{\min} + \overline{u}_{\max}}{2}\right)^2 + \frac{\beta}{2k^2}(\overline{u}_{\max} - \overline{u}_{\min}), \qquad c_i > 0, \tag{6.51}$$

where $c - \overline{u} \equiv \hat{\omega}k$, $c_r - \overline{u} \equiv \hat{\omega}_r k$, $c_r = \omega_r k$, $c_i = \omega_i k$. These are called the Pedlosky's theorem (Pedlosky, 1964, 1979)[77]. In addition, Linzen and Rosenthal (1983) and Lindzen et al. (1983) proposed to apply a concept called *overreflection* to the tropical barotropic instability proiblems, in which the unstable wave is replaced by a reflection of neutral Rossby wave at the critical point (5.30) with reflectivity > 1. This gives a unified understanding with the wave-mean flow interaction (Section 5.4): at the critical point, if the flow is stable, the mean flow accelerates by

[76]This is an extension of the so-called Rayleigh's inflection point theorem in the fluid dynamics with $\beta = 0$: if the flow is unstable, the velocity profile must have an inflection point $d^2\overline{u}/dy^2 = 0$ inside the domain.

[77](6.50) and (6.51) are respectively extensions for $\beta \neq 0$ of the Rayleigh's theorem (an unstable wave must have a critical point (5.30) in the domain) and the Howard's semicircle theorem (the unstable eigenvalues are in a semicircle on the real-axis domain in the Gauss' complex plane; Howard, 1961) obtained originally for $\beta = 0$.

absorbing the waves; whereas if unstable the waves amplify by extracting energy from the mean flow. For further details of the instability problems see dynamics textbooks (e.g., Chapter VII of Charney, 1973; Pedlosky, 1979; Lindzen, 1980; Holton, 1992).

After the approach by barotropic instability did not succeed, the neutral and forced wave theories mentioned in Chapter 5 were developed. The equatorial zone within the deformation radius (4.21) is a "waveguide" (Gill, 1982) for the equatorial waves constituting the MJO. As mentioned in Section 4.1, if the Earth was an "aqua-planet" without any lands, there would be basically zonal structures (right-hand side panel of Fig. 4.7), and the ITCZ near the equator is not homogeneous but involves the MJO/ISVs. In other words a steady zonally-elongated limit or a zonal/seasonal average ISVs become the Hadley circulations (Gill, 1980; Kosaka and Matsuda, 2005).

Those waves are also favorable for the CISK and WISHE mechanisms mentioned in the previous section, which are considered more plausible also for the ISVs. In particular the wave-CISK mechanism (Y. Hayashi, 1970; Lindzen, 1974), which is not assuming the Ekman pumping, is regarded as playing the major role to generate the ISVs such as the MJO, after the pioneering successful numerical experiment of "aqua planet" by Y.-Y. Hayashi and Sumi (1984), which also showed that the ISVs/MJO are the major features over the equatorial atmosphere-ocean system (without land or over the actual open ocean), replacing the steady homogeneous ITCZ imaged since Hadley. When we include the localized heating Q' and substitute the Ooyama's cumulus parameterization (6.23) and the equivalent depth (5.12), the thermodynamic equation (5.7) for equatorial waves may be rewritten as

$$\frac{\overline{D}\phi'}{Dt} + gh\left(\frac{\partial u'}{\partial x} + \frac{\partial v'}{\partial y}\right) \approx \eta'\left(\frac{\partial u'}{\partial x} + \frac{\partial v'}{\partial y}\right), \qquad \eta' > 0. \tag{6.52}$$

From (5.19) gh is square of the phase velocity $\hat{\omega}/k$ (relative to the media moving by the mean flow) of the equatorial Kelvin wave (and gravity waves with $f = 0$) free from any forcing. If the heating exists and is sufficiently strong ($\eta' > gh$), we have $\hat{\omega}^2 < 0$ and expect that any unstable modes ($\hat{\omega} = i\omega_i,\ \omega_i > 0$) exist (Chang and Lim, 1988). Numaguti and Hayashi (1991) examined the aqua-planet model results as a Kelvin wave-CISK, and showed that the results are quite sensitive to the cumulus parameterization scheme. The MJO is noted also as a trigger (or miniature) of the interannual variations such as ENSO (Lau et al., 1989; Lau and Peng, 1990) and IOD. On the other hand, the WISHE mechanism (Emanuel, 1987; Neelin et al., 1987) is expected to work in case of an easterly wave-like situation: wind speed, evaporation and latent heating are stronger in the eastern side (where perturbed wind is also easterly) of a convective updraft area than in the western side. This differential latent heating may intensify the eastward propagating (Kelvin or inertio-gravity) wave with the phase structure that the eastern side is warmer than the western side.

These semi-theoretical approaches, however, are still only qualitatively successful, and have not yet explained the actual dominant time and space scales (zonal wavenumbers and phase velocity of 1−3 and ~5 m/s). The too sensitive dependence upon the cumulus parameterization scheme (Numaguti and Hayashi, 1991) has not yet been settled. On the other hand a cloud-resolving model (Miura et al., 2007: Nasuno et al., 2009; Liu et al., 2009) show successful simulation results for some MJO events. Numerical experiments using this model (Takasuka et al., 2015) confirm that MJO/ISVs on an aqua planet are substantially modified if a land such as the IMC blocks the "waveguide" completely. However, a completely satisfactory theory for the MJO/ISVs has not yet been established, so that their prediction is still not good (Waliser, 2012). For further details see several overview articles (Madden and Julian,

1994; Lau and Waliser, 2005; Zhang, 2005, 2013; Yoneyama et al., 2008, 2013).

Zhang (2013) mentioned that the MJO is "bridging weather and climate". In the tropical marine atmosphere and probably also in the extratropics (including the predictability reason) it would be true. However, in the tropical land the annual cycle (which is basic in the extratropical climatology) is only the second component, but the diurnal cycle is the first. In this meaning the ISVs including MJO in the tropics are like the interannual variations. Of course at least the atmosphere is borderless in space and time, and we need to establish a seamless theoretical meteorology and climatology connecting the tropical marine, tropical land and extratropical atmospheres. Probably the MJO/ISVs over the ocean and the diurnal cycle over lands are both important and collaborating to maintain the energy and water cycles in the Earth's climate system.

Exercise 6

(1) Now T = 20C and RH = 80%. How cold does it become to make cloud or rain?
(2) At sea level T=20C and RH=80%. How high is the cloud bottom if it exists?
(3) What is necessary to realize the cloud bottom as estimated in (2) ?
(4) If a cloud is generated by 1 km^3 saturated air with T=20C, p=1000 hPa and ρ=1 kg/m^3 and disappears after making rainfall over an area of 1 km^2, how heavy rain falls?

Answers:

(1) Roughly in a phase diagram (exactly by solving 2nd eq. of (7)), $e = e_s$ (T=20C) × 0.8 ≈ 23 hPa × 0.8 ≈ 18 hPa, which is ≈ e_s (T=16C, the dew point temperature). Thus, if T cools down to 16C, it may be cloudy or rainy.
(2) From (1) the cloud bottom (or lifting condensation level=LCL) must be T=16C. Using "dry" lapse late Γ below the cloud bottom, the bottom is (20C−16C)/Γ ≈ 400 m height.
(3) In general a T-profile (as observed by rawinsonde) is slower than Γ, and LCL is warmer than the dew point. Clouds are not generated by air staying at LCL, but by air lifted from the ground (for example by a mountain slope, or by convection forced by hot ground).
(4) The cloud involves water of 1 kg/m^3 × 10^9 m^3×23 hPa/1000 hPa = 2.3 × 10^7 kg. Using the density of water 10^3 kg/m^3, the rainfall amount is 2.3 × 10^7 kg/(10^3 kg/m^3)/(10^6 m^2) = 2.3 × 10^{-2} m = 23 mm.

Acknowledgment

Contents of this article were prepared for a two-week lecture series carried out in the "Short-term Expert Training Course on Weather Forecasting I, Japan International Collaboration Agency (JICA) - Sri Lanka Department of Meteorology Improving of Meteorological Observation, Weather Forecasting and Dissemination Project", 21 November - 1 December 2016 at Sri Lanka Department of Meteorology. The author would like to express sincere thanks to the Director General Mr. Lalith Chandrapala, Director Mr. K. H. S. M. Premalal, Director Mr. Athula K. Kurunanayake, Deputy Director Ms. Anusha R. Warnasuriya and Deputy Director Ms. J. M. S. P. Jayawardena for their hospitality and collaborations, and to the JICA Expert Dr. Masahito Ishihara for his leading, hospitality and advice during the lectures and for his suggestion and comments on writing this article.

The author's teaching tropical meteorology has been done as a lecture and an associate professor at Kyoto University and a professor at Kobe University, and a senior and principal scientist at the Japan Agency for Marine-Earth Science and Technology (JAMSTEC) in Japan, and a visiting scientist at many university and institutes in Indonesia and other Southeast Asian countries. In particular the author would like to acknowledge Dr. Fadli Syamsudin of the Agency for the Assessment and Application of Technology (BPPT) of Indonesia for his collaboration and support during the "Hydrometeorological Array for IntraSeasonal Variability-Monsoon Automonitoring, Japan Earth Observation System Promotion Program" (JEPP-HARIMAU, 2005−10, funded by the Ministry of Education, Culture, Sports, Science and Technology (MEXT) of Japan) and the "Climate Variability Study and Societal Application through Indonesia - Japan Maritime Continent COE - Radar-Buoy Network Optimization for Rainfall Prediction, Science and Technology Research Partnership for Sustainable Development" (SATREPS-MCCOE, 2009−14, funded by the Japan Science and Technology Agency (JST) and JICA). In parallel, the author has been a visiting lecturer at Udayana University and Yamaguchi University since 2007, for which hospitality and advice by late Professor Yasuhiro Sugimori, Professor Tasuku Tanaka and Dr. Takahiro Osawa are also acknowledged.

Studies on subjects related to the contents of this article have been collaborated with many researchers mainly in Japan and Indonesia. In particular the author would like to thank late Professor Shoichiro Fukao, Professor Jun Matsumoto, Dr. Hiroyuki Hashiguchi, Dr. Shuichi Mori, Dr. Wu Pei-Ming, Dr. Shin-Ya Ogino, Dr. Hamada Jun-Ichi and Dr. Kimpei Ichiyanagi among them.

References

Aldrian, E., and D. Susanto, 2003: Identification of three dominant rainfall regions within Indonesia and their relationship to sea surface temperature. *Int. J. Climatol.,* **23**, 1435-1452.

Andrews, D. G., 2000: *An Introduction to Atmospheric Physics*. Cambridge University Press, 229pp.

Andrews, D. G., J. R. Holton and C. B. Leovy, 1987: *Middle Atmosphere Dynamics*. Academic Press, 489pp.

Andrews, D. G., and M. E. McIntyre, 1976. Planetary waves in horizontal and vertical shear: The generalized Eliassen–Palm relation and the mean zonal acceleration. *J. Atmos. Sci.*, **33**, 2031–2048.

Arakawa, A., and W. H. Schubert, 1974: Interaction of a cumulus cloud ensemble with the large-scale environment, Part I. *J. Atmos. Sci.*, **31**, 674–701.

Arakawa, O., and A. Kitoh, 2005: Rainfall diurnal variation over the Indonesian maritime continent simulated by 20 km-mesh GCM. *SOLA*, **1**, 109–112.

Araki, R., M. D. Yamanaka, F. Murata, H. Hashiguchi, Y. Oku, T. Sribimawati, M. Kudsy and F. Renggono, 2006: Seasonal and interannual variations of diurnal cycles of local circulation and cloud activity observed at Serpong, West Jawa, Indonesia. *J. Meteor. Soc. Japan*, **84A**, 171–194.

Asai, T., 1970: Three-dimensional features of thermal convection in a plane Couette flow. *J. Meteor. Soc. Japan*, **48**, 18–29.

Asai, T., 1972. Thermal instability of a shear flow turning the direction with height. *J. Meteor. Soc. Japan*, **50**, 525–532.

Ashok, K., S. K. Behera, S. A. Rao, H. Weng and T. Yamagata, 2007: El Niño Modoki and its possible teleconnection. *J. Geophys. Res.*, **112**, C11007, doi:10.1029/2006JC003798.

Barry, R. G., and R. J. Chorley, 2003: *Atmosphere, Weather and Climate, 8th Ed.*, Routledge, 421pp.

Battisti, D. S., and A. C. Hirst, 1989: Interannual variability in a tropical atmosphere-ocean model: Influence of the basic state, ocean geometry and nonlinearity. *J. Atmos. Sci.*, **46**, 1687–1712

Bessho, K., K. Date, M. Hayashi, A. Ikeda, T. Imai, H. Inoue, Y. Kumagai, T. Miyakawa, H. Murata, T. Ohno, A. Okuyama, R. Oyama, Y. Sasaki, Y. Shimazu, K. Shimoji, Y. Sumida, M. Suzuki, H. Taniguchi, H. Tsuchiyama, D. Uesawa, H. Yokota and R. Yoshida, 2016: An introduction to Himawari-8/9: Japan's new-generation Geostationary Meteorological Satellites. *J. Meteor. Soc. Japan*, **94**, 151−183.

Bjerknes, J., 1969: Atmospheric teleconnections from the equatorial Pacific. *Mon. Wea. Rev.*, **97**, 163–172.

Booker, J. R., and F. P. Bretherton, 1967: The critical layer for internal gravity waves in a shear flow. *J. Fluid Mech.*, **27**, 513−539.

Brewer, A. W., 1949: Evidence for a world circulation provided by the measurements of Helium and Water vapour distribution in the stratosphere. *Quart. J. Roy. Meteor. Soc.*, **75**, 351-363.

Broecker, W. S., 1991: The great ocean conveyor. *Oceanography*, **4**(2), 79-89.

Chan, J. C. L., and K.S. Liu, 2004: Global warming and western North Pacific typhoon activity from an observational perspective, *J. Climate*, **17**, 4590–4602.

Chang, C.-P., and H. Lim, 1988: Kelvin wave-CISK: A possible mechanism for the 30–50 day oscillations. *J. Atmos. Sci.*, 45, 1709–1720.

Chang, C.-P., C.-H. Liu and H.-C. Kuo, 2003: Typhoon Vamei: An equatorial tropical cyclone formation. *Geophys. Res. Lett.*, **30**, L1150, doi:10.1029/2002GL016365.

Chang, C.-P., Z. Wang, J. Ju and T. Li, 2004a: On the relationship between western Maritime Continent monsoon rainfall and ENSO during northern winter. *J. Climate*, **17**, 665–672.

Chang, C.-P., P. A. Harr, J. C. McBride and H. H. Hsu, 2004b: Maritime continent monsoon: Annual cycle and boreal winter variability. *East Asia Monsson*, C. P. Chang ed., 107-152.

Chang, C.-P., Z. Wang, J. L. McBride and C.-H. Liu, 2005: Annual cycle of Southeast Asia-Maritime Continent rainfall and the asymmetric monsoon transition. *J. Climate*, **18**, 287–301.

Charney, J. G., 1973: Planetary fluid dynamics. *Dynamic Meteorology*, P. Morel, Ed., D. Reidel Pub. Co., 97–351. (Springer)

Charney, J. G., and A. Eliassen, 1964: On the growth of the hurricane depression. *J. Atmos. Sci.*, **21**, 68–75.

Cheang, B. K., 1977: Synoptic features and structures of some equatorial vortices over the South China Sea in the Malaysian region during the winter monsoon, December 1973. *Pure Appl. Geophys*., **115**, 1303–1333.

Chen, H., P. Malanotte-Rizzoli, T.-Y. Koh and G. Song, 2014: The relative importance of the wind-driven and tidal circulations in Malacca Strait. *Continental Shelf Res.*, **88**, 92–102.

Chen, T.-C., 2002: A north Pacific short-wave train during the extreme phases of ENSO. *J Climate*, **15**, 2359–2376.

Chen, T.-C., J.-D. Tsay, M.-C. Yen and J. Matsumoto, 2013: The winter rainfall of Malaysia. *J. Climate*, **26**, 936–958.

Chen, T.-C., J.-D. Tsay, J. Matsumoto and J. Alpert, 2015: Development and formation mechanism of the Southeast Asian winter heavy rainfall events around the South China Sea. Part I: Formation and propagation of cold surge vortex. *J. Climate*, **28**, 1417–1443.

Corby, G. A., 1954: The airflow over mountains: A review of the state of current knowledge. *Quart. J. Roy. Meteor. Soc.*, **80**, 491–521.

Cunnold, D., F. Alyea, N. Phillips and R. Prinn, 1975: A three-dimensional dynamical-chemical model of atmospheric ozone. *J. Atmos. Sci.*, **32**, 170–194.

Dengler, K., 1997: A numerical study of the effects of land proximity and changes in sea surface temperature on hurricane tracks. *Quart. J. Roy. Meteor.. Soc.*, **123**, 1307–1321.

Dobson, G. M. B., 1956: Origin and distribution of polyatomic molecules in the atmosphere. *Proc. Roy. Soc. London*, **A236**, 187-193.

Dunkerton, T. J., 1979: On the role of the Kelvin wave in the westerly phase of the semiannual zonal wind oscillation. *J. Atmos. Sci.*, **36**, 32–41.

Dunkerton, T. J., 1981: On the inertial stability of the equatorial middle atmosphere. *J. Atmos. Sci.*, **38**, 2354–2364.

Dunkerton, T. J., 1982: Theory of the mesopause semiannual oscillation. *J. Atmos. Sci.*, **39**, 2681–2690.

Dunkerton, T. J., 1983: A nonsymmetric equatorial inertial instability. *J. Atmos. Sci.*, **40**, 807–813.
Durran, D. R., 1990: Mountain waves and downslope winds. *Atmospheric Processes over Complex Terrain*, W. Blumen Ed., American Meteorological Society, 59–82.
Eliassen, A., and E. Palm, 1961: On the transfer of energy in stationary mountain waves. *Geofys. Publ.*, **22**(3), 1–23.
Emanuel, K. A., 1987: An air-sea interaction model of intraseasonal oscillations in the tropics. *J. Atmos. Sci.*, **44**, 2324–2430.
Emanuel, K. A., 1994: *Atmospheric Convection*. Oxford Univ. Press, 580pp.
Emanuel, K. A., 2005: Increasing destructiveness of tropical cyclones over the past 30 years. *Nature*, **436**, 686–688.
Estoque, M., 1962: The sea breeze as a function of the prevailing synoptic situation. *J. Atmos. Sci.*, **19**, 244–250.
Fiondella, F., 2009: Can we blame El Niño? https://www.climate.gov/news-features/understanding-climate/can-we-blame-el-ni%C3%B1o
Fovell, R. G. 2005. Convective initiation ahead of the sea-breeze front. *Mon. Wea. Rev.*, **133**, 264–278.
Fritts, D. C., and T. J. Dunkerton, 1984: A quasi-linear study of gravity wave saturation and self-acceleration. *J. Atmos. Sci.*, **41**, 3272–3289.
Fudeyasu, H., K. Ichiyanagi, A. Sugimoto, K Yoshimura, A. Ueta, M. D. Yamanaka and K. Ozawa, 2008a: Isotope ratios of precipitation and water vapor observed in Typhoon Shanshan. *J. Geophys. Res.*, **113**, D12113, doi:doi:10.1029/2007JD009313.
Fudeyasu, H., Y. Wang, M. Satoh, T. Nasuno, H. Miura and W. Yanase, 2008b: Global cloud-system-resolving model NICAM successfully simulated the lifecycles of two real tropical cyclones. *Geophys. Res. Lett.*, **35**, L22808, doi:10.1029/2008GL036003
Fudeyasu, H., K. Ichiyanagi, K. Yoshimura, S. Mori, N. Sakurai, Hamada J.-I., M. D. Yamanaka, J. Matsumoto and F. Syamsudin, 2011: Effects of large-scale moisture transport and mesoscale processes on precipitation isotope ratios observed at Sumatera, Indonesia. *J. Meteor. Soc. Japan*, **89A**, 49-59.
Fujita, M., F. Kimura and M. Yoshizaki, 2010: Morning precipitation peak over the Strait of Malacca under a calm condition. *Mon. Wea. Rev.*, **138**, 1474-1486.
Fujita, M., K. Yoneyama, S. Mori, T. Nasuno and M. Satoh, 2011: Diurnal convection peaks over the eastern Indian Ocean off Sumatra during different MJO phases. *J. Meteor. Soc. Japan*, **89A**, 317-330.
Fujiwara, M., 1965: Raindrop-size distribution from individual storms. *J. Atmos. Sci.*, **22**, 585–591.
Fujiwhara, S., 1923: On the growth and decay of vortical systems. *Quart. J. Roy. Meteor. Soc.*, **49**, 75–104.
Fukao, S., 2006: Coupling Processes in the Equatorial Atmosphere (CPEA): A project overview. *J. Meteor. Soc. Japan*, **84A**, 1–18.
Fukao, S., and K. Hamazu, 2014: *Radar for Meteorological and Atmospheric Observations*. Springer, 537pp.
Gage, K. S., and G. D. Nastrom, 1985: On the spectrum of atmospheric velocity fluctuations seen by MST/ST radar and their interpretation. *Radio Sci.*, **20**, 1339–1347.
Garcia, R. R., and F. Sassi, 1999: Modulation of the mesospheric semiannual oscillation by the quasibiennial oscillation. *Earth Planets Space*, **51**, 563–569.
Gill, A. E., 1980: Some simple solutions for heat-induced tropical circulation. *Quart. J. Roy. Meteor. Soc.*, **106**, 447–462.
Gill, A., E., 1982: *Atmosphere-Ocean Dynamics*. Academic Press, 662pp.
Gordon, A. L., 2005: Oceanography of the Indonesian seas and their throughflow. *Oceanography*, **18**(4), 14–27.
Hadi, T. W., T. Tsuda, H. Hashiguchi and S. Fukao, 2000: Tropical sea-breeze circulation and related atmospheric phenomena observed with *L*-band boundary layer radar in Indonesia. *J. Meteor. Soc. Japan*, **78**, 123–140.
Hadi, T. W., T. Horinouchi, T. Tsuda, H. Hashiguchi and S. Fukao, 2002: Sea-breeze circulation over Jakarta, Indonesia: A climatology based on boundary layer radar observations. *Mon. Wea. Rev.*, **130**, 2153–2166.
Hadley, G., 1735: Concerning the cause of the general trade-winds. *Phil. Trans.*, **39**, 58–62.
Hall, J. D., A. J. Matthews and D J. Karoly, 2001: The modulation of tropical cyclone activity in the Australian region by the Madden–Julian oscillation. *Mon. Wea. Rev.*, **129**, 2970–2982.
Halley, E., 1686: An historical account of the trade winds, and monsoons, observable in the seas between and near the Tropicks, with an attempt to assign the phisical cause of the said winds. *Phil. Trans.*, **16**, 153-168.
Hamada, J.-I., S. Mori, M. D. Yamanaka, U. Haryoko, S. Lestari, R. Sulistyowati and F. Syamsudin, 2012: Interannual rainfall variability over northwestern Jawa and its relation to the Indian Ocean dipole and El Niño-southern oscillation events, *SOLA*, **8**, 69‑72.
Hamada, J.-I., M. D. Yamanaka, J. Matsumoto, S. Fukao, P. A. Winarso and T. Sribimawati, 2002: Spatial and temporal variations of the rainy season over Indonesia and their link to ENSO. *J. Meteor. Soc. Japan*, **80,** 285–310.
Hamada J.-I., M. D. Yamanaka, S. Mori, Y. I. Tauhid and T. Sribimawati, 2008: Differences of rainfall characteristics between coastal and interior areas of central western Sumatera, Indonesia. *J. Meteor. Soc. Japan*, **86**, 593–611.
Hamid, E. Y., Z.-I. Kawasaki and R. Mardiana, 2001: Impact of the 1997–98 El Niño event on lightning activity over Indonesia. *Geophys. Res. Lett.*, **28**, 147–150.
Hara, M., T. Yoshikane, H. G. Takahashi, F. Kimura, A. Noda and T. Tokioka, 2009: Assessment of the diurnal cycle of precipitation over the Maritime Continent simulated by a 20 km mesh GCM using TRMM PR data. *J. Meteor. Soc. Japan*, **87A**, 413–424.
Hartmann, D. L., 1994: *Global Physical Climatology*, Academic Press, 411pp.
Hashiguchi, H., S. Fukao, T. Tsuda, M. D. Yamanaka, D. L. Tobing, T. Sribimawati, S. W. B. Harijono and H. Wiryosumarto, 1995a: Observations of the planetary boundary layer over equatorial Indonesia with an *L*-band clear-air Doppler radar: Initial results. *Radio Sci.*, **30**, 1043–1054.
Hashiguchi, H., S. Fukao, M. D. Yamanaka, T. Tsuda, S. W. B. Harijono and H. Wiryosumarto, 1995b: Boundary layer radar observations of the passage of the convection center over Serpong, Indonesia (6°S, 107°E) during the TOGA-COARE intensive observation period. *J. Meteor. Soc. Japan*, **73**, 535–548.
Hashiguchi, H., M. D. Yamanaka, T. Tsuda, M. Yamamoto, T. Nakamura, T. Adachi, S. Fukao, T. Sato and D. L. Tobing, 1995c: Diurnal variations of the planetary boundary layer observed with an *L*-band clear-air Doppler radar. *Boundary-Layer Meteor.*, **74**, 419-424.
Hashiguchi, H., S. Fukao, M. D. Yamanaka and T. Tsuda, 1997: Frequency spectra of wind velocity fluctuations between 1 hour and 1

month in the atmospheric boundary layer over equatorial Indonesia. *J. Geomag. Geoelectr.*, **49**, S187–S195.
Hattori, M., S. Mori, and J. Matsumoto, 2011: The cross-equatorial northerly surge over the maritime continent and its relationship to precipitation patterns. *J. Meteor. Soc. Japan*, **89A**, 27-47.
Hayashi, Y., 1970: A theory of large-scale equatorial waves generated by condensation heat and accelerating the zonal wind. *J. Meteor. Soc. Japan*, **48**, 140-160.
Hayashi, Y.-Y., 1987: Linear theory of two dimensional steady Rossby waves. *Meteor. Res. Note, Meteor. Soc. Japan*, **156**, 29–48 (in Japanese).
Hayashi, Y.-Y., and T. Matsuno, 1984: Amplitude of Rossby wavetrains on a sphere. *J. Meteor. Soc. Japan*, **62**, 377–387.
Hayashi, Y.-Y., and A. Sumi, 1985: The 30-40 day oscillations simulated in an "aqua planet" model. *J. Meteor. Soc. Japan*, **64**, 451−467.
Haylock, M., and J. McBride, 2001: Spatial coherence and predictability of Indonesian wet season rainfall. *J. Climate*, **14**, 3882–3887.
Held, I. M., and A. Y. Hou, 1980: Nonlinear axially symmetric circulations in a nearly inviscid atmosphere. *J. Atmos. Sci.*, **37**, 515–533.
Hendon, H. H., 2003: Indonesian rainfall variability: Impacts of ENSO and local air–sea interaction. *J. Climate*, **16**, 1775–1790.
Hendon, H. H., and B. Liebmann, 1990: The intraseasonal (30–50 day) oscillation of the Australian summer monsoon. *J. Atmos. Sci.*, **47**, 2909–2923.
Hendon, H. H., and K. Woodberry, 1993: The diurnal cycle of tropical convection. *J. Geophys. Res.*, **98**, 16623–16637.
Hidayat, R., and S. Kizu, 2010: Influence of the Madden-Julian Oscillation on Indonesian rainfall variability in austral summer. *Int. J. Climatol.*, **30**, 1816-1825.
Hidayat, S., and M. Ishii, 1998: Spatial and temporal distribution of lightning activity around Java. *J. Geophys. Res.*, **103**, 14001–14009.
Hirota, I., 1978: Equatorial waves in the upper stratosphere and mesosphere in relation to the semiannual oscillation of the zonal wind. *J. Atmos. Sci.*, **35**, 714–722.
Hirota, I., 1979: Kelvin waves in the equatorial middle atmosphere observed by the Nimbus 5 SCR. *J. Atmos. Sci.*, **36**, 217–222.
Holton, J. R., 1982: The role of gravity wave induced drag and diffusion in the momentum budget of the mesosphere. *J. Atmos. Sci.*, **39**, 791–799
Holton, J. R., 1992: *An Introduction to Dynamic Meteorology*, 3rd Ed., Academic Press, 511pp.
Holton, J. R., P. H. Haynes, M. E. McIntyre, A. R. Douglass, R. B. Rood and L. Pfister 1995: Stratosphere-troposphere exchange. *Rev. Geophys.*, **33**, 403-439.
Holton, J. R., and R. S. Lindzen, 1972: An updated theory for the quasi-biennial cycle of the tropical stratosphere. *J. Atmos. Sci.*, **29**, 1076–1080.
Horel, J. D., and J. M. Wallace, 1981: Planetary-scale atmospheric phenomena associated with the southern oscillation. *Mon Wea. Rev.*, **109**, 813–829.
Horinouchi, T., and S. Yoden, 1996: Excitation of transient waves by localized episodic heating in the tropics and their propagation into the middle atmosphere. *J. Meteor. Soc. Japan*, **74**, 189–210.
Horinouchi, T., T. Nakamura and J.-i. Kosaka, 2002: Convectively generated mesoscale gravity waves simulated throughout the middle atmosphere. *Geophys. Res. Lett.*, **29**(21), L2007, doi:10.1029/2002GL016069.
Horinouchi, T., S. Pawson, K. Shibata, U. Langematz, E. Manzini, M. A. Giorgetta, F. Sassi, R. J. Wilson, K. Hamilton, J. de Grandpré and A. A. Scaife, 2003: Tropical cumulus convection and upward-propagating waves in middle-atmospheric GCMs. *J. Atmos. Sci.*, **60**, 2765–2782.
Hoskins, B. J., and D. J. Karoly, 1981: The steady linear response of a spherical atmosphere to thermal and orographic forcing. *J. Atmos. Sci.*, **38**, 1179–1196.
Houze, R. A. Jr., 1993: *Cloud Dynamics*. Academic Press, 573pp.
Houze, R. A., Jr., S. G. Geotis, F. D. Marks Jr. and A. K. West, 1981: Winter monsoon convection in the vicinity of north Borneo. Part I: Structure and time variation of the clouds and precipitation. *Mon. Wea. Rev.*, **109**, 1595–1614.
Howard, L. N., 1961: Note on a paper of John W. Miles. *J. Fluid Mech.*, **10**, 509–512.
Ichikawa, H., and T. Yasunari, 2007: Propagating diurnal disturbances embedded in the Madden–Julian Oscillation. *Geophys. Res. Lett.*, **34**, L18811, doi:10.1029/2007GL030480
Ichiyanagi, K., 2007: Review: Studies and Applications of Stable Isotopes in Precipitation. *J. Japan. Assoc. Hydrol. Sci.*, **37**(4), 165-185.
IPCC (Intergovernmental Panel on Climate Change), 2007: *Climate Change 2007 - The Physical Science Basis: Working Group I Contribution to the Fourth Assessment Report of the IPCC*, Cambridge University Press, 1009pp.
Ishihara, M., Z. Yanagisawa, H. Sakakibara, K. Matsuura and J. Aoyagi, 1986: Structure of a typhoon rainband observed by two Doppler radars. *J. Meteor. Soc. Japan*, **64**, 923–939.
Israelachvili, J. N., 1992: *Intermolecular and Surface Force, 2nd Ed.*, Academic Press, 450pp.
Iwasaki, T., S. Yamada and K. Tada, 1989a: A parameterization scheme of orographic gravity wave drag with two different vertical partitionings, Part I: Impacts on medium-range forecasts. *J. Meteor. Soc. Japan*, **67**, 11-21.
Iwasaki, T., S. Yamada and K. Tada, 1989b: A parameterization scheme of orographic gravity wave drag with two different vertical Partitionings, Part II: Zonally averaged budget analysis based on transformed Eulerian-mean (TEM) method. *J. Meteor. Soc. Japan*, **67**, 29-41.
Johnson, R. H., 1992: Heat and moisture sources and sinks of Asian monsoon precipitating systems. *J. Meteor. Soc. Japan*, **70**, 353–372.
Johnson, R. H., 2011: Diurnal cycle of monsoon convection. *The Global Monsoon System: Research and Forecast*, 2nd Ed., C.-P. Chang et al. (eds.), World Scientific Pub. Co., 257–276.
Johnson, R. H., and P. E. Ciesielski, 2013: Structure and properties of Madden--Julian Oscillations deduced from DYNAMO sounding arrays. *J. Atmos. Sci.*, **70**, 3157–3179.
Johnson, R. H., and D. C. Kriete, 1982: Thermodynamic and circulation characteristics of winter monsoon tropical mesoscale convection. *Mon. Wea. Rev.*, **110**, 1898–1911.

Johnson, R. H., and D. L. Priegnitz, 1981: Winter monsoon convection in the vicinity of north Borneo. Part II: Effects on large-scale fields. *Mon. Wea. Rev.*, 109, 1615–1628.
Jones, W. L., 1967: Propagation of internal gravity waves in fluids with shear and rotation. *J. Fluid Mech.*, **30**, 439–448.
Kamimera, H., S. Mori, M.D. Yamanaka and F. Syamsudin, 2012: Modulation of diurnal rainfall cycle by the Madden-Julian oscillation based on one-year continuous observations with a meteorological radar in West Sumatera. *SOLA*, **8**, 111–114.
Kanamori, H., T. Yasunari and K. Kuraji, 2013: Modulation of the diurnal cycle of rainfall associated with the MJO observed by a dense hourly rain gauge network at Sarawak, Borneo. *J. Climate*, **26**, 4858-4875.
Kato, S., 1966: Diurnal atmospheric oscillation, I: Eigenvalues and Hough functions. *J. Geophys. Res.*, **71**, 3201–3209.
Kato, S., 1980: *Dynamics of the Upper Atmosphere*. D. Reidel, 233pp.
Kawashima, M., Y. Fujiyoshi, M. Ohi, T. Honda, T. Kozu, T. Shimomai and H. Hashiguchi, 2006: Overview of Doppler radar observations of precipitating cloud systems in Sumatera Island during the first CPEA campaign. *J. Meteor. Soc. Japan*, **84A**, 33-56.
Kawashima, M., Y. Fujiyoshi, M. Ohi, T. Honda, S. Mori, N. Sakurai, Y. Abe, W. Harjupa, F. Syamsudin, and M. D. Yamanaka, 2011: Case study of an intense wind event associated with a mesoscale convective system in west Sumatera during the HARIMAU2006 campaign. *J. Meteor. Soc. Japan*, **89A**, 239-257.
Kawatani, Y., and K. Hamilton, 2013: Weakened stratospheric quasibiennial oscillation driven by increased tropical mean upwelling. *Nature*, **497**, 478–481.
Kawatani, Y., K. Sato, T. J. Dunkerton, S. Watanabe, S. Miyahara and M. Takahashi, 2010a: The roles of equatorial trapped waves and internal inertia-gravity waves in driving the quasi-biennial oscillation, Part I: Zonal mean wave forcing. *J. Atmos. Sci.*, **67**, 963–980.
Kawatani, Y., K. Sato, T. J. Dunkerton, S. Watanabe, S. Miyahara and M. Takahashi, 2010b: The roles of equatorial trapped waves and internal inertia-gravity waves in driving the quasi-biennial oscillation, Part II: Three-dimensional distribution of wave forcing. *J. Atmos. Sci.*, **67**, 981–997.
Kida, H., 1983a: General circulation of air parcels and transport characteristics derived from a hemispheric GCM. Part 1. A determination of advective mass flow in the lower stratosphere. *J. Meteor. Soc. Japan*, **61**, 171–187.
Kida, H., 1983b: General circulation of air parcels and transport characteristics derived from a hemispheric GCM. Part 2. Very long-term motions of air parcels in the troposphere and stratosphere. *J. Meteor. Soc. Japan*, **61**, 510–523.
Kimura, R., 1975: Dynamics of steady convections over heat and cool islands. *J. Meteor. Soc. Japan*, **53**, 440–457.
Klingaman, W. K., and N. P. Klingaman, 2013: *The Year without Summer: 1816 and the Volcano That Darkened the World and Changed History*. St. Martin's, 338pp.
Kodama, Y.-M., M. Tokuda and F. Murata, 2006: Convective activity over the Indonesian maritime continent during CPEA-I as evaluated by lightning activity and Q1 and Q2 profiles. *J. Meteor. Soc. Japan*, **84A**, 133-149.
Kosaka, Y., and Y. Matsuda, 2005: Roles of Rossby and gravity waves on circulation associated with tropical and subtropical heating. *J. Meteor. Soc. Japan*, **83**, 481–498.
Koseki, S., T.-Y. Koh, and C.-K. Teo, 2013: Effects of the cold tongue in the South China Sea on the monsoon, diurnal cycle and rainfall in the Maritime Continent. *Quart. J. Roy. Meteor. Soc.*, 139, 1566–1582.
Kozu, T., K. K. Reddy, S. Mori, M. Thurai, J. T. Ong, D. N. Rao and T. Shimomai, 2006: Seasonal and diurnal variations of raindrop size distribution in Asian monsoon region. *J. Meteor. Soc. Japan*, **84A**, 195–209.
Krishnamurti, T. N., 1971: Tropical east–west circulations during the northern summer. *J. Atmos. Sci.*, **28**, 1342–1347.
Krishnamurti, T. N., M. Kanamitsu, W. J. Koss, and J. D. Lee, 1973: Tropical east–west circulations during the northern winter. *J. Atmos. Sci.*, **30**, 780–787.
Kubota, H., 2012: Variability of typhoon tracks and genesis over the western North Pacific. *Cyclones: Formation, Triggers and Control*, K. Oouchi and H. Fudeyasu Eds., Nova Science Publ., 95–114.
Kubota, H., and J. C. L. Chan, 2009: Interdecadal variability of tropical cyclone landfall in the Philippines from 1902 to 2005. *Geophys. Res. Lett.*, **36**, L12802, doi:10.1029/2009GL038108.
Kubota, H., and Ts. Nitta, 2001: Diurnal variations of tropical convection observed during the TOGA-COARE. *J. Meteor. Soc. Japan*, **79**, 815–830.
Kubota, H., R. Shirooka, Hamada J.-I. and F. Syamsudin, 2011: Interannual rainfall variability over the eastern maritime continent. *J. Meteor. Soc. Japan*, **89A**, 111–122.
Kubota, H., J. C. L. Chan, J. Matsumoto and E. W. L. Ginn, 2012: Shifts in typhoon tracks over the western North Pacific during the 20th century based on the recovery of historical data. *30th AMS Conference on Hurricanes and Tropical Meteorology*, The American Meteorological Society, 1B.7.
Kuo, H. L., 1949: Dynamic instability of two-dimensional nondivergent flow in a barotropic atmosphere. *J. Meteor.*, **6**, 105–122.
Kuo, H. L., 1974: Further studies of the parameterization of the influence of cumulus convection on large-scale flow. *J. Atmos. Sci.*, **31**, 1232–1240.
Kurita, N., K. Ichiyanagi, J. Matsumoto, M. D. Yamanaka and T. Ohata, 2009: The relationship between the isotopic content of precipitation and the precipitation amount in tropical regions. *J. Geochem. Explor.*, **102**, 113-122.
Lamb, D., 2003: Cloud microphysics. *Encyclopedia of Atmospheric Sciences*, Holton, J. R., J. A. Curry and J. A. Pyle, Eds., 459–467.
Lau, K.-M., and P. H. Chan, 1986: Aspects of the 40–50 day oscillation during the northern summer as inferred from outgoing longwave radiation. *Mon. Wea. Rev.*, **114**, 1354–1367.
Lau, K.-M., and L. Peng, 1990: Origin of low frequency (intraseasonal) oscillations in the tropical atmosphere. Part III: Monsoon dynamics. *J. Atmos. Sci.*, **47**, 1443–1462.
Lau, K.-M., and D. E. Waliser (eds), 2005: *Intraseasonal Variability in the Atmosphere-Ocean Climate System*, Praxis Publ., 436 pp.
Lau, K.-M., C.-H. Sui and T. Nakazawa, 1989 Dynamics of westerly wind burst, supercloud clusters, 30-60 day oscillations and ENSO:

A unifying view. *J. Meteor. Soc. Japan*, **67**, 205–219
Lau, K. M., M. K. Kim and K. M. Kim, 2006: Asian summer monsoon anomalies induced by aerosol direct forcing: the role of the Tibetan Plateau. *Clim. Dyn.*, **26**, 855–864.
Lestari, S., Hamada J.-I., F. Syamsudin, Sunaryo, J. Matsumoto and M. D. Yamanaka, 2016: ENSO influences on rainfall extremes around Sulawesi and Maluku Islands in the eastern Indonesian maritime continent. *SOLA*, **12**, 37-41.
Liebmann, B., H. H. Hendon and J. D. Glick, 1994: The relationship between tropical cyclones of the western Pacific and Indian Oceans and the Madden-Julian oscillation. *J. Meteor. Soc. Japan*, **72**, 401–412.
Lin, Y.-L., 2007: *Mesoscale Meteorology*. Cambridge University Press, 630pp.
Lindzen, R. S., 1966: On the theory of the diurnal tide. *Mon. Wea. Rev.*, **94**, 295–301.
Lindzen, R. S., 1974: Wave-CISK in the tropics. *J. Atmos. Sci.*, **31**, 156–179.
Lindzen, R. S., 1981: Turbulence and stress owing to gravity wave and tidal breakdown. *J. Geophys. Res.*, **86**, 9707–9714.
Lindzen, R. S., 1990: *Dynamics in Atmospheric Physics*. Cambridge University Press, 310pp.
Lindzen, R. S., and J. R. Holton, 1968: A theory of the quasi-biennial oscillation. *J. Atmos. Sci.*, **25**, 1095–1107.
Lindzen, R. S., and A. Y .Hou 1988: Hadley circulations for zonally averaged heating centered off the equator. *J. Atmos. Sci.*, **45**, 2416–2427.
Lindzen, R. S., and A. J. Rosenthal, 1983: Charney's problem for baroclinic instability applied to barotropic instability. *J. Atmos. Sci.*, **40**, 1029–1034.
Lindzen, R. S., B. Farrel and A. J. Rosenthal, 1983: Absolute barotropic instability and monsoon depressions. *J. Atmos. Sci.*, **40**, 1178–1184.
Liu, P., M. Satoh, B. Wang, H. Fudeyasu, T. Nasuno, T. Li, H. Miura, H. Taniguchi, H. Masunaga, X. Fu and H. Annamalai, 2009: An MJO simulated by the NICAM at 14-and 7-km resolutions. *Mon. Wea. Rev.*, **137**, 3254–3268.
Lorenz, E. N., 1963: Deterministic nonperiodic flow. *J. Atmos. Sci.*, **20**, 130–141.
Love, B. S., A. J. Matthews and G. M. S. Lister, 2011: The diurnal cycle of precipitation over the Maritime Continent in a high-resolution atmospheric model. *Quart. J. Roy. Meteor. Soc.*, **137**, 934-–947.
Lukas, R., T. Yamagata and J. P. McCreary, 1996: Pacific low-latitude western boundary currents and the Indonesian throughflow. *J. Geophys. Res.*, **101**, 12209–12216.
Lunine, J. I., 1999: *Earth: Evolution of a Habitable World*. Cambridge University Press, 319pp.
Madden, R. A., and P. R. Julian, 1971: Detection of a 40-50 day oscillation in the zonal wind in the tropical Pacific. *J. Atmos. Sci.*, **28**, 702–708.
Madden, R. A., and P. R. Julian,, 1972: Description of global-scale circulation cells in the tropics with a 40-50 day period. *J. Atmos. Sci.*, **29**, 1109–1123.
Madden, R. A., and P. R. Julian, 1994: Observations of the 40–50-day tropical oscillation: A review. *Mon. Wea. Rev.*, **122**, 814–837.
Maloney, E. D., and D. L. Hartmann, 2001: The Madden–Julian oscillation, barotropic dynamics, and North Pacific tropical cyclone formation. Part I: Observations. *J. Atmos. Sci.*, **58**, 2545–2558.
Manabe, S., and R. Strickler, 1964: Thermal equilibrium of the atmosphere with convective adjustment. *J. Atmos. Sci.*, **21**, 361–385.
Mapes, B. E., T. T. Warner, M. Xu and A. J. Negri, 2003a: Diurnal patterns of rainfall in northwestern South America. Part I: Observations and context. *Mon. Wea. Rev.*, **131**, 799–812.
Mapes, B. E., T. T. Warner and M. Xu, 2003b: Diurnal patterns of rainfall in northwestern South America. Part III: Diurnal gravity waves and nocturnal convection offshore. *Mon. Wea. Rev.*, **131**, 830–844.
Marshall, J., and R. A. Plumb, 2008 *Atmosphere, Ocean, and Climate Dynamics: An Introductory Text*. Academic Press, 319pp.
Marzuki, H. Hashiguchi, M.K. Yamamoto, M. Yamamoto, S. Mori, M.D. Yamanaka, R.E. Carbone and J.D. Tuttle, 2013: Cloud episode propagation over the Indonesian maritime continent from 10 Years of infrared brightness temperature observations. *Atmos. Res.*, **120-121**, 268-286.
Matsuda, Y., 1980: Dynamics of the four-day circulation in the Venus atmosphere. *J. Meteor. Soc. Japan*, **58**, 443–470.
Matsumoto, J., 1992: The seasonal changes in Asian and Australian monsoon regions. *J. Meteor. Soc. Japan*, **70**, 257–273.
Matsumoto, J., and T. Murakami, 2000: Annual changes of tropical convective activities as revealed from equatorial symmetric OLR data. *J. Meteor. Soc. Japan*, **78**, 543–561.
Matsumoto, J., B. Wang, G.-X. Wu, J.-P. Li, P.-M. Wu, M. Hattori, S. Mori, M. D. Yamanaka, Hamada J.-I., F. Syamsudin, T. Koike, K. Tamagawa, E. Ikoma, H. Kinutani, H. Kamahori, K. Kamiguchi and Y. Harada, 2017: An overview of the Asian Monsoon Years 2007-2012 (AMY) and multi-scale interactions in the extreme rainfall events over the Indonesian maritime continent. *The Global Monsoon System: Research and Forecast, 3rd Ed.*, C.-P. Chang, H.-C. Kuo, N.-C. Lau, R. H. Johnson, B. Wang and M. C. Wheeler (eds), World Scientific Series on Asia-Pacific Weather and Climate: Vol.9, World Scientific Publication Company, 365-386.
Matsuno, T., 1966: Quasi-geostrophic motions in the equatorial area. *J. Meteor. Soc. Japan*, **44**, 25–43.
Matsuno, T., 1982: A quasi one-dimensional model of the middle atmosphere circulation interacting with internal gravity waves. *J. Meteor. Soc. Japan*, **60**, 215-226
McBride J. L., M. R. Haylock and N. Nicholls N., 2003, Relationships between the Maritime Continent heat source and the El Niño-Southern Oscillation phenomenon. *J. Climate*, **16**, 2905–2914
McPhaden, M. J., 1999: Genesis and evolution of the 1997–98 El Niño, *Science*, **283**, 950–954.
Mega, T., M. K. Yamamoto, H. Luce, Y. Tabata, H. Hashiguchi, M. Yamamoto, M. D. Yamanaka and S. Fukao, 2010: Turbulence generation by Kelvin-Helmholtz instability in the tropical tropopause layer observed with a 47-MHz range imaging radar. *J. Geophys. Res.*, **115**, D18115, doi:10.1029/2010JD013864.
Mega, T., M. K. Yamamoto, M. Abo, Y. Shibata, H. Hashiguchi, N. Nishi, T. Shimomai, Y. Shibagaki, M. Yamamoto, M. D. Yamanaka, S. Fukao and T. Manik, 2012: First simultaneous measurement of vertical air velocity, particle fall velocity, and hydrometeor

sphericity in stratiform precipitation: Results from 47-MHz wind profiling radar and 532-nm polarization lidar observations. *Radio Sci.*, **47**, RS3002, doi:10.1029/2011RS004823.
Milanković, 1941: *Kanon der Erdbestrahlung und Seine Anwendung auf das Eiszeitenproblem*. (Japanese translation by Kashiwaya et al., 1992, Kokin Shoin, 516pp.)
Miles, J. W., 1961: On the stability of heterogeneous shear flows. *J. Fluid Mech.*, **10**, 496–508.
Mitchell, J. M., 1976: An overview of climatic variability and its causal mechanisms. *Quaternary Res.*, **6**, 481-493.
Miura, H., M. Satoh, T. Nasuno, A. T. Noda and K. Oouchi, 2007: A Madden-Julian oscillation event realistically simulated by a global cloud-resolving model. *Science*, **318**, 1763-1765.
Miyahara, S., 1981: Zonal mean winds induced by solar diurnal tides in the lower thermosphere. *J. Meteor. Soc. Japan*, **59**, 303–319.
Miyakoda, K., 1963: Some characteristic features of winter circulation in the troposphere and the lower stratosphere. *Tech. Rep.*, No.14, Dept. Geophys. Sci., Univ. Chicago, 93pp.
Moncrieff, M. W., D. E. Waliser, M. J. Miller, M. E. Shapiro, G. Asrar, and J. Caughey, 2012: Multiscale convective organization and the YOTC Virtual Global Field Campaign. *Bull. Amer. Meteor. Soc.*, 93, 1171–1187.
Mori, S., J.-I. Hamada, Y. I. Tauhid, M. D. Yamanaka, N. Okamoto, F. Murata, N. Sakurai and T. Sribimawati, 2004: Diurnal rainfall peak migrations around Sumatera Island, Indonesian maritime continent observed by TRMM satellite and intensive rawinsonde soundings. *Mon. Wea. Rev.*, **132**, 2021-2039.
Mori, S., Hamada J.-I., N. Sakurai, H. Fudeyasu, M. Kawashima, H. Hashiguchi, F. Syamsudin, A. A. Arbain, R. Sulistyowati, J. Matsumoto and M. D. Yamanaka, 2011: Convective systems developed along the coastline of Sumatera Island, Indonesia observed with an X-band Doppler radar during the HARIMAU2006 campaign. *J. Meteor. Soc. Japan*, **89A**, 61–81.
Murakami, T., and J. Matsumoto, 1994: Summer monsoon over the Asian Continent and western North Pacific. *J. Meteor. Soc. Japan*, **72**, 719–745.
Murata, F., M. D. Yamanaka, M. Fujiwara, S.-Y. Ogino, H. Hashiguchi, S. Fukao, M. Kudsy, T. Sribimawati, S. W. B. Harijono and E. Kelana, 2002: Relationship between wind and precipitation observed with a UHF radar, GPS rawinsonde and surface meteorological instruments at Kototabang, West Sumatera during September-October 1998. *J. Meteor. Soc. Japan*, **80**, 347-360.
Murata, F., M. D. Yamanaka, H. Hashiguchi, S. Mori, M. Kudsy, T. Sribimawati, B. Suhardi and Emrizal, 2006: Dry intrusions following eastward-propagating synoptic-scale cloud systems over Sumatera Island. *J. Meteor. Soc. Japan*, **84**, 277–294.
Murgatroyd, R. J., and F. Singleton, 1961: Possible meridional circulations in the stratosphere and mesosphere. *Quart. J. Roy. Meteorol. Soc.*, **87**: 125–135.
Nakajima, S., Y.-Y. Hayashi and Y. Abe, 1992: A study on the "runaway greenhouse effect" with a one-dimensional radiative-convective equilibrium model. *J. Atmos. Sci.*, **49**, 2256–2266.
Nakazawa, T., 1988: Tropical super clusters within intraseasonal variations over the western Pacific. *J. Meteor. Soc. Japan*, **66**, 823–839.
Nakazawa, T., 1995: Intraseasonal oscillations during the TOGA-COARE IOP. *J. Meteor. Soc. Japan*, **73**, 305–319.
Nastrom, G. D., and K. S. Gage, 1985: A climatology of atmospheric wavenumber spectra of wind and temperature observed by commercial aircraft. *J. Atmos. Sci.*, **42**, 950–960.
Nasuno, T., H. Miura, M. Satoh, A. T. Noda and K. Oouchi, 2009: Multi-scale organization of convection in a global numerical simulation of the December 2006 MJO event using explicit moist processes. *J. Meteor. Soc. Japan*, **87**, 335–345
Naujokat, B., 1986: An update of the observed quasi-biennial oscillation of the stratospheric winds over the tropics. *J. Atmos. Sci.*, **43**, 1873-1877.
Neale, R., and J. Slingo, 2003: The Maritime Continent and its role in the global climate: A GCM study. *J. Climate*, **16**, 834–848.
Neelin, J. D., I. M. Held and K. H. Cook, 1987: Evaporation-wind feedback and low-frequency variability in the tropical atmosphere. *J. Atmos. Sci.*, **44**, 2341–2348.
Newell, R. E., and S. Gould-Stewart, 1981: A Stratospheric Fountain? *J. Atmos. Sci.*, **38**, 2789–2796.
Nieuwolt, S., 1968: Diurnal rainfall variation in Malaya. *Ann. Assoc. Amer. Geographers*. **58**(2), 313–326.
Niino, H., 1987: The linear theory of sea-land breeze circulation. *J. Meteor. Soc. Japan*, **65**, 901–921.
Nitta, Ts, 1987: Convective activities in the tropical western pacific and their impact on the northern hemisphere summer circulation. *J. Meteor. Soc. Japan*, **65**, 373–390.
Nitta, Ts, and T. Motoki, 1987: Abrupt enhancement of convective activity and low-level westerly burst during the onset phase of the 1986-87 El Nino. *J. Meteor. Soc. Japan*, **65**, 497–506.
Nitta, Ts., and S. Sekine, 1994: Diurnal variation of convective activity over the tropical western Pacific. *J. Meteor. Soc. Japan*, **72**, 627–641.
Nitta, Ts, T. Mizuno and K. Takahashi, 1992: Multiscale convective systems during the initial phase of the 1986/87 El Niño. *J. Meteor. Soc. Japan*, **70**, 447–466.
Nodzu, M. I., S.-Y. Ogino, Y. Tachibana and M. D. Yamanaka, 2006: Climatological description on seasonal variations of temperature inversion layers over the Indochina Peninsula. *J. Climate*, **19**, 3307-3319.
Numaguti, A., 1993: Dynamics and energy balance of the Hadley circulation and the tropical precipitation zones: Significance of the distribution of evaporation. *J. Atmos. Sci.*, **50**, 1874-1887.
Numaguti, A., and Y.-Y. Hayashi, 1991: Behavior of Cumulus Activity and the Structures of Circulations in an" Aqua Planet" Model. *J. Meteor. Soc. Japan*, **69**, 541–561.
Okamoto, N., M. D. Yamanaka, S.-Y. Ogino, H. Hashiguchi, N. Nishi, T. Sribimawati and A. Numaguti, 2003: Seasonal variation of tropospheric wind over Indonesia: Comparison between collected operational rawinsonde data and NCEP reanalysis for 1992-99. *J. Meteor. Soc. Japan*, **81**, 829–850.
Ogino, S.-Y., M. D. Yamanaka and S. Fukao, 1995: Meridional variation of lower stratospheric gravity wave activity: A quick look at Hakuho-Maru J-COARE cruise rawinsonde data. *J. Meteor. Soc. Japan*, **73**, 407–413.

Ogino, S.-Y., M. D. Yamanaka, S. Mori and J. Matsumoto, 2016: How much is the precipitation amount over the tropical coastal region? *J. Climate*, **29**, 1231-1236.

Ogura, Y., 1997: *Fundamentals of Meso-Meteorology*. University of Tokyo Press, 215pp. (in Japanese)

Ogura, Y., and M. Yoshizaki, 1988: Numerical study of orographic-convective precipitation over the eastern Arabian Sea and the Ghat Mountains during the summer monsoon. *J. Atmos. Sci.*, **45**, 2097–2122.

Ohsawa, T., H. Ueda, T. Hayashi, A. Watanabe and J. Matsumoto, 2001: Diurnal variations of convective activity and rainfall in tropical Asia. *J. Meteor. Soc. Japan*, **79**, 333–352.

Oouchi, K., J. Yoshimura, H. Yoshimura, R. Mizuta, S. Kusunoki and A. Noda, 2006: Tropical cyclone climatology in a global-warming climate as simulated in a 20 km-mesh global atmospheric model: Frequency and wind intensity analyses. *J. Meteor. Soc. Japan*, **84**, 259–276.

Ooyama, K., 1969: Numerical simulation of the life cycle of tropical cyclones. *J. Atmos. Sci.*, **26**, 3–40.

Osprey, S. M., N. Butchart, J. R. Knight, A. A. Scaife, K. Hamilton, J. A. Anstey, V. Schenzinger and C. Zhang, 2016: An unexpected disruption of the atmospheric quasi-biennial oscillation. *Science*, **353**, 1424–1427.

Palmén, E., and C. R. Newton, 1969: *Atmospheric Circulation Systems: Their Structure and Physical Interpretation*. Academic Press, 603pp.

Palmer, T. N., G. J. Shutts and R. Swinbank, 1986: Alleviation of a systematic westerly bias in general circulation and numerical weather prediction models through an orographic gravity wave drag parameterization. *Quart. J. Roy. Meteor. Soc.*, **112**, 1001-1039

Peatman, S. C., A. J. Matthews and D. P. Stevens, 2014: Propagation of the Madden-Julian Oscillation through the Maritime Continent and scale interaction with the diurnal cycle of precipitation. *Quart. J. Roy. Meteor. Soc.*, **140**, 814–825.

Pedlosky, J., 1964: The stability of currents in the atmosphere and the oceans, Part I. *J. Atmos. Sci.*, **27**, 201–219.

Pedlosky, J., 1979: *Geophysical Fluid Dynamics*. Springer, New York, 707pp.

Peixoto, J. P., and A. H. Oort, 1992: *Physics of Climate*. Springer-Verlag, 520pp.

Pezza, A. B., and I. Simmonds, 2005: The first South Atlantic hurricane: Unprecedented blocking, low shear and climate change. *Geophys. Res. Lett.*, **32**, L15712, doi:10.1029/2005GL023390.

Philander, S. G., T. Yamagata and R. C. Pacanowski, 1984: Unstable air-sea interaction in the tropics. *J. Atmos. Sci.*, **41**, 604–613.

Phillips, N. A., 1966: The equations of motion for a shallow rotating atmosphere and the "traditional approximation". *J. Atmos. Sci.*, **23**, 626–628.

Plumb, R. A., 1984: The quasi-biennial oscillation. *Dynamics of the Middle Atmosphere*, J. R. Holton and T. Matsuno, Eds., Terrapub-D.Reidel, 217–251.

Plumb, R. A., and A. D. McEwan, 1978: The instability of a forced standing wave in a viscous stratified fluid: A laboratory analogue of .the quasi-biennial oscillation. *J. Atmos. Sci.*, **35**, 1827–1839.

Qian, J.-H., 2008: Why precipitation is mostly concentrated over islands in the Maritime Continent. *J. Atmos. Sci*., **65**, 1428–1441.

Ramage, C. S., 1968: Role of a tropical "maritime continent" in the atmospheric circulation. *Mon.Wea. Rev.*, **96**, 365–369.

Ramage, C. S., 1971: *Monsoon Meteorology*. Academic Press, 296p

Rauniyar, S. P., and K. J. E. Walsh, 2011: Scale interaction of the diurnal cycle of rainfall over the Maritime Continent and Australia: Influence of the MJO. *J. Climate*, **24**, 325–348.

Reed, R. J., W. J. Campbell, L. A. Rasmussen, and D. G. Rogers, 1961: Evidence of downward-propagating annual wind reversal in the equatorial stratosphere. *J. Geophys. Res.*, **66**, 813–818.

Rees D., J.J. Barnett and K. Labitske (eds.), 1990: *COSPAR International Reference Atmosphere 1986, Part II: Middle Atmosphere Models*. *Adv. Space Res.*, **10**(12), 1–519.

Reid, J. S., E. J. Hyer, R. S. Johnson, B. N. Holben, R. J. Yokelson, J. Zhang, J. R. Campbell, S. A. Christopher, L. D. Girolamo, L. Giglio, R. E. Holz, C. Kearney, J. Miettinen, E. A. Reid, F. J. Turk, J. Wang, P. Xian, G. Zhao, R. Balasubramanian, B. N. Chew, S. Janjai, N. Lagrosas, P. Lestari, N.-H. Lin, M. Mahmud, A. X. Nguyen, B. Norris, N. T. K. Oanh, M. Oo, Santo V. Salinas, E. J. Welton and S. C. Liew, 2013: Observing and understanding the Southeast Asian aerosol system by remote sensing: An initial review and analysis for the Seven Southeast Asian Studies (7SEAS) program. *Atmos. Res.*, **122**, 403–468.

Renggono, F., H. Hashiguchi, S. Fukao, M. D. Yamanaka, S.-Y. Ogino, N. Okamoto, F. Murata, S. W. B. Harijono, M. Kudsy, M. Kartasasmita, and G. Ibrahim, 2001: Precipitating clouds observed by 1.3-GHz L-band boundary layer radars in equatorial Indonesia. *Ann. Geophys.*, **19**, 889–897.

Renggono, F., M. K. Yamamoto, H. Hashiguchi, S. Fukao, T. Shimomai, M. Kawashima and M. Kudsy, 2006: Raindrop size distribution observed with the Equatorial Atmosphere Radar (EAR) during the Coupling Processes in the Equatorial Atmosphere (CPEA-I) observation campaign. *Radio Sci.*, **41**, RS5002, doi:10.1029/2005RS003333.

Rotunno, R., 1983: On the linear theory of the land and sea breeze. *J. Atmos. Sci.*, **40**, 1999–2009.

Saito, K., T. Keenan, G. Holland and K. Puri, 2001: Numerical simulation of the diurnal evolution of tropical island convection over the maritime continent. *Mon. Wea. Rev.*, **129**, 378-400.

Saji, N. H., B. N. Goswami, P. N. Vinayachandran and T. Yamagata, 1999: A dipole mode in the tropical Indian Ocean. *Nature*, **401**, 360–363.

Sakazaki, T., M. Fujiwara, X. Zhang, M. E. Hagan, and J. M. Forbes, 2012: Diurnal tides from the troposphere to the lower mesosphere as deduced from TIMED/SABER satellite data and six global reanalysis data sets. *J. Geophys. Res.*, **117**, D13108, doi:10.1029/2011JD017117.

Sakazaki, T., K. Sato, Y. Kawatani and S. Watanabe, 2015: Three-dimensional structures of tropical nonmigrating tides in a high-vertical-resolution general circulation model. *J. Geophys. Res. Atmos.*, **120**, 1759–1775.

Sakurai, N., F. Murata, M. D. Yamanaka, H. Hashiguchi, S. Mori, J.-I. Hamada, Y.-I. Tauhid, T. Sribimawati and B. Suhardi, 2005: Diurnal cycle of migration of convective cloud systems over Sumatera Island. *J. Meteor. Soc. Japan*, **83**, 835–850.

Sakurai, N., M. Kawashima, Y. Fujiyoshi, H. Hashiguchi, T. Shimomai, S. Mori, Hamada J.-I., F. Murata, M. D. Yamanaka, Y. I. Tauhid, T. Sribimawati, and B. Suhardi, 2009: Internal structures of migratory cloud systems with diurnal cycle over Sumatera Island during CPEA-I campaign. *J. Meteor. Soc. Japan*, **87**, 157-170.

Sakurai, N., S. Mori, M. Kawashima, Y. Fujiyoshi, J-I. Hamada, S. Shimizu, H. Fudeyasu, Y. Tabata, W. Harjupa, H. Hashiguchi, M. D. Yamanaka, J. Matsumoto, Emrizal and F. Syamsudin, 2011: Migration process and 3D wind field of precipitation systems associated with a diurnal cycle in west Sumatera: Dual Doppler radar analysis during the HARIMAU2006 campaign. *J. Meteor. Soc. Japan*, **89**, 341-361.

Sasaki, T., P.-M. Wu, S. Mori, J.-I. Hamada, Y. I. Tauhid, M. D. Yamanaka, T. Yoshikane and F. Kimura, 2004: Vertical moisture transport above the mixed layer around mountains in western Sumatera. *Geophys. Res. Lett.*, **31**, L08106, doi:10.1029/2004GL019730.

Sato, K., T. Kumakura and M. Takahashi, 1999: Gravity waves appearing in a high-resolution GCM simulation. *J. Atmos. Sci.*, **56**, 1005–1018.

Sato, T., H. Miura, M. Satoh, Y. N. Takayabu and Y. Wang, 2009: Diurnal cycle of precipitation in the tropics simulated in a global cloud-resolving model. *J. Climate*, **22**, 4809–4826.

Satoh, M., T. Matsuno, H. Tomita, H. Miura, T. Nasuno and S. Iga, 2008: Nonhydrostatic icosahedral atmospheric model (NICAM) for global cloud resolving simulations. *J. Comput. Phys.*, **227**, 3486–3514.

Schmidt, F. H., and J. H. A. Ferguson, 1951: Rainfall types based on wet and dry period ratios for Indonesia with western New Guinee. *Verhandelingen Djawatan Meteorologi dan Geofisik*, **42**, 77pp.

Scott, J. R., 1956: The zonal wind in the upper troposphere and weather at Singapore. *Quart. J. Roy. Meteor. Soc.*, **82**, 340–341.

Seto, T. H., M. K. Yamamoto, H. Hashiguchi, S. Fukao, M. Abo, T. Kozu, and M. Kudsy, 2006: Observational study on westerly wind burst over Sumatera, Indonesia by the Equatorial Atmosphere Radar: A case study during the first CPEA observation campaign. *J. Meteor. Soc. Japan*, **84A**, 95–112.

Shibagaki, Y., M. D. Yamanaka, M. Fukase-Kita, H. Hashiguchi, Y. Maekawa and S. Fukao, 2003: Meso-alpha-scale wind field and precipitating clouds in Typhoon 9426 (Orchid) observed by the MU radar. *J. Meteor. Soc. Japan*, **81**, 211-228.

Shibagaki, Y., T. Kozu, T. Shimomai, S. Mori, F. Murata, Y. Fujiyoshi, H. Hashiguchi and S. Fukao, 2006a: Evolution of a super cloud cluster and the associated wind fields observed over the Indonesian maritime continent during the first CPEA Campaign. *J. Meteor. Soc. Japan*. **84A**, 19–31.

Shibagaki, Y., T. Shimomai, T. Kozu, S. Mori, Y. Fujiyoshi, H. Hashiguchi, M. K. Yamamoto, S. Fukao and M. D. Yamanaka, 2006b: Multi-scale convective systems associated with an intraseasonal oscillation over the Indonesian maritime continent. *Mon. Wea. Rev.*, **134**, 1682–1696.

Shigehisa, Y., 1983: Normal modes of the shallow water equations for zonal wavenumber zero. *J. Meteor. Soc. Japan*, **61**, 479–494.

Shimizu, A. and T. Tsuda, 1997: Radiosonde observations of equatorial atmosphere dynamics over Indonesia. *J. Geophys. Res.*, **102**, 26159–26172.

Simmons, A. J., J. M. Wallace and G. W. Branstator, 1983: Barotropic wave propagation and instability, and atmospheric teleconnection patterns. *J. Atmos. Sci.*, **40**, 1363–1392.

Sorooshian, S., X. Gao, K. Hsu, R. A. Maddox, Y. Hong, H. V. Gupta and B. Imam, 2002: Diurnal variability of tropical rainfall retrieved from combined GOES and TRMM satellite information. *J. Climate*, **15**, 983–1001

Stull, R. B., 1988: *Introduction to Boundary-Layer Meteorology*. Kluwer Academic Publishers, 666pp.

Stull, R. B., 2006: The atmospheric boundary layer. *Atmospheric Science: An Introductory Survey*, 2nd Ed., M. J. Wallace and P. V. Hobbs, 375–417.

Stull, R. B., 2015: *Practical Meteorology: An Algebra-based Survey of Atmospheric Science*. Dept. of Earth, Ocean & Atmos. Sci., Univ. of British Columbia, 924pp. Free access: https://www.eoas.ubc.ca/books/Practical_Meteorology/

Sugimoto, N., I. Matsui, A. Shimizu, M. Pinandio and S. Sugondo, 2000: Climatological characteristics of cloud distribution and planetary boundary layer structure in Jakarta, Indonesia revealed by lidar observation. *Geophys. Res. Lett.*, **27**, 2909–2912.

Sui, C.-H., K.-M. Lau, 1992: Multiscale phenomena in the tropical atmosphere over the western Pacific. *Mon. Wea. Rev.*, **120**, 407–430.

Sulistyowati, R., R. I. Hapsari, F. Syamsudin, S. Mori, S. T. Oishi and M. D. Yamanaka, 2014: Rainfall-driven diurnal variations in the Ciliwung River, West Jawa, Indonesia. *SOLA*, **10**, 141−144.

Sun, W.-Y., and I. Orlanski, 1981a: Large mesoscale convection and sea breeze circulation, Part I: Linear stability analysis. *J. Atmos. Sci.*, **38**, 1675–1693.

Sun, W.-Y., and I. Orlanski, 1981b: Large mesoscale convection and sea breeze circulation, Part II: Non-linear numerical model. *J. Atmos. Sci.*, **38**, 1694–1706.

Suwarman, R., K. Ichiyanagi, M. Tanoue, K. Yoshimura, S. Mori, M. D. Yamanaka, N. Kurita and F. Syamsudin, 2013: The variability of stable isotopes and water origin of precipitation over the maritime continent. *SOLA*, **9**, 74-78.

Tabata, A., H. Sakakibara, M. Ishihara, K. Matsuura and Z. Yanagisawa, 1992: A general view of the structure of Typhoon 8514 observed by dual-Doppler radar: From outer rainbands to eye-wall clouds. *J. Meteor. Soc. Japan*, **70**, 897–917.

Tabata, Y., H. Hashiguchi, M. K. Yamamoto, M. Yamamoto, M. D. Yamanaka, S. Mori, F. Syamsudin, and T. Manik, 2011b: Observational study on diurnal precipitation cycle in equatorial Indonesia using 1.3-GHz wind profiling radar network and TRMM precipitation radar, *J. Atmos. Solar Terr. Phys.*, **73**, 1031−1042.

Takasuka, D., T. Miyakawa, M. Satoh and H. Miura, 2015: Topographical effects on internally produced MJO-like disturbances in an aqua-planet version of NICAM. *SOLA*, **11**, 170-176.

Takayabu, Y. N., and Ts. Nitta, 1993: 3−5 day-period disturbances coupled with convection over the tropical Pacific Ocean. *J. Meteor. Soc. Japan*, **71**, 221−246.

Takayabu, Y. N., K.-M. Lau and C.-H. Sui, 1996: Observation of a quasi-2-day wave during TOGA COARE. *Mon. Wea. Rev.*, **124**, 1892–1913.

Takayabu, Y. N., T. Iguchi, M. Kachi, A. Shibata and H. Kanzawa, 1999: Abrupt termination of the 1997−98 El Niño in response to a Madden-Julian oscillation. *Nature*, **402**. 279−282.
Takeda, T., and M. Ikeyama, 1984: Time variation of cloud amount with about 30-days period in the western North Pacific region. J. Meteor. Soc. Japan, *J. Meteor. Soc. Japan*, **62**, 162−175.
Tanaka, H., and M. D. Yamanaka, 1985: Atmospheric circulation in the lower stratosphere induced by the mesoscale mountain wave breakdown. *J. Meteor. Soc. Japan*, **63**, 1047−1054.
Tanaka, H., and N. Yoshizawa, 1985: Quasi-biennial oscillation and its analog under the assumption of wave self-acceleration. *J. Atmos. Sci.*, **42**, 2350–2359.
Tangang, F. T., L. Juneng, 2004: Mechanisms of Malaysian rainfall anomalies. *J. Climate*, **17**, 3616−3622.
Tangang, F. T., L. Juneng, E. Salimun, P. N. Vinayachandran, Y. K. Seng, C. J. C. Reason, S. K. Behera and T. Yasunari, 2008: On the roles of the northeast cold surge, the Borneo vortex, the Madden-Julian Oscillation, and the Indian Ocean Dipole during the extreme 2006/2007 flood in southern Peninsular Malaysia. *Geophys. Res. Lett.*, **35**, L14S07, doi:10.1029/2008GL033429.
Teshiba, M., H. Fujita, H. Hashiguchi, Y. Shibagaki, M. D. Yamanaka and S. Fukao, 2005: Detailed structure within a tropical cyclone "eye". *Geophys. Res. Lett.*, **32**, L24805, doi:10.1029/2005GL023242.
Thompson, W. J., and J. M. Wallace, 1998: The Arctic oscillation signature in the wintertime geopotential height and temperature fields. *Geophys. Res. Lett.*, **25**, 1297–1300.
Trenberth, K. E., J. T. Fasullo and J. Kiehl, 2009: Earth's global energy budget. *Bull. Amer. Meteor. Soc.*, **90**, 311-323.
Trilaksono, N. J., S. Otsuka, S. Yoden, K. Saito and S. Hayashi, 2011: Dependence of model-simulated heavy rainfall on the horizontal resolution during the Jakarta flood event in January−February 2007. *SOLA*, **7**, 193−196.
Trilaksono, N. J., S. Otsuka and S. Yoden, 2012: A time-lagged ensemble simulation on the modulation of precipitation over west Java in January–February 2007. *Mon. Wea. Rev.*, **140**, 601–616.
Tsuda, T., Y. Murayama, H. Wiryosumarto, S. W. B. Harijono and S. Kato, 1994a: Radiosonde observations of equatorial atmosphere dynamics over Indonesia: 1. Equatorial waves and diurnal tides. *J. Geophys. Res.*, **99**, 10491–10505.
Tsuda, T., Y. Murayama, H. Wiryosumarto, S. W. B. Harijono, and S. Kato, 1994b: Radiosonde observations of equatorial atmosphere dynamics over Indonesia: 2. Characteristics of gravity waves. *J. Geophys. Res.*, **99**, 10507–10516,
Tsuda, T., M. Nishida, C. Rocken and R. H. Ware, 2000: A global morphology of gravity wave activity in the stratosphere revealed by the GPS occultation data (GPS/MET). *J. Geophys. Res.*, 105, 7257–7273.
Van Andel, T. H., 1994: *New Views on an Old Planet: A History of Global Change.* Cambridge University Press, 458pp.
van Bemmelen, W., 1913: Die Erforschungdes tropischen Luftoszeans in Niederländische-Ost-Indien. *Luftfahrt und Wissenschaft*, **5**, 1–50 (in German).
van Bemmelen, W., 1922: Land- und Seebrise in Batavia. *Beitr. Phys. Frei. Atmos.*, **10**, 169–177. (in German).
Veryard, R. G., and R. A. Ebdon, 1961: Fluctuations in tropical stratosphere winds. *Meteor. Mag.*, **90**, 125–143.
Virts, K. S., J. M. Wallace, M. L. Hutchins and R. H. Holzworth, 2013a: Highlights of a new ground-based, hourly global lightning climatology. *Bull. Amer. Meteor. Soc.*, **94**, 1381–1391.
Virts, K. S., J. M. Wallace, M. L. Hutchins and R. H. Holzworth, 2013b: Diurnal lightning variability over the Maritime Continent: Impact of low-level winds, cloudiness, and the MJO. *J. Atmos. Sci.*, **70**, 3128–3146.
Waliser, D. E., 2012: Predictability and forecasting. *Intraseasonal Variability of the Atmosphere–Ocean Climate System*, 2nd ed. W. K.-M. Lau and D. E. Waliser, Eds., Springer, 433–476.
Walker, G. T., 1923: Correlation in seasonal variations of weather, VIII: A preliminary study of world weather. *Memoirs of the Indian Meteorological Department*, **24**(4), 75–131.
Wallace, J. M., and P. V. Hobbs, 2006: *Atmospheric Science: An Introductory Survey, 2nd Ed.*, Academic Press, 483pp.
Wallace, J. M., and V. E. Kousky, 1968: Observational evidence of Kelvin waves in the tropical stratosphere. *J. Atmos. Sci.*, **25**, 900–907.
Wang, B., and L. Ho, 2002: Rainy season of the Asian-Pacific summer monsoon. *J. Climate*, **17**, 386–398.
Wang, B., and H. Rui, 1990: Synoptic climatology of transient tropical intraseasonal convection anomalies: 1975–1985. *Meteor. Atmos. Phys.*, **44**, 43–61.
Warner, T. T., B. E. Mapes and M. Xu, 2003: Diurnal patterns of rainfall in northwestern South America. Part II: Model simulations. *Mon. Wea. Rev.*, **131**, 813–829.
Webster, P. J., 1994: The role of hydrographic processes in ocean-atmosphere interactions. *Rev. Geophys.*, **32**, 427–476.
Webster, P. J., and R. Lukas,, 1992: TOGA COARE: The coupled ocean-atmosphere response experiment. *Bull, Amer. Meteor. Soc.*, **73**, 1377-1416.
Webster, P. J., V. O. Magaña, T. N. Palmer, J. Shukla, R. A. Tomas, M. Yanai and T. Yasunari, 1998: Monsoons: Processes, predictability, and the prospects for prediction, *J. Geophys. Res.*, **103**, 14451–14510,
Webster, P. J., C. Clark, G. Cherikova, J. Fasullo, W. Han, J. Loschnigg and K. Sahami, 2002: The monsoon as a self-regulating coupled ocean-atmosphere system. *International Geophys.*, **83**, 198-219.
Webster, P. J., G. J. Holland, J. A. Curry and H.-R. Chang, 2005: Changes in tropical cyclone number, duration, and intensity in a warming environment. *Science*, **309**, 1844–1846. [Corrections and clarifications (2006), **311**, 470.]
Wheeler, M. C., and H. H. Hendon, 2004: An alll-season real-time multivariate MJO index: Development of an index for monitoring and prediction. *Mon. Wea. Rev.*, **132**, 1917–1932.
Widiyatmi, I., M. D. Yamanaka, H. Hashiguchi, S. Fukao, T. Tsuda, S.-Y. Ogino, S. W. B. Harijono and H. Wiryosumarto, 1999: Quasi-four-day mode observed by the boundary layer radar at Serpong (6S, 107E), Indonesia. *J. Meteor. Soc. Japan*, **77**, 1177–1184.
Widiyatmi, I., H. Hashiguchi, S. Fukao, M. D. Yamanaka, S.-Y. Ogino, K. S. Gage, S. W. B. Harijono, S. Diharto and H. Djojodihardjo, 2001: Examination of 3-6 day disturbances over equatorial Indonesia based on boundary layer radar observations during 1996-1999

at Serpong, Biak and Bukittinggi. *J. Meteor. Soc. Japan*, **79**, 317–331.
Willoughby, H. E., 1999: Hurricane heat engines. *Nature*, **401**, 649-650.
Winchester, S., 2003: *Krakatoa: The Day the World Exploded: August 23, 1883*. Perennial, 416pp.
Wu, P.-M., J.-I. Hamada, S. Mori, Y. I. Tauhid, M. D. Yamanaka and F. Kimura, 2003: Diurnal variation of precipitable water over a mountaneous area in Sumatera Island. *J. Appl. Meteor.*, **42**, 1107-1115.
Wu, P.-M., M. Hara, H. Fudeyasu, M. D. Yamanaka, J. Matsumoto, F. Syamsudin, R. Sulistyowati and Y. S. Djajadihardja, 2007: The impact of trans-equatorial monsoon flow on the formation of repeated torrential rains over Java Island. *SOLA*, **3**, 93–96.
Wu, P.-M., M. D. Yamanaka and J. Matsumoto, 2008a: The formation of nocturnal rainfall offshore from convection over western Kalimantan (Borneo) Island. *J. Meteor. Soc. Japan*, **86A**, 187–203.
Wu, P.-M., S. Mori, J.-I. Hamada, M. D. Yamanaka, J. Matsumoto and F. Kimura, 2008b: Diurnal variation of rainfall and precipitable water over Siberut Island off the western coast of Sumatera Island. *SOLA*, **4**, 125–128.
Wu, P.-M., J.-I. Hamada, M. D. Yamanaka and J. Matsumoto, 2009a: The impact of orographically-induced gravity wave on the diurnal cycle of rainfall over southeast Kalimantan Island. *Atmos. Ocean. Sci. Lett.*, **2**, 35–39.
Wu, P.-M., M. Hara, J.-I. Hamada, M. D. Yamanaka and F. Kimura, 2009b: Why heavy rainfall occurs frequently over the sea in the vicinity of western Sumatera Island during nighttime. *J. Appl. Meteor. Climatol.*, **48**, 1345–1361.
Wu, P.-M., Y. Fukutomi and J. Matsumoto, 2011: An observational study of the extremely heavy rain event in northern Vietnam during 30 October–1 November 2008. *J. Meteor. Soc. Japan*, **89A**, 331–344.
Wu, P.-M., A. A. Arbain, S. Mori, Hamada J.-I., M. Hattori, F. Syamsudin and M. D. Yamanaka, 2013: The effects of an active phase of the Madden-Julian oscillation on the extreme precipitation event over western Java Island in January 2013, *SOLA*, **9**, 79–83.
Xie, S.-P., H. Xu, N. H. Saji, Y. Wang and W. T. Liu, 2006: Role of narrow mountains in large-scale organization of Asian monsoon convection. *J. Climate*, **19**, 3420–3429.
Yamanaka, M. D., 2016: Physical climatology of Indonesian maritime continent: An outline to comprehend observational studies. *Atmos. Res.*, **178-179**, 231–259.
Yamanaka, M. D., and H. Tanaka, 1984: Propagation and breakdown of internal inertio-gravity waves near critical levels in the middle atmosphere. *J. Meteor. Soc. Japan*, **62**, 1–17.
Yamanaka, M. D., S. Mori, Wu P.-M., Hamada J.-I., N. Sakurai, H. Hashiguchi, M. K. Yamamoto, Y. Shibagaki, M. Kawashima, Y. Fujiyoshi, T. Shimomai, T. Manik, Erlansyah, W. Setiawan, B. Tejasukmana, F. Syamsudin, Y. S. Djajadihardia, and J. T. Anggadiredja, 2008: HARIMAU radar-profiler network over Indonesian maritime continent: A GEOSS early achievement for hydrological cycle and disaster prevention. *J. Disaster Res.*, **3**, 78–88.
Yamanaka, M. D., S.-Y. Ogino, P.-M. Wu, Hamada J.-I., S. Mori, J. Matsumoto and F. Syamsudin, 2017: Maritime continent coastlines controlling Earth's climate. *Prog. Earth Planet Sci.*, MAHASRI Special Issue, submitted.
Yanai, M., and T. Maruyama, 1966: Stratospheric wave disturbances propagating over the equatorial Pacific. *J. Meteor. Soc. Japan*, **44**, 291–294.
Yanai, M., S. Esbensen and J. H. Chu, 1973: Determination of bulk properties of tropical cloud clusters from large-scale heat and moisture budgets. *J. Atmos. Sci.*, **30**, 611–627.
Yang, G.-Y., and J. Slingo, 2001: The diurnal cycle in the tropics. *Mon. Wea. Rev.*, **129**, 784–801.
Yasunari, T., 1979: Cloudiness fluctuations associated with the Northern Hemisphere summer monsoon. *J. Meteor. Soc. Japan*, **57**, 227–242.
Yokoi, S., and J. Matsumoto, 2008: Collaborative effects of cold surge and tropical depression–type disturbance on heavy rainfall in central Vietnam. *Mon. Wea. Rev.*, **136**, 3275–3287.
Yoneyama, K., Y. Masumoto, Y. Kuroda, M. Katsumata, K. Mizuno, Y. N. Takayabu, M. Yoshizaki, A. Shareef, Y. Fujiyoshi, M. J. McPhaden, V. S. N. Murty, R. Shirooka, K. Yasunaga, H. Yamada, N. Sato, T. Ushiyama, Q. Moteki, A. Seiki, M. Fujita, K. Ando, H. Hase, I. Ueki, T. Horii, C. Yokoyama and T. Miyakawa, 2008: MISMO field experiment in the equatorial Indian Ocean. *Bull. Amer. Meteor. Soc.*, **89**, 1889-1903.
Yoneyama, K., C. Zhang and C. N. Long, 2013: Tracking pulses of the Madden–Julian oscillation. *Bull. Amer. Meteor. Soc.*, **94**, 1871–1891.
Zhang, C., 2005: Madden-Julian oscillation. *Rev. Geophys.*, **43**, RG2003, doi:10.1029/2004RG000158.
Zhang, C., 2013: Madden-Julian oscillation bridging weather and climate. *Bull. Amer. Meteor. Soc.*, **43**, 1849–1870.
Zhang, C., and J. Ling, 2017: Barrier effect of the Indo-Pacific Maritime Continent on the MJO: Perspectives from tracking MJO precipitation. *J. Climate*, **30**, 3439–3459.